The Thesis Committee for Graham Stephen Hogsett
Certifies that this is the approved version of the following thesis:

Defining Structurally Acceptable Mechanical Properties of High-Strength Reinforcing Steel Bars through Low-Cycle Fatigue Testing

APPROVED BY
SUPERVISING COMMITTEE:

Supervisor: _____
Michael D. Engelhardt

Co-Supervisor: _____
Wassim M. Ghannoum

Defining Structurally Acceptable Mechanical Properties of High-Strength Reinforcing Steel Bars through Low-Cycle Fatigue Testing

by

Graham Stephen Hogsett

Thesis

Presented to the Faculty of the Graduate School of

The University of Texas at Austin

in Partial Fulfillment

of the Requirements

for the Degree of

Master of Science in Engineering

The University of Texas at Austin

December 2017

Dedication

This thesis is dedicated to my parents, for their constant love, support and encouragement.

Acknowledgements

The generous financial support of the Charles Pankow Foundation, the Concrete Reinforcing Steel Institute, and the American Concrete Institute Foundation Strategic Development Council made this work possible and is greatly appreciated. The steel and fabrication donations of member mills of the Concrete Reinforcing Steel Institute are also greatly appreciated, as is their substantial financial and technical commitment to developing new high-strength reinforcing bars.

I would like to acknowledge the technical and administrative staff at the Ferguson Structural Engineering Laboratory (FSEL): David Braley, Dennis Fillip, Liz Clayton, Michelle Damvar, Truman Oliver, and in particular Dr. Michael Brown for his patience and near daily help.

Drit Sokoli always managed to find the time to talk through any difficulties and give thoughtful advice. His guidance and endless curiosity was an influential driving force through this project. I am grateful for Alex Mackey introducing me to the laboratory environment, but more importantly for his friendship. I am thankful to have worked around so many bright minds at FSEL whose passionate work ethic and achievements are both humbling and inspiring.

I would like to thank Dr. Michael Engelhardt for his review, insights and perspectives on not only academics, but on life. Lastly, I would like to express my gratitude and appreciation for Dr. Wassim Ghannoum for giving me this opportunity, continually challenging me, keeping things in perspective, and being patient. Without his expertise and advice, this research would not have been possible.

Abstract

Defining Structurally Acceptable Mechanical Properties of High-Strength Reinforcing Steel Bars through Low-Cycle Fatigue Testing

Graham Stephen Hogsett, M.S.E.

The University of Texas at Austin, 2017

Supervisor: Michael D. Engelhardt

Co-Supervisor: Wassim M. Ghannoum

Low-cycle fatigue tests were performed on high-strength reinforcing bars currently being developed in the United States, to quantify mechanical properties and fatigue life under simulated seismic conditions. Reinforcing bars with yield strengths ranging for about 60ksi to over 100ksi were tested. The high-strength bars with yield strengths exceeding 80ksi were obtained from three manufacturers that produce high-strength bars using the main three manufacturing techniques in use in the United States. Primary variables considered also include chemical composition, geometric deformations, bar grade, clear gripping span, loading protocol, and manufacturing process. The results of monotonic and cyclic tests are presented and comparisons are made based on the variables listed. A previously proposed fatigue model is considered and recalibrated for the new testing data.

TABLE OF CONTENTS

LIST OF TABLES

LIST OF FIGURES

LIST OF EQUATIONS

1. INTRODUCTION

1.1 MOTIVATION

In an effort to meet the increasing challenges of structural designs, high-strength reinforcing steel bars are increasing in popularity. Higher strength reinforcing bars allow for measurable reductions in the amount of steel required in design, thus providing benefits in constructability, as well as economic and environmental benefits derived from reduced material quantities. High-strength reinforcing bars (HSRB) are defined in this report as bars having a yield strength that is higher than 80ksi. For simplicity, this report also uses the term grade to refer to the approximate yield strength provided by the manufacturer in kips per square inch (ksi). For example, grade 60 bars have a yield strength that is around 60ksi.

Current code provisions as laid out in ACI 318-14, set the reinforcement strength limit for gravity systems at 80ksi, but for seismic applications, the maximum reinforcement strength is limited to 60ksi. This limitation is in part due to well-known changes in the mechanical behavior of steel as its strength increases, namely, higher strength steel has a greater yield strain and a lower fracture strain. Additionally, uncertainties about the toughness and fatigue performance of newly developed HSRB have also contributed to maintaining the status quo in the ACI 318 design code. Experimental evidence has shown that HSRB in concrete members can experience much larger strains at any given member deformation level. Tests conducted by Sokoli and Ghannoum (2016) showed that grade 100 bars experienced as much as 100% larger strain demands than equivalent grade 60 bars. Additional design decisions concerning the limitations on the spacing of transverse reinforcement to prevent buckling of HSRB must also be evaluated.

Recent fatigue testing has revealed a high variability in the resistance to fatigue of HSRB being developed in the U.S., with some exhibiting much higher and others much lower fatigue

lives than the benchmark grade 60 bars (Slavin and Ghannoum, 2015, Ghannoum and Slavin, 2016). Additionally, it is well known that the fatigue life of steel decreases exponentially with increased strain demands. These results spurred the reinforcing bar industry to seek further improvements in production methods and chemical compositions to improve the ductility and toughness of high-strength reinforcing bars. Further evaluation of the mechanical properties of HSRB and their effects on low-cycle fatigue life are crucial for assessing any potential change in fracture and associated collapse risk associated with the switch from regular grade 60 bars to HSRB.

1.2 OBJECTIVES AND SCOPE

This study is part of a broader project whose ultimate objectives are to evaluate any changes in bar fracture and seismic risk associated with switching to HSRB, and to define the acceptable mechanical properties for HSRB for use in seismic applications based on those risks. As part of that effort, mechanical tests were conducted in this study to quantify the mechanical properties of experimental batches of high-strength bars and aid the development process of those new types of bars. Monotonic tension tests along with low-cycle fatigue tests were performed on grade 60 and high-strength reinforcing bars in order to evaluate their performance under simulated seismic conditions. The results allowed comparison between the performance of HSRB and equivalent grade 60 bars. This study builds on a precursor study by Ghannoum and Slavin (2016), in which similar monotonic tension tests and low-cycle fatigue tests were performed on grade 60 bars and earlier productions of HSRB.

High-strength reinforcement produced using the three main manufacturing techniques in the U.S. and produced by three different manufacturers is assessed. This study also considered the additional variables of bar grade, up to grade 100, clear griping span, loading strain protocol,

and geometric deformations. A series of batches with various production adjustments were tested for each manufacturer to help guide the development of the bars. Bar testing is still ongoing as part of the broader project, which encompass steel from the main five manufacturers of reinforcing bars in the U.S. Results of tests completed to date are presented here.

2. BACKGROUND

2.1 METALLURGY

The four main production methods currently used in the United States to produce high-strength reinforcing bars are: micro-alloying, quenching and tempering, a proprietary combination of alloying and microstructure manipulation, and cold-working. Each of these methods results in different mechanical properties. Although steel produced by cold-working shows an increase in yield strength, due to a reduction in ductility and ratio of tensile strength to yield strength (T/Y), this method is not used for producing bars in seismic applications. Differences between the other three production methods, the resulting metallurgy, and its influence on the mechanical properties of reinforcing bars are discussed in this section.

2.1.1 Micro-alloying

Micro-alloying is the process of producing high-strength steel by alloying the steel with small amounts of vanadium (V), titanium (Ti), or niobium (Nb) to achieve solid solution strengthening and interstitial solution hardening. In this study, the bars produced by micro-alloying were done so using vanadium. Benefits of using vanadium over titanium and niobium include, more control over the strengthening effects and less temperature control required during rolling. Micro-alloyed bars using vanadium are able to maintain their weldability and ductility while achieving a yield strength above 100ksi. Additional effects of micro-alloying with vanadium on the mechanical properties of bars include a relatively high T/Y ratio, between 1.2 to 1.4 for high-strength bars, and a reduction in fracture elongation.

2.1.2 Quenching and Tempering

Quenching and tempering allows for the production of high-strength steel using inexpensive carbon steel through temperature manipulation during manufacturing. The quenching part of the process consists of rapidly cooling the bars down after they have been heated to the austenitic phase. This rapid cooling creates a hard and brittle layer around the exterior of the bar, while the core of the bar retains heat and is allowed to cool slowly. During the slow cooling, the core of the bar is transformed from austenite to a combination of ferrite, perlite and bainite and therefore decreasing the hardness while increasing the ductility. The hot bar core also reheats and tempers the outer layers after quenching. As a result of this process, the exterior and interior core of the bar show a significant difference in their mechanical properties. The exterior of the bar is harder and more brittle compared to the softer and more ductile core. Quenching and tempering typically produces large gains in yield strength but relatively modest gains in tensile strength, producing bars with a relatively low T/Y ratio on the order of 1.10 to 1.15 for grade 100 bars. Fracture elongation is typically higher than that of bars produced by micro-alloying.

2.1.3 Proprietary Combination of Alloying and Micro Structure Manipulation

The proprietary combination of alloying and micro structure manipulation method has been patented by MMFX (MMFX Technologies Corporation, 2012). During this process, manipulation of the microstructure is used to obtain the desired mechanical properties. The result of this production technique is bar that demonstrates a stress-strain relationship that does not show a well-defined yield point, exhibit a relatively high T/Y ratio, but have relatively low fracture elongations. The MMFX steel bars satisfy the ASTM A1035 specifications (ASTM

A1035/A1035M-16a, 2016). ACI 318-14 allows for the use of A1035 grade 100 bars in confinement applications.

2.2 LOW-CYCLE FATIGUE

Brown and Kunnath (2004): Low-Cycle Fatigue Failure of Reinforcing Steel Bars

The authors of this paper defined their objective as to gain understanding of the low-cycle fatigue failure of longitudinal steel reinforcement as well as developing a fatigue life relationship to characterize response. The test setup and conditions were designed to replicate the behavior of longitudinal reinforcement in reinforced concrete columns subjected to large inelastic cyclic loading. As concrete typically spalls at a relatively small strains compared to the strains experienced in longitudinal bars during a seismic event, the concrete cover contribution to bar buckling restraint is limited. For this reason, the authors completed all bar fatigue testing in air. Specimens were swaged using aluminum sleeves to reduce stress concentrations during gripping.

All tests were conducted on bars satisfying ASTM A615 from a single source. Focusing on bar sizes representative of those commonly used as longitudinal steel, unmachined #6, #7, #8, and #9 bars were used in the tests. Bars were cycled at constant fully reversed strain amplitudes ranging between 1.5% and 3.0%, or a total strain range of 3.0% to 6.0%. These strains were measured across the entire gage length of the specimen. The gage length for all tests was six times the nominal bar diameter ($6d_b$) based off of transverse reinforcement spacing limits for seismically detailed columns in ACI 318-02.

The authors found that the fatigue life model proposed by Koh and Stephens (1991) best matched the fatigue results from reinforcement. The authors observed that at lower strain amplitudes, as bar diameter increased fatigue life increased. However, as strain amplitudes

increased, the trend reversed with smaller diameter bars showing longer fatigue life than larger diameter bars. These relations suggest that larger bars experience a more significant deterioration in fatigue life with increasing strain amplitudes. Lastly, the authors found that using energy-based models for predicting fatigue life were generally less reliable and accurate than models based on the number of cycles to failure. The authors suggest this inaccuracy may be a result of energy dissipation per cycle decreasing with an increasing number of cycles.

NIST GCR 14-917-30 (2014): Use of High-Strength Reinforcement in Earthquake Resistant Concrete Structures

This report evaluates recent research to determine whether code provisions should be updated to allow for the use of high-strength reinforcement in seismic design. The authors discuss the effects of transverse bar spacing on longitudinal bar buckling restraint. When buckling occurs in longitudinal reinforcement the ductility and energy dissipation capacity of the member decrease. In addition to member level effects, buckling can cause cracking near transverse deformations in the buckled bar and eventually fracture. Figure 2-1 shows the cracking along the transverse deformations for a buckled bar.

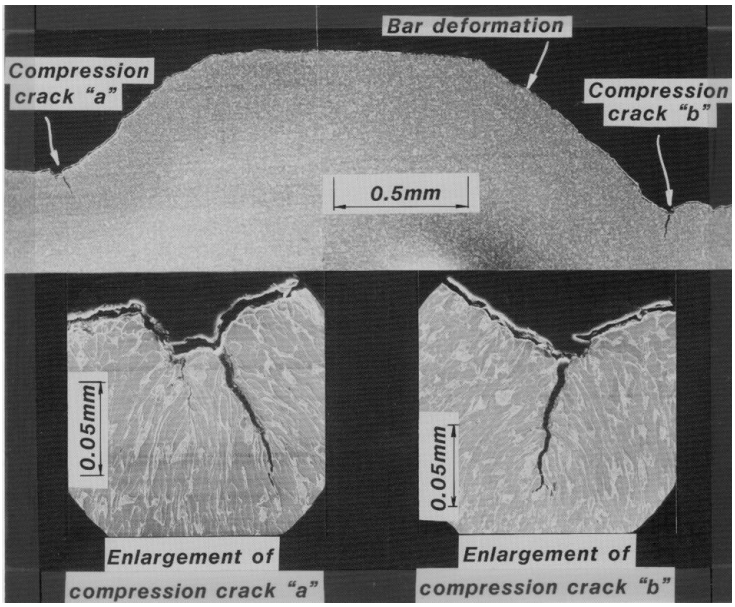

Figure 2-1: Cracking along the root of the deformation in the compressed side of a buckled reinforcing bar: electron microscope view of cracking (from NIST GCR 14-917-30, 2014)

Theoretical compressive stress-strain relationships based on known tensile stress-strain relationships were calculated by discretizing the cross section of the bars into fibers. This allowed for geometric nonlinearities to be considered upon buckling. Analyses were conducted at clear spans of $4d_b$, $5d_b$, and $6d_b$ assuming full fixity at the ends of the bars. These idealized conditions ignore the effects of stiffness of the transverse reinforcement, longitudinal bar concrete cover and core longitudinal bar interaction. The authors found that for strains under 0.025, the three clear spans investigated showed little variation in the compressive stress-strain response for grade 60 and grade 80 bars. For strains above 0.025, the effects of buckling begin to influence response and the results from each clear span deviate from one another. For grade 100 bars, the response for $6d_b$ begins to deviate at a smaller strain than the grade 60 and grade 80 bars. Based on these findings, it was recommended that a transverse spacing of 6 times the nominal bar diameter of the longitudinal reinforcement for grade 60 and grade 80 reinforcement. For grades above 80, this recommendation was lowered to 5 times the diameter of the

longitudinal reinforcement. The authors note that current construction tolerances would need to be updated to reflect these provisions.

Slavin and Ghannoum (2015): Defining Structurally Acceptable Properties of High-Strength Steel Bars through Material and Column Testing

The authors of this study conducted low-cycle fatigue testing on high-strength reinforcing bars (HSRB) that were representative of the production methods and practices in the United States at the time of reporting. This allowed for a direct comparison of behavior and results with the standard grade 60 steel that the current ACI 318-14 design code allows when designing in seismic regions. As the majority of the research to date had been conducted on the monotonic tension-test properties, such as the Tensile/Yield strength ratio (T/Y) and fracture elongation, focus in the study was directed to the cyclic behavior. The cyclic loading protocols chosen involved strains that exceeded the elastic strains, causing a relatively low number of cycles before failure occurred, representative of seismic conditions.

Low-cycle fatigue tests were conducted on three sizes of bars, #5, #8, and #11, three grades, grade 60, 80 and 100, produced by two manufacturers. This recently completed testing program on HSRB provided the impetus for improving their mechanical properties and conducting further material testing within this study. Five primary parameters were varied in the test program: 1. Production method, 2. Steel strength, 3. Bar size, 4. Strain loading protocol, and 5. Unbraced length of the bar specimen. A summary of the effects of each parameter is provided below.

1. Production Method

Two different production methods of two different manufacturers were compared, the first being micro-allowing (Manufacturer 1) and the second being a combination of micro-alloying along with quenching and tempering (Manufacturer 2). The two processes proved to be comparable, with Manufacturer 2 exhibiting an overall fatigue life across all cases that is only 19% higher. Table 2-1 and Table 2-2 show the results for #5 and #8 bars respectively.

		Loading Protocol		
		+4%, 0%		+4%, -1%
		Clear-Span		Clear-Span
Manufacturer	Grade	$5d_b$	$6d_b$	$6d_b$
1	60	30.6 (3)	43.2 (5)	N/A
	80	N/A	16 (3)	N/A
	100	39 (4)	36.5 (4)	12 (3)
2	60	55 (4)	19.3 (3)	N/A
	80	N/A	85.5(4)	N/A
	100	23 (4)	33.3 (3)	14 (3)

Table 2-1: Mean number of half-cycles to fracture for #5 bars with the number of coupons tested per bar type noted in parentheses (from Slavin and Ghannoum, 2015)

		Loading Protocol					
		+2%, -2%			+4%, -1%		
		Clear-Span			Clear-Span		
Manufacturer	Grade	$4d_b$	$5d_b$	$6d_b$	$4d_b$	$5d_b$	$6d_b$
1	60	46.7 (3)	44 (3)	32 (3)	33.3 (3)	25 (2)	20 (3)
	80	36.7 (3)	N/A	14.7 (3)	18 (3)	N/A	11.3 (3)
	100	68 (4)	42 (5)	28.5 (4)	27.3 (3)	18.5 (4)	12.7 (3)
2	60	69.3 (4)	36 (3)	24 (4)	25.3 (3)	17.3 (3)	14.7 (3)
	100	57.3 (3)	N/A	26.7 (3)	28.5 (4)	18 (3)	12 (3)

Table 2-2: Mean number of half-cycles to fracture for #8 bars with the number of coupons tested per bar type noted in parentheses (from Slavin and Ghannoum, 2015)

2. Steel Strength

Both the grade 80 #5 and grade 80 #8 bars produced by manufacturer 1 exhibited a decrease in fatigue life performance compared to the grade 60 A706 bars produced by the same manufacturer. The grade 100 #5 bar results for manufacturer 1 indicated a comparable fatigue life to the grade 60 A706. In general, the grade 100 #8 bars from manufacturer 1 performed worse than their grade 60 counterpart, but surpassed the results from grade 80 #8. The authors were not able identify the reason for the decrease in fatigue life for the grade 80 bars when compared to both the grade 60 and grade 100 bars from the same manufacturer.

The grade 80 #5 bars produced by manufacturer 2 showed significantly superior fatigue life than the grade 60 #5 bars produced by the same manufacturer. There was some variability with the grade 100 #5 bars produced by manufacturer 2, with the bars performing comparably to the baseline grade 60 for the larger clear spans, but much worse (nearly 60%) for the smaller clear spans. The authors did not test any grade 80 #8 bars from manufacturer 2, but grade 100 #8 bars from manufacturer 2 were able to approximately match the fatigue performance of equivalent grade 60 bars.

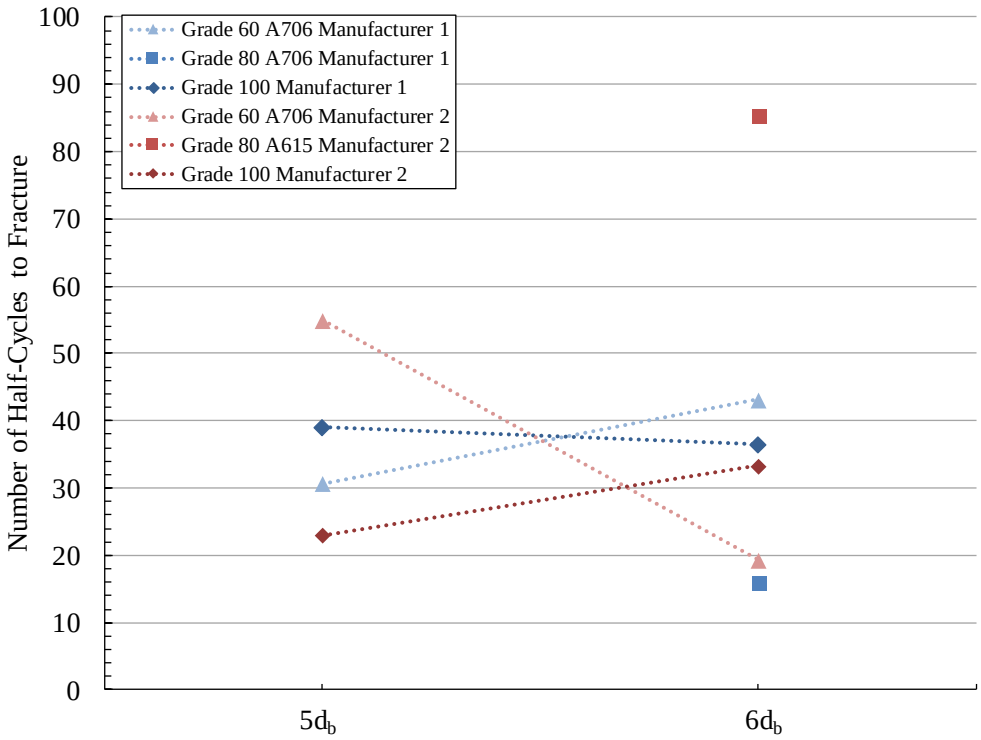

Figure 2-2: Effects of steel grade and clear span on low-cycle fatigue life for #5 bars tested under the +4% to 0% loading protocol (from Slavin and Ghannoum, 2015)

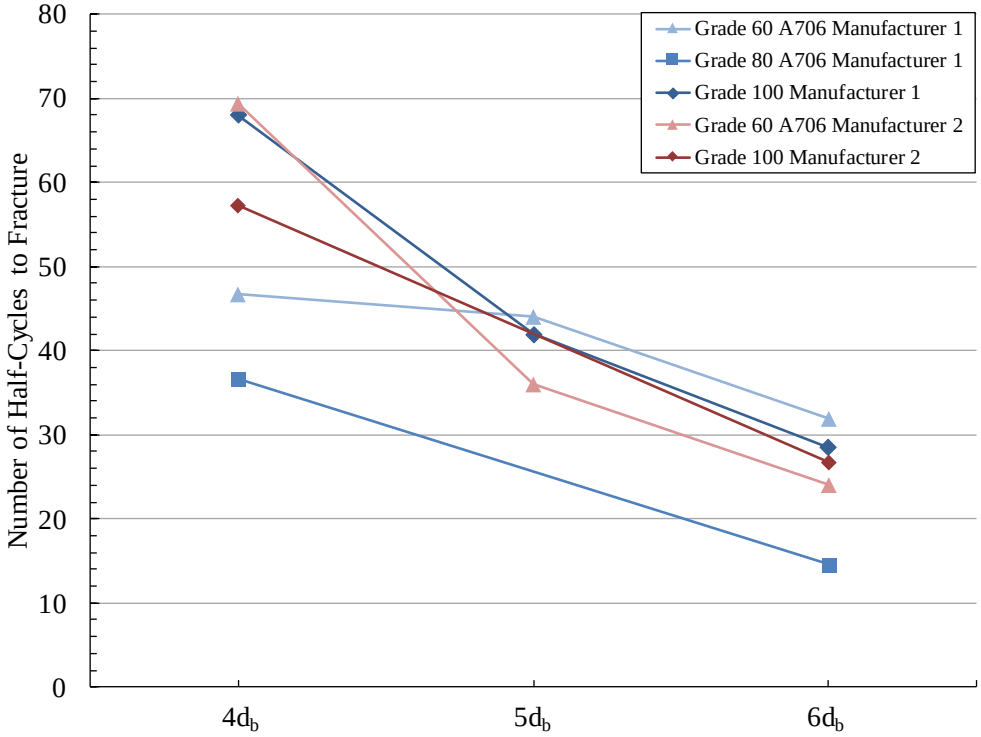

Figure 2-3: Effects of steel grade and clear span on low-cycle fatigue life for #8 bars tested under the +2% to -2% loading protocol (from Slavin and Ghannoum, 2015)

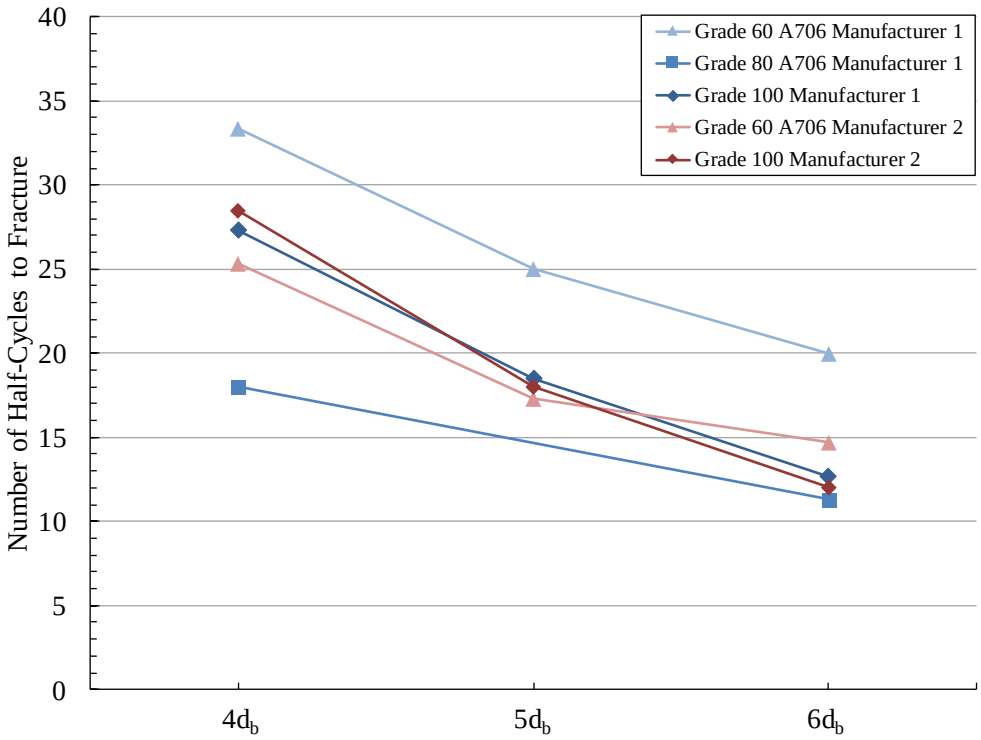

Figure 2-4: Effects of steel grade and clear span on low-cycle fatigue life for #8 bars tested under the +4% to -1% loading protocol (from Slavin and Ghannoum, 2015)

3. Bar Size

Bar size was shown to be the less significant of the parameters in the study. A general trend of an increase in bar size leading to a decrease in fatigue life was observed. Figure 2-5 and Figure 2-6 illustrate the effects of bar size on fatigue life under a total strain range of 4% for manufacturer 1 and manufacturer 2 respectively.

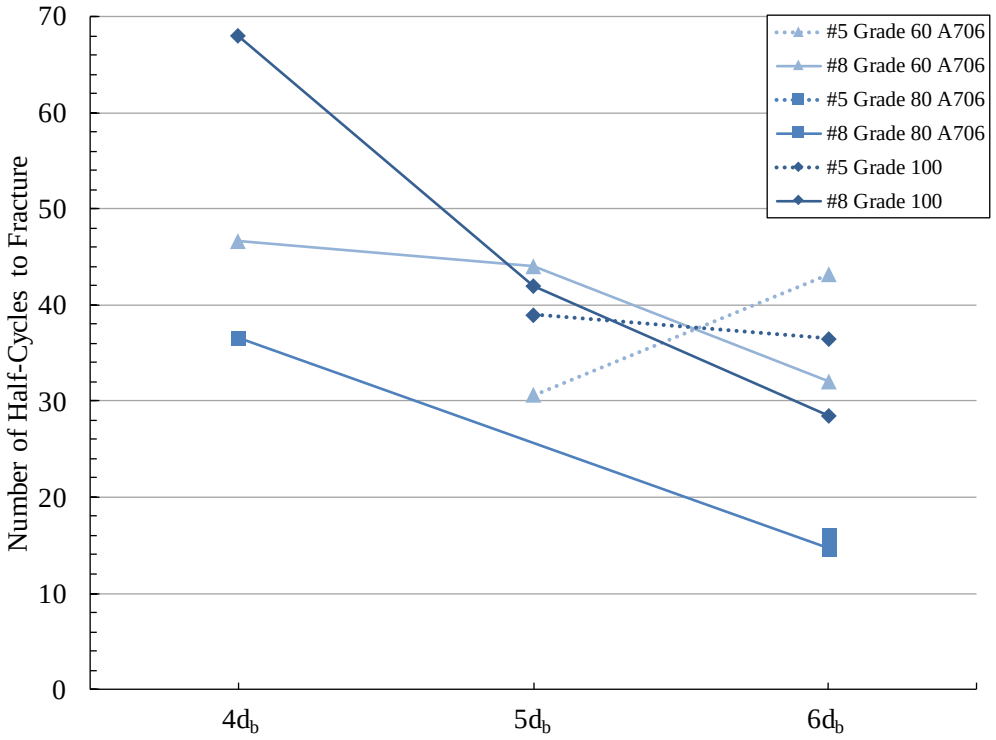

Figure 2-5: Effects of bar size and clear span on low-cycle fatigue life for #5 and #8 bars produced by manufacturer 1 and tested with a total strain range of 4% (from Slavin and Ghannoum, 2015)

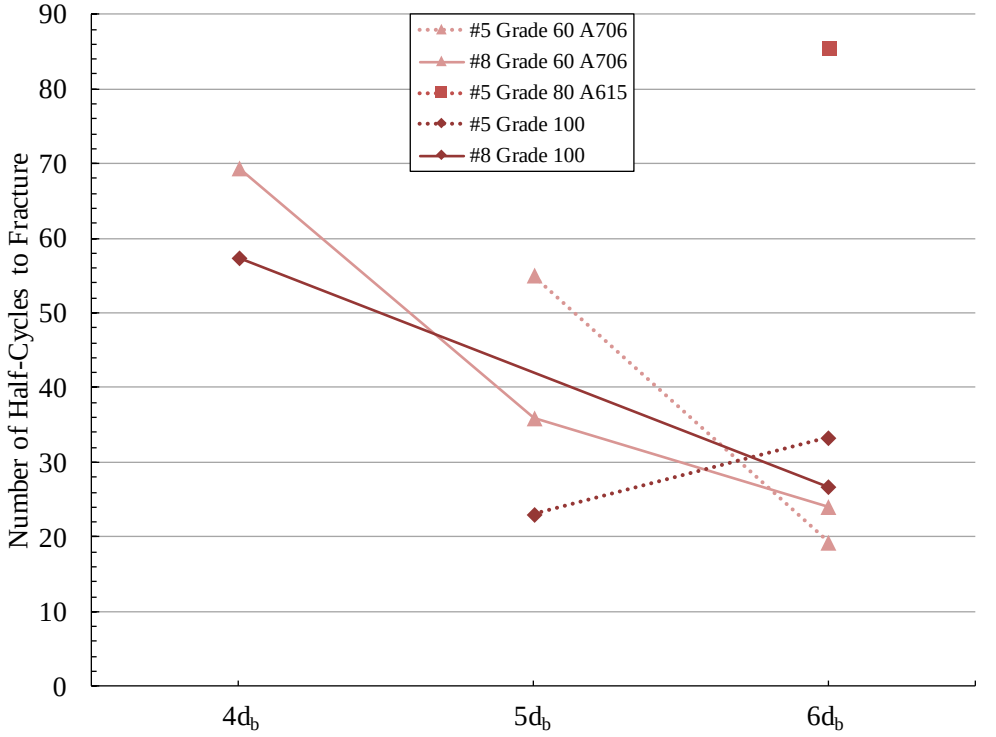

Figure 2-6: Effects of bar size and clear span on low-cycle fatigue life for #5 and #8 bars produced by manufacturer 2 and tested with a total strain range of 4% (from Slavin and Ghannoum, 2015)

4. Loading Protocol

The authors of the previous study were able to demonstrate that with an increase in higher total strain ranges, a decrease in the number of half-cycles to failure occurred. The loading protocol of +4% to -1% (a 5% total strain range) exhibited on average only 51% of the fatigue life of bars tested with the loading protocol of +2% to -2% (a total strain range of 4%). Figure 2-7 and Figure 2-8 illustrate this relationship for #8 bars.

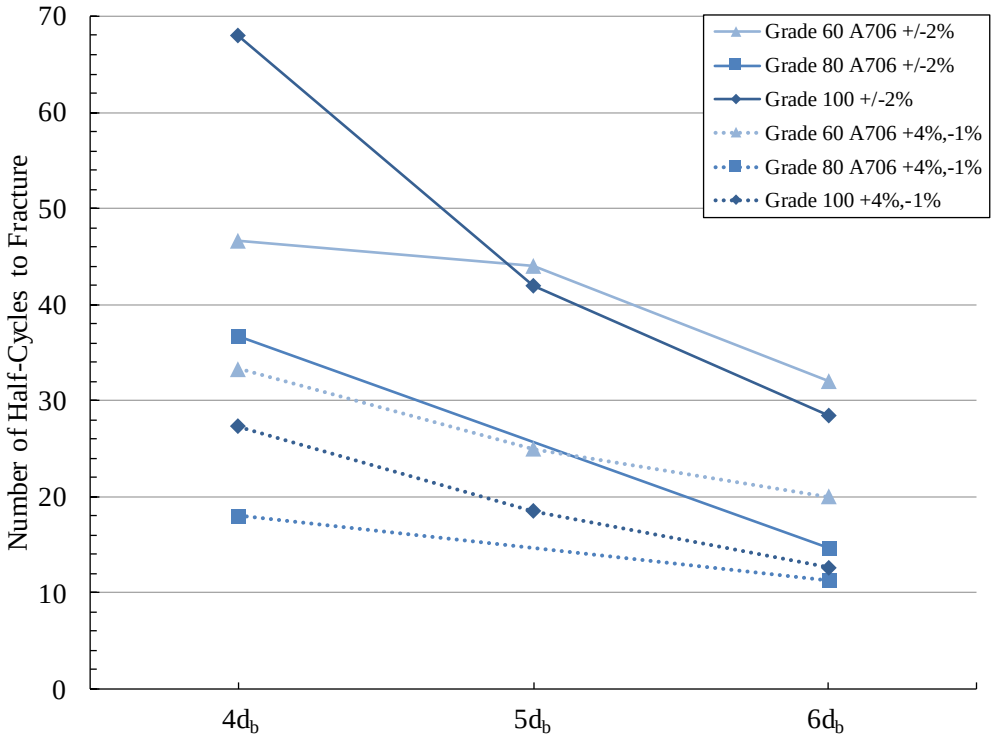

Figure 2-7: Relationship between loading protocol and low-cycle fatigue life for #8 bars produced by manufacturer 1 (from Slavin and Ghannoum, 2015)

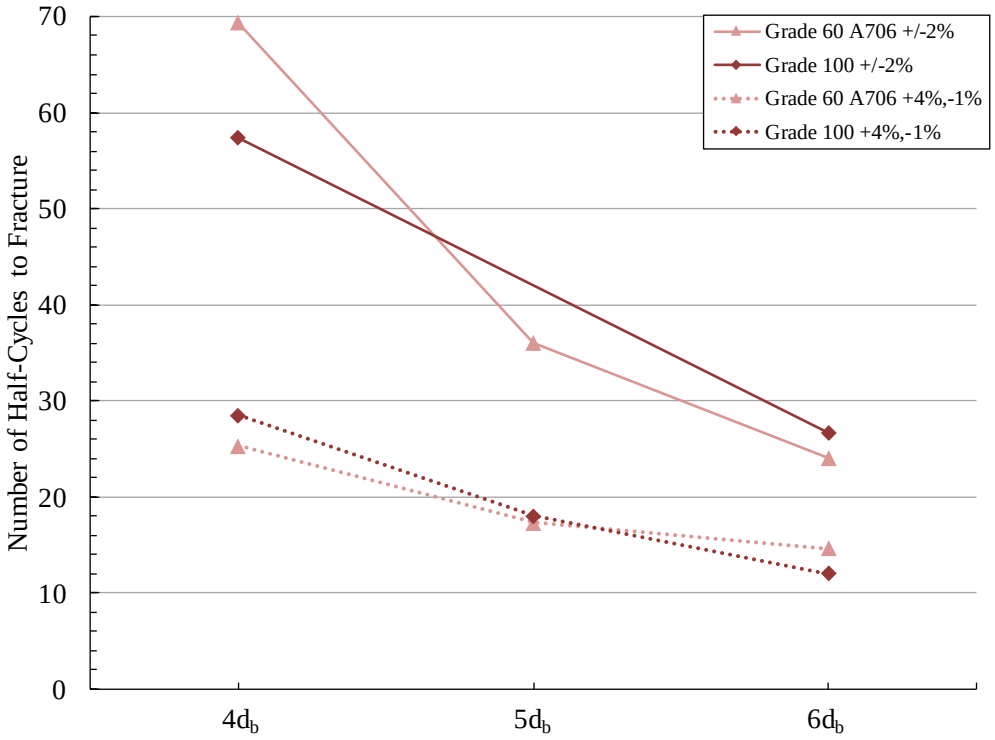

Figure 2-8: Relationship between loading protocol and low-cycle fatigue life for #8 bars produced by manufacturer 2 (from Slavin and Ghannoum, 2015)

5. Unbraced Length

The authors concluded, as the clear griping span or unbraced length increased, the specimens had a lower average fatigue life, despite all other parameters. The bars with the longer unbraced span experienced greater curvature due to larger buckling amplitudes and the associated higher local strain demands that reduced the fatigue life of bars.

Lastly, the authors proposed an equation for predicting the number of half-cycles to fracture as a function of total strain range cycled as seen below as Equation 2-1. Coefficients for the equations were derived from the low-cycle fatigue tests and are presented in Table 2-3. Figure 2-9 and Figure 2-10 show the curve fit for the equation and experimental results.

$$\text{Half-Cycles to Failure} = c*(\text{Total Strain Range})^{d}$$

Equation 2-1: Fatigue life modeling with fatigue life as the dependent variable

Manufacturer	Grade	Clear Span	c	d
1	60	$4d_b$	5.14E-03	-2.87
		$5d_b$	5.92E-03	-2.77
		$6d_b$	7.92E-03	-2.59
	80	$4d_b$	2.48E-03	-2.97
		$6d_b$	6.60E-03	-2.43
	100	$4d_b$	2.40E-05	-4.62
		$5d_b$	8.14E-05	-4.06
		$6d_b$	1.49E-04	-3.77
2	60	$4d_b$	3.59E-04	-3.75
		$5d_b$	8.49E-04	-3.31
		$6d_b$	1.49E-03	-3.03
	100	$4d_b$	1.90E-06	-5.42
		$5d_b$	2.60E-06	-5.25
		$6d_b$	1.65E-05	-4.46

Table 2-3: Summary of material coefficients for fatigue life equations for #8 bars (from Slavin and Ghannoum, 2015)

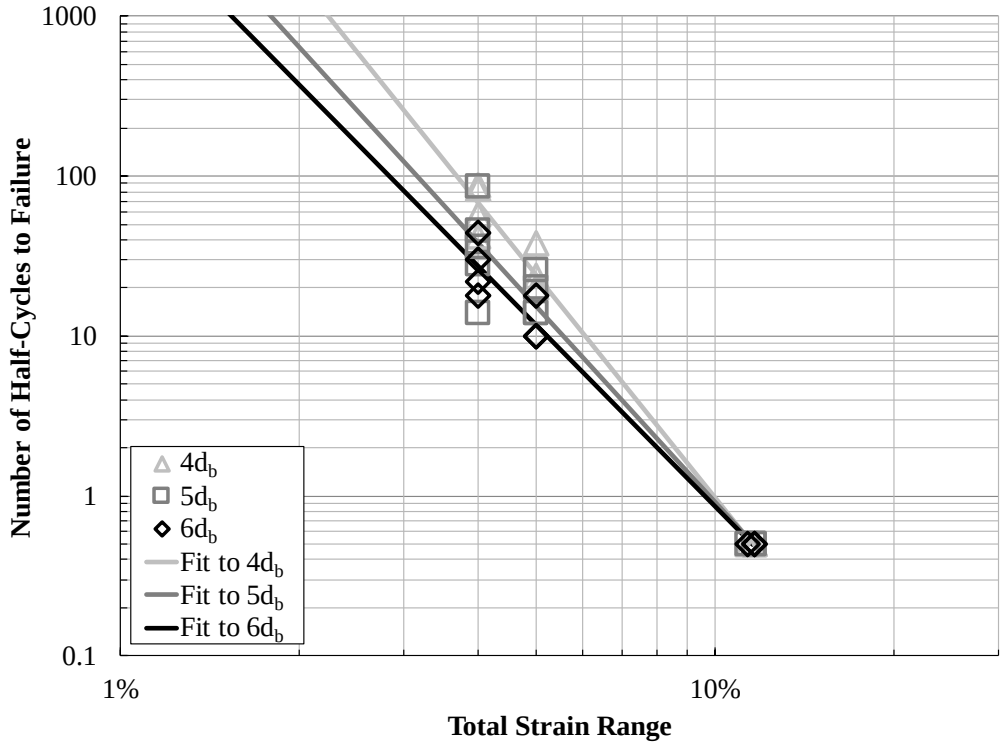

Figure 2-9: Relationship between half-cycles to failure and total strain range for grade 100 #8 bars produced by manufacturer 1 (from Slavin and Ghannoum, 2015)

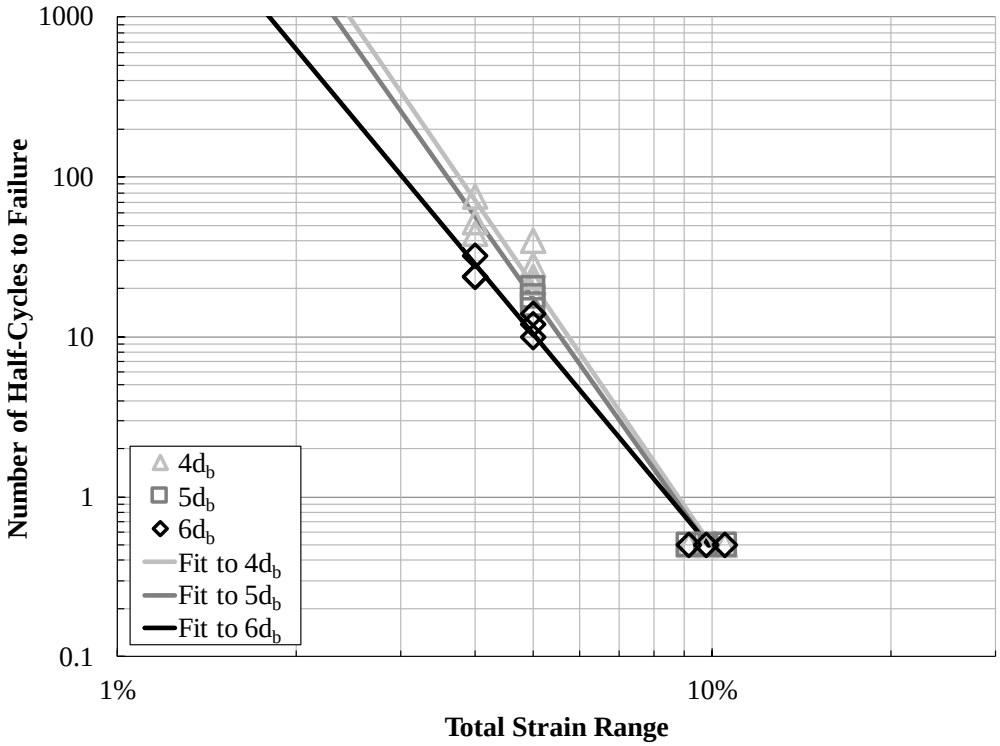

Figure 2-10: Relationship between half-cycles to failure and total strain range for grade 100 #8 bars produced by manufacturer 2 (from Slavin and Ghannoum, 2015)

3. EXPERIMENTAL PROGRAM

3.1 TEST MATRIX

As mentioned in the introduction, the study reported herein is part of a broader study aimed at quantifying the fatigue performance of regular and high-strength reinforcing bars representative of the current production methods in the United States. Parameters known to have a substantial impact on fatigue life were varied explicitly in the experimental program. These primary parameters were: manufacturer or manufacturing process, bar size, steel grade, unbraced or clear span, and strain protocol.

Low-cycle fatigue tests were conducted on bars from three different manufacturers that are representative of the current production methods in the United States. Manufacturer 1 produces high-strength reinforcing bars using a micro-alloying process, manufacturer 2 uses a quenching and tempering process with minimal micro-alloying, while manufacturer 3 produces high-strength reinforcing bars satisfying the ASTM A1035 specifications using a patent micro-structure manipulation process.

In a precursor study to this one, Ghannoum and Slavin (2016) tested bars from manufacturers 1 and 2. These manufacturers implemented adjustments to their production methods for high-strength reinforcing bars (HSRB) to identify practices that could improve the fatigue life of the bars. Manufacturers 1 and 2 delivered several batches with varying properties for testing in this study. Batch number designation was based in this study on the shipment in which the heat of bars arrived and may not be numbered sequentially. For example, the first delivery from manufacturer 1 contained only grade 80 #8 bars (batch 1), while the second delivery contained three different grades of #8 bars that were all identified as batch 2. This batch

numbering scheme was used to facilitate tracking of bar production history and adjustments. Bars tested by Ghannoum and Slavin (2016) are identified as batch 0.

Except for batch 2, manufacturer 1 (M1) grade 80 batches varied only in chemical composition, had similar deformation geometries, and were produced using the same processes and in the same mill. Notably, the chemical variations attempted by manufacturer 1 included modifying the source of the Vanadium used in the micro-alloying process, as well as adjusting the equivalent carbon content. M1 batch 2 bars were produced in a different mill owned by the manufacturer, but still using similar production processes. The main difference between batch 2 bars and other batch bars was the deformation geometry discussed in more detail in section 3.6.

In the batches of bars produced by manufacturer 2 (M2) and tested in this study as well as the batch 0 #5 grade 80 bars from the same manufacturer, the deformation base radius was softened in an attempt to improve fatigue performance of the bars.

Batch 1 of grade 100 #8 bars produced by manufacturer 3 (M3) came from an unrelated study on bending performance of HSRB (Zhao and Ghannoum, 2016) and was left outdoors for approximately two years before being tested in this study.

Focus was placed on two sizes of reinforcement representative of steel bars used in concrete frame construction. #5 bars were chosen to represent bars typically used as transverse reinforcement and #8 bars were chosen to represent longitudinal reinforcement. A concerted effort was made to replicate experiments from the study by Ghannoum and Slavin (2016) in both experimental design and specimen selection so that the results from the previous study could be compared against the results from the current study. Therefore the fatigue performance of the grade 60 bars from the previous study were mainly used to set benchmark fatigue performance for HSRB. Testing in this study focused mainly on bars of higher grade than grade 60,

particularly those bars that showed significantly lower fatigue performance compared with grade 60 benchmark values in the previous study. Grade 60 bars from manufacturer 2 were tested in this study, as that manufacturer adjusted its bar deformation geometries across all grades and so benchmark grade 60 values needed to be redefined for that manufacturer.

#5 bars were gripped at a single clear span of 6 times the nominal bar diameter ($6d_b$). Due to geometric constraints in the test machine, clear spans smaller than $6d_b$ were not possible for #5 bars. Three different clear gripping spans were used in testing of the #8 bars: $4d_b$, $6d_b$, and $8d_b$. As the severity of buckling in the bars is related to the clear span, the spans used in this study were selected to bracket expect buckling length of longitudinal bars in concrete members subjected to seismic loading. A $4d_b$ clear span resulted in minimal bar buckling, while the $6d_b$ and $8d_b$ clear spans resulted in significant buckling amplitudes and buckling lengths representative of those observed in seismically detailed frame members. Current code provisions in ACI 318-14 limit hoop spacing for seismically detailed frame members to $6d_b$.

Tests were conducted in strain control by cycling bars in a uniaxial testing machine to predefined strain peaks that remained constant in a given test. Strain protocols were selected to allow comparison with prior research (Brown and Kunnath, 2004, Ghannoum and Slavin, 2016) and to be representative of the high end of strain ranges experienced during a seismic event by longitudinal bars in concrete frame and wall members. The #5 bars were subjected to a single partially reversed strain protocol (Table 3-1). This partially reversed loading protocol with only tensile strains is representative of the strains experienced by transverse bars of flexural members in plastic hinge regions sustaining large inelastic deformations (Sokoli, 2014). For #8 bars, in addition to the two partially reversing strain protocols used in the preceding study (primary strain protocols), three additional protocols were added to better quantify the relationship between

strain amplitude and fatigue performance (secondary strain protocols, Table 3-2). In this study, a positive strain value is used to denote a tensile strain while a negative strain values is used to signify compressive strains.

Bar Size	Primary
#5	+4% to 0%

Table 3-1: Strain protocols for #5 bars

Bar Size	Primary		Secondary		
#8	+2% to -2%	+4% to -1%	+4% to 0%	+4% to -2%	+6% to 0%

Table 3-2: Strain protocols for #8 bars

3.2 SPECIMEN NOMENCLATURE

A nomenclature was used to distinguish the various bar types tested in this study. Typically, three or more bar specimens were tested per bar type and test parameters, to obtain a more robust estimate of mean fatigue life and the associated coefficient of variation values. The nomenclature selected, however, does not distinguish between individual bars of the same type and tested under the same parameters. Each type of bar is designated by the following nomenclature:

Manufacturer#-Batch#-Grade–Bar Size

Example **M1-B1-80-#8**

Additionally, to distinguish individual tests by clear gripping span, the following addition to the nomenclature are sometimes used:

Manufacturer#-Batch#-Grade–Bar Size-Clear Span

Example **M1-B1-80-#8-6d_b**

Table 3-3 and Table 3-4 provide a list of the different bar types tested in the previous and current study.

Mfr	Bar Size	Grade	Batch	ID
1	#5	60	0	M1-B0-60-#5
		80	0	M1-B0-80-#5
		100	0	M1-B0-100-#5
	#8	60	0	M1-B0-60-#8
		80	0	M1-B0-80-#8
		100	0	M1-B0-100-#8
2	#5	60	0	M2-B0-60-#5
		80	0	M2-B0-80-#5
		100	0	M2-B0-100-#5
	#8	60	0	M2-B0-60-#8
		100	0	M2-B0-100-#8

Table 3-3: Bar types tested by Ghannoum and Slavin (2016)

Mfr	Bar Size	Grade	Batch	ID
1	#5	80	1	M1-B1-80-#5
	#8	60	2	M1-B2-60-#8
		80	1	M1-B1-80-#8
			2	M1-B2-80-#8
			3	M1-B3-80-#8
			4	M1-B4-80-#8
			5	M1-B5-80-#8
		100	2	M1-B2-100-#8
2	#5	80	1	M2-B1-80-#5
			2	M2-B2-80-#5
		100	1	M2-B1-100-#5
	#8	60	3	M2-B3-60-#8
		80	1	M2-B1-80-#8
			3	M2-B3-80-#8
		100	1	M2-B1-100-#8
			3	M2-B3-100-#8
3	#5	100	1	M3-B1-100-#5
	#8	100	1	M3-B1-100-#8
			2	M3-B2-100-#8

Table 3-4: Bar types tested in this study

3.3 MONOTONIC TENSION TESTS

Monotonic tension tests were conducted in conformance with procedures specified in

ASTM A370 - Standard Methods and Definitions for Mechanical Testing of Steel Products and

ASTM E8 - Standard Test Methods for Tension Testing of Metallic Materials for each batch of bars tested. The force-strain response of each specimen was collected during the test. Force was obtained via the load cell on the testing machine and divided by the nominal bar area as specified in ACI 318-14 to calculate stress. Strains were measured over an 8 inch gage length via digital image correlation software discussed below in section 3.5.

From the stress-strain response, mechanical monotonic properties were derived including yield strength, tensile strength, elastic modulus, yield strain, uniform strain and fracture strain. As not all bars had a clear yield point, the modulus of elasticity was defined as the initial elastic slope of the stress-strain curve to approximately 50% of the specified yield strength. Yield stress was extracted using the 0.2% method as detailed in ASTM E8 with yield strain defined as the strain at which yield stress first occurs. The tensile or ultimate strength represents the maximum recorded stress during a test. Uniform strain was calculated in accordance with ASTM E8, as the average of the two strains corresponding to 99.5% of the tensile strength. Fracture strain is the last strain at which force was measured in the specimen. The ratio of tensile strength to yield strength (T/Y) as well as the ratio of fracture strain to uniform strain were also evaluated from monotonic test data. Lastly, the hardening strain was extracted as the strain at which the stress is reaches 1.01 times the yield stress, such that the difference between the hardening strain and yield strain reflects the strain length of the yield plateau.

3.4 LOW-CYCLE FATIGUE TESTS

All load-cycle fatigue tests were performed in a universal test machine with an axial capacity of 550 kips and two independent hydraulic gripping mechanisms. Each specimen was placed six inches into the gripping mechanisms to provide rotational fixity, simulating the boundary conditions that occur along longitudinal bars between transverse hoops. Both the top

and bottom end sections of a bar that were to be gripped in the machine were swaged with ASTM 6063 aluminum tubing. This was necessary not only to distribute more evenly the applied grip pressure on the specimens, but to prevent any stress concentrations from developing at the grip interface. The swaging increased the likelihood of fracture occurring away from the grips and in the clear span. Any tests in which failure occurred at or near the gripping mechanisms was deemed to be unsuccessful and removed from subsequent analysis. Specimens were orientated such that weak axis buckling would occur perpendicular to the field of view of the monochromatic camera used in data acquisition. Specimens were cycled until fracture occurred. A minimum of three successful tests per bar type and test parameters were conducted to quantify the variability in results. Figure 3-1 and Figure 3-2 show the experimental setup.

Figure 3-1: Front view of experimental setup showing test frame and DIC Camera

Figure 3-2: Side view of experimental setup showing test frame and DIC Camera

3.5 INSTRUMENTATION

The force applied to each of the bars was recorded from the load cell of the test machine. Due to the low strength of the aluminum swaging relative to the steel bars, the aluminum tubing experienced deformations during testing, which lead to discrepancies between actual bar deformations and the recordings of the actuator displacement. Therefore tests were conducted via strain control measured in real time from targets attached directly to the bar surface. Bar strains were obtained using a digital image correlation (DIC) system dubbed the Ghannoum Vision System (GVIS). The system is described in detail in (Sokoli et al. 2014). A series of high-resolution images were recorded at a rate of several frames per second by a single

monochromatic digital camera. A typical image obtained from the system can be seen in Figure 3-3.

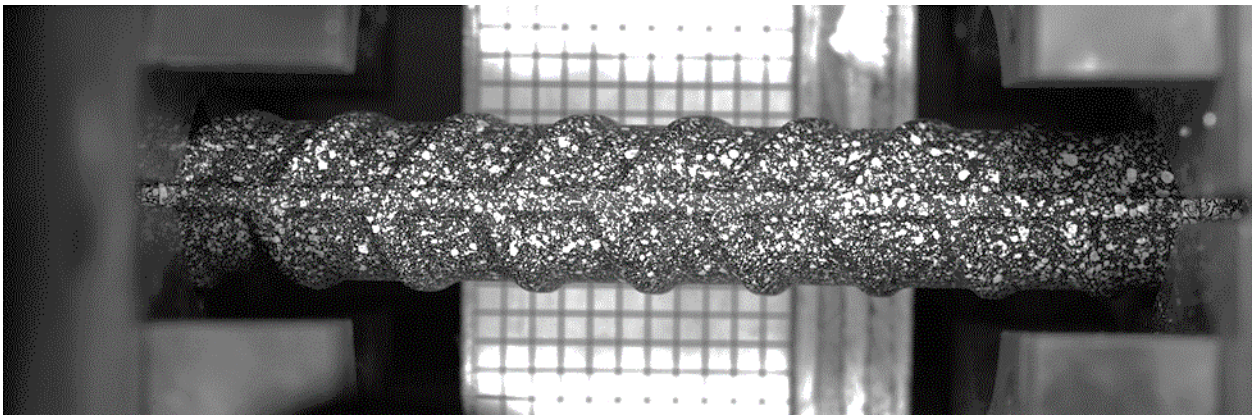

Figure 3-3: Typical image obtained from the GVIS system

The DIC software tracked the location of targets on the surface of the bars between subsequent frames. The GVIS system is able to provide strain resolutions on the order of 10^{-4} (Sokoli, et al. 2014). High-contrast surface targets were glued at each end of the bar specimens. For monotonic testing, three sets of targets were spaced eight inches apart in pairs to ensure that strains across the failure plane would be captured. For cyclic testing, two targets were placed as close to the grips as allowable, to avoid regions of bar curvature which were generated during buckling. Therefore, all strains recorded in cyclic tests occurred just inside of the clear span of the grips. Figure 3-4 shows a prepared specimen before it was tested.

Figure 3-4: Specimen preparation with targets and aluminum tubing attached

Using the strain delivered by the GVIS system, a closed loop control system was implemented that allowed for automating the test procedure through strain control. For cyclic testing, the average value between sets of targets on either end of the specimen was calculated in real time and sent as feedback to the load frame control software. This automation allowed for tests to run continually from beginning to end without requiring user input. The applied strain protocol was sinusoidal with respect to time. All tests were conducted so that tension strains were imposed first prior to reversing loading direction. For cyclic tests in which the mean of the strain range of the protocol was not zero, the bars were first ramped to the mean or the bounding strains, before the sinusoidal procedure began. The rate of cyclic testing was selected to be at an average strain rate of 0.00025 in/in/s across the sinusoidal loading protocol, which was in close agreement with the rate used by Ghannoum and Slavin (2016).

3.6 GEOMETRIC PROPERTIES OF DEFORMATIONS

Three geometric parameters of the transverse bar deformations were considered for correlation with the cyclic fatigue performance of reinforcing bars: the ratio of the smaller of the two radii at the base of the deformation (R_{min}) to the height of the deformation (H), the ratio of the larger of the two radii at the base of the deformation (R_{max}) to the height of the deformation, and the ratio of the height of the deformation to the nominal diameter of the bar (d_b). Three measurements were taken and the average is reported. The severity of curvature of the transverse ribs causes stress concentrations from which fracture can propagate. Measurements were taken using the same high resolution monochromatic camera used in the tests. Figure 3-5 shows an example image of bar deformations and overlaid measurements.

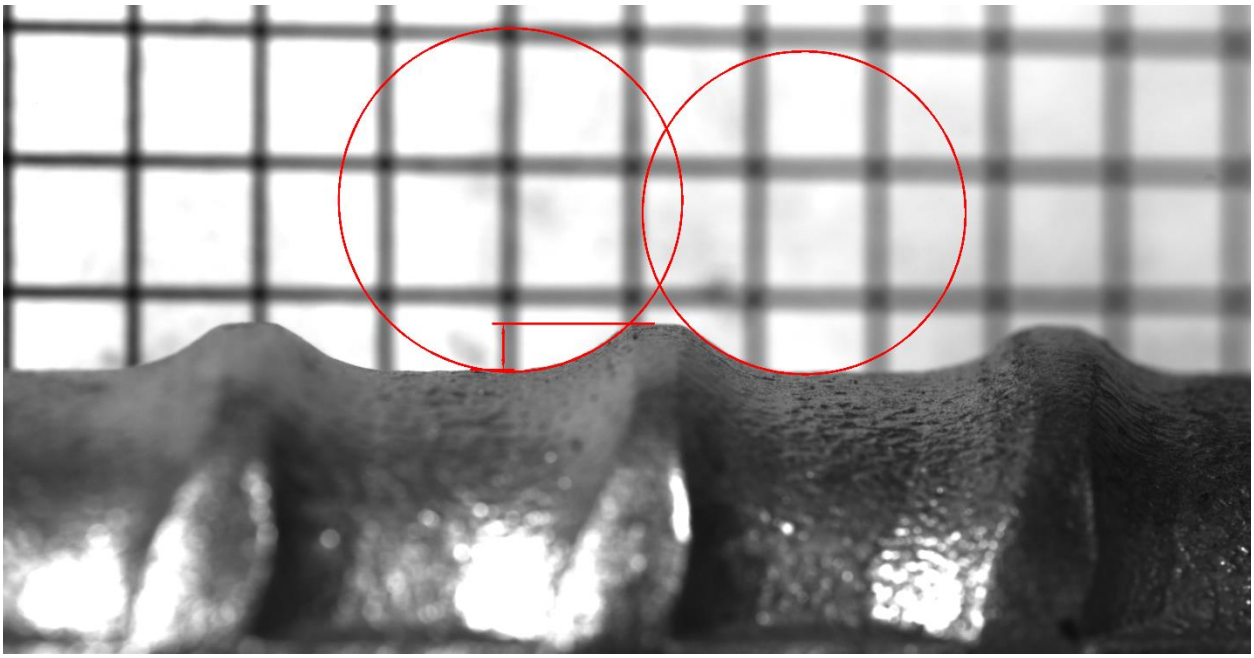

Figure 3-5: Example of geometric deformation measurements for M1-B4-80-#8

Table 3-5 presents all of the bar deformation measurements for manufacturer 1. Except for bars of batch 2, bars produced by manufacturer 1 and tested in this study did not deviate significantly in deformation properties from those tested by Ghannoum and Slavin (2016). While the different grades of M1 #8 bars from batch 0 had variations between their bar deformation properties, the bars from the current study had consistent bar deformations throughout all grades. The most significant differences were seen in the increased height of deformation to bar diameter ratio across #8 bars of this study compared to batch 0 #8 bars, and the decreased deformation radii in the grade 100 #8 bars of this study compared to other bars.

ID	R_{min}/H	R_{max}/H	H/d_b
M1-B0-60-#5	2.55	3.00	0.0618
M1-B0-80-#5	1.27	2.18	0.0813
M1-B0-100-#5	1.32	1.72	0.0707
M1-B1-80-#5	1.64	2.02	0.0751
M1-B0-60-#8	2.72	2.97	0.0617
M1-B0-80-#8	3.54	3.81	0.0756
M1-B0-100-#8	3.22	4.94	0.0632
M1-B2-60-#8	1.34	2.95	0.0750
M1-B1-80-#8	2.89	3.61	0.0681
M1-B2-80-#8	2.47	2.58	0.0696
M1-B3-80-#8	2.49	2.98	0.0624
M1-B4-80-#8	3.41	3.68	0.0719
M1-B5-80-#8	2.77	3.65	0.0677
M1-B2-100-#8	1.54	1.93	0.0812

Table 3-5: Bar deformation geometry for bars produced by manufacturer 1

Batch 2 of the #8 bars produced by manufacturer 1 had surface geometry that differed significantly from any other bars. These bars were produced by a different mill than the other batches from that manufacturer. The grade 60 and grade 80 bars from M1-B2 had a single secondary longitudinal rib running along one of the longitudinal primary ribs, as can be seen in Figure 3-6 and Figure 3-7. The grade 100 bars had two additional smaller longitudinal ribs on the same side of one of the primary longitudinal ribs. Figure 3-8 shows a front facing view of a grade 100 bar from batch 2 containing the secondary longitudinal ribs, and Figure 3-9 provides a view of the side of the same bar. The side opposite to the one seen in Figure 3-9 does not contain any additional longitudinal rib. This asymmetric cross sectional geometry is important to note as it played an important role in determining the axis of buckling during cyclic testing.

Figure 3-6: Front view of longitudinal geometry for M1-B2-60-#8

Figure 3-7: Front view of longitudinal geometry for M1-B2-80-#8

Figure 3-8: Front view of longitudinal geometry for M1-B2-100-#8

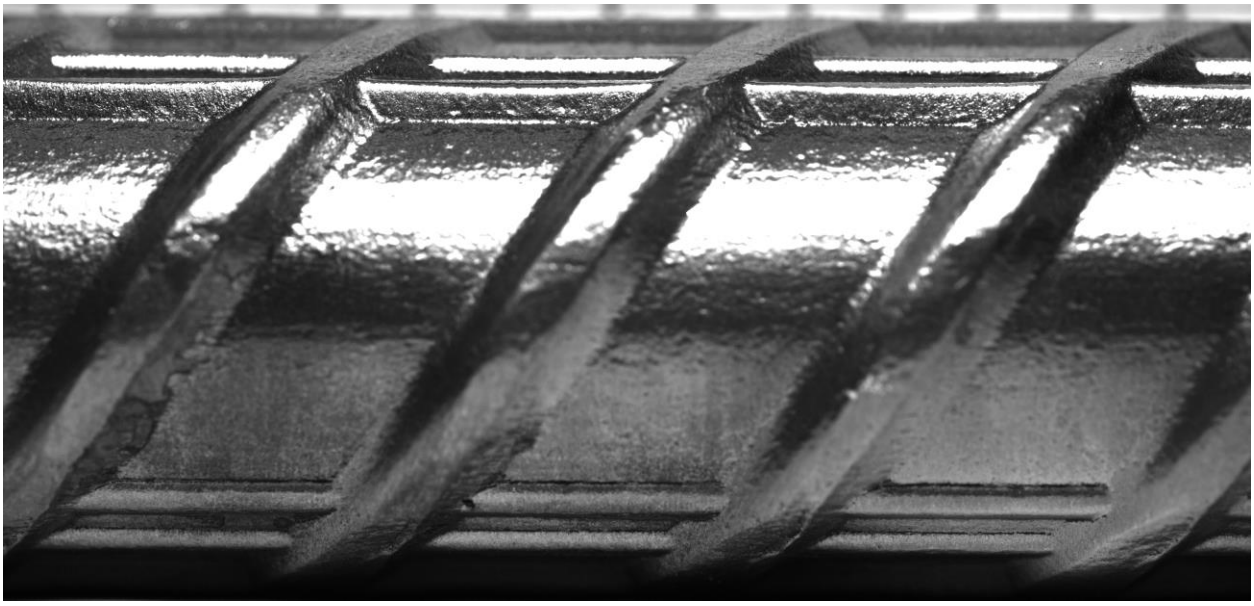

Figure 3-9: Side view of longitudinal geometry for M1-B2-100-#8

Table 3-6 tabulates the geometric properties of deformation for bars produced by manufacturer 2. As intended by manufacturer 2, bars tested in this study as well as the #5 grade 80 bars from the previous study showed significantly larger deformation radii than those of bars tested in the previous study. This can be seen most prevalently in the ratio of R_{max} to height of

the deformation. It is noted that the adjustments in deformation properties of bars produced by M2 brought them nearer to those of bars produced by M1.

ID	R_{min}/H	R_{max}/H	H/d_b
M2-B0-60-#5	1.13	2.06	0.0639
M2-B0-80-#5	3.01	3.52	0.0755
M2-B0-100-#5	0.43	0.69	0.0735
M2-B1-80-#5	3.79	4.33	0.0709
M2-B2-80-#5	2.27	2.46	0.0751
M2-B1-100-#5	1.91	6.47	0.0661
M2-B0-60-#8	1.30	2.59	0.0611
M2-B0-100-#8	0.63	0.86	0.0753
M2-B3-60-#8	1.98	2.78	0.0655
M2-B1-80-#8	1.86	2.87	0.0839
M2-B3-80-#8	2.07	3.72	0.0882
M2-B1-100-#8	2.96	3.25	0.0857
M2-B3-100-#8	2.15	3.46	0.0778

Table 3-6: Bar deformation geometry for bars produced by manufacturer 2

Table 3-7 presents the deformation geometry measurements for bars produced by manufacturer 3. Both batches of #8 bars from manufacturer 3 showed comparable deformation properties to those of bars from the other manufacturers. However, the #5 bars had a significantly higher ratio of deformation radii to height, representing a much softer curvature. In addition, some of the #5 bars from manufacturer 3 had a relatively low height of bar deformation and relatively faint longitudinal rib. Both of these geometric properties can be seen in Figure 3-10.

ID	R_{min}/H	R_{max}/H	H/d_b
M3-B1-100-#5	8.32	9.37	0.0510
M3-B1-100-#8	1.68	2.44	0.0778
M3-B2-100-#8	1.54	4.87	0.0592

Table 3-7: Bar deformation geometry for bars produced by manufacturer 3

Figure 3-10: Deformation geometry for M3-B1-100-#5

4. TEST RESULTS AND GENERAL OBSERVATIONS

4.1 MONOTONIC TENSION TESTS

Three monotonic tension tests were conducted in accordance with ASTM A370 for each bar type in the batch. The average mechanical properties of three specimens per bar type are summarized in Table 4-1, Table 4-2, Table 4-3. The methods for calculating the values presented in the tables are discussed in section 3.3 In the tables below, hardening strain is defined as the strain at which the stress first reaches 1% above yield. Figure 4-1 through Figure 4-19 show the stress-strain relationship for each batch of bars tested in this study with the different colors denoting each specimen tested and the dashed red line denoting the 0.2% offset used to calculate yield strength.

Bar Size	Grade	Batch	Yield Strength (ksi)	Tensile Strength (ksi)	T/Y Ratio	Elastic Modulus (ksi)	Yield Strain	Hardening Strain	Yield Plateau Length	Uniform Strain	Fracture Strain	Fracture Strain / Uniform Strain
#5	80	1	87.73	117.84	1.34	26,200	0.34%	0.61%	0.27%	8.65%	11.79%	1.36
#8	60	2	64.01	89.16	1.39	27,800	0.24%	1.40%	1.17%	12.96%	20.85%	1.61
	80	1	83.89	114.61	1.37	27,500	0.31%	0.59%	0.29%	9.35%	15.11%	1.62
		2	81.50	109.28	1.34	28,000	0.29%	0.84%	0.55%	10.62%	16.03%	1.51
		3	81.39	117.40	1.44	29,100	0.28%	0.54%	0.26%	9.13%	13.84%	1.52
		4	84.05	113.68	1.35	29,100	0.30%	0.62%	0.32%	9.80%	16.14%	1.65
		5	87.66	113.47	1.29	28,800	0.31%	0.61%	0.30%	9.33%	14.68%	1.57
	100	2	109.44	138.72	1.27	27,900	0.40%	0.68%	0.28%	9.07%	12.47%	1.37

Table 4-1: Summary of material properties calculated from monotonic tension tests for manufacturer 1

Bar Size	Grade	Batch	Yield Strength (ksi)	Tensile Strength (ksi)	T/Y Ratio	Elastic Modulus (ksi)	Yield Strain	Hardening Strain	Yield Plateau Length	Uniform Strain	Fracture Strain	Fracture Strain / Uniform Strain
#5	80	1	84.67	109.05	1.29	26,000	0.33%	1.48%	1.15%	9.65%	14.26%	1.48
		2	84.55	103.16	1.22	23,900	0.35%	1.49%	1.13%	9.16%	14.11%	1.54
	100	1	102.73	121.79	1.19	26,200	0.39%	0.80%	0.41%	7.11%	10.75%	1.51
#8	60	3	70.37	94.78	1.35	27,400	0.27%	1.31%	1.04%	11.97%	18.51%	1.55
	80	1	88.31	106.23	1.20	27,300	0.33%	1.26%	0.93%	8.75%	13.98%	1.60
		3	99.86	118.71	1.19	29,000	0.35%	0.72%	0.37%	6.50%	10.17%	1.56
	100	1	103.16	120.44	1.17	28,200	0.37%	0.72%	0.35%	6.46%	11.33%	1.75
		3	102.06	121.79	1.19	27,600	0.37%	1.08%	0.71%	8.32%	13.22%	1.59

Table 4-2: Summary of material properties calculated from monotonic tension tests for manufacturer 2

Bar Size	Grade	Batch	Yield Strength (ksi)	Tensile Strength (ksi)	T/Y Ratio	Elastic Modulus (ksi)	Yield Strain	Hardening Strain	Yield Plateau Length	Uniform Strain	Fracture Strain	Fracture Strain / Uniform Strain
#5	100	1	121.34	162.06	1.34	27,700	0.45%	0.66%	0.21%	5.02%	9.30%	1.85
#8	100	1	122.36	164.20	1.34	29,000	0.43%	0.64%	0.21%	5.29%	11.38%	2.15
		2	116.97	159.77	1.37	28,400	0.42%	0.63%	0.22%	5.48%	12.11%	2.21

Table 4-3: Summary of material properties calculated from monotonic tension tests for manufacturer 3

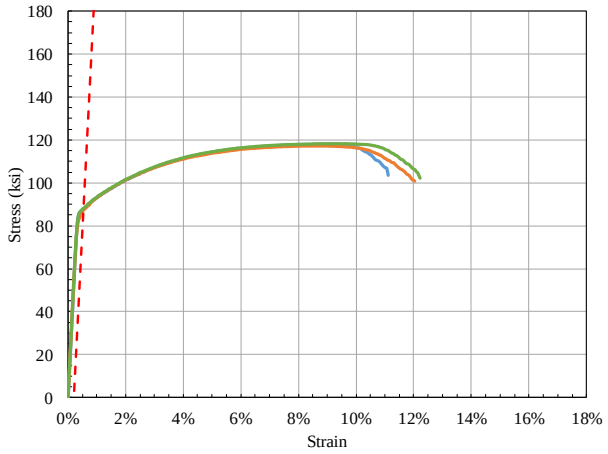

Figure 4-1: Stress-strain curves from monotonic tension tests of from M1-B1-80-#5

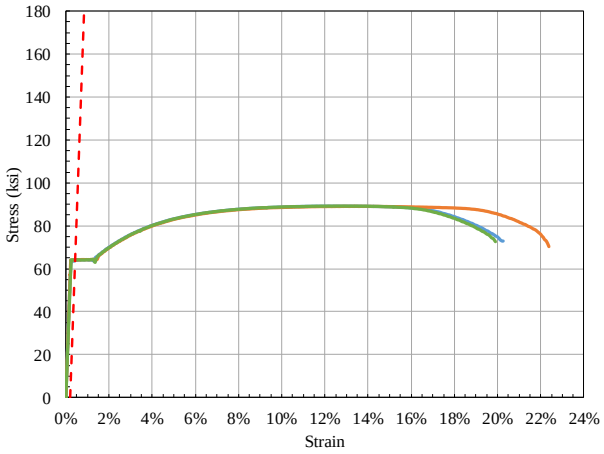

Figure 4-2: Stress-strain curves from monotonic tension tests of from M1-B2-60-#8

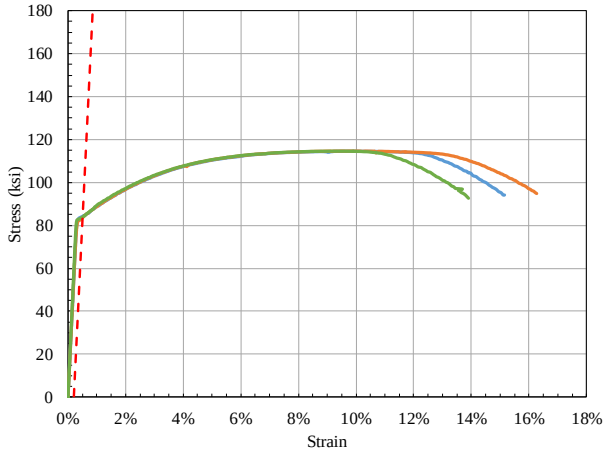

Figure 4-3: Stress-strain curves from monotonic tension tests of from M1-B1-80-#8

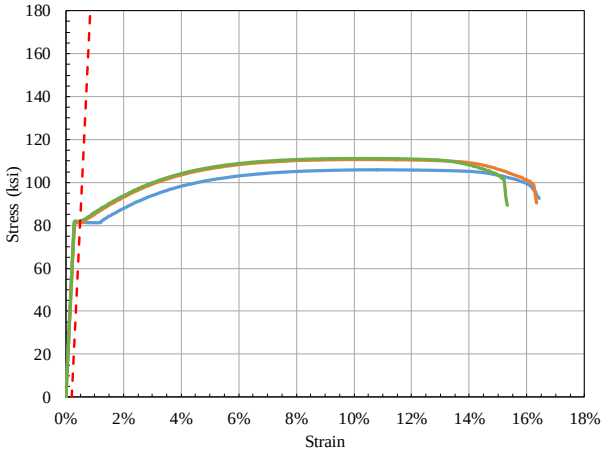

Figure 4-4: Stress-strain curves from monotonic tension tests of from M1-B2-80-#8

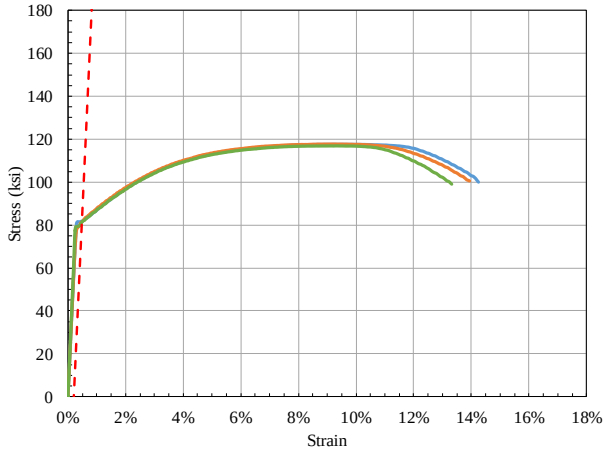

Figure 4-5: Stress-strain curves from monotonic tension tests of from M1-B3-80-#8

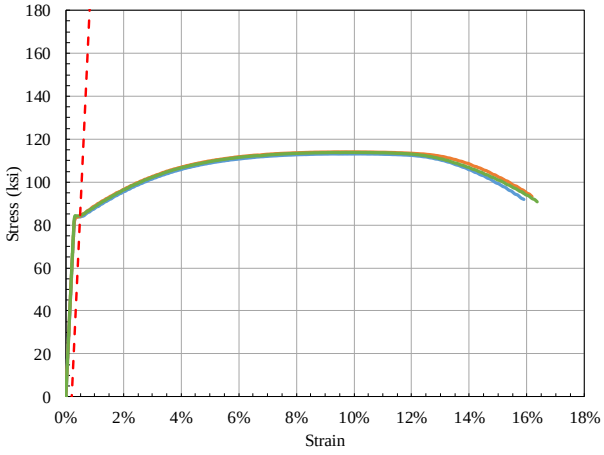

Figure 4-6: Stress-strain curves from monotonic tension tests of from M1-B4-80-#8

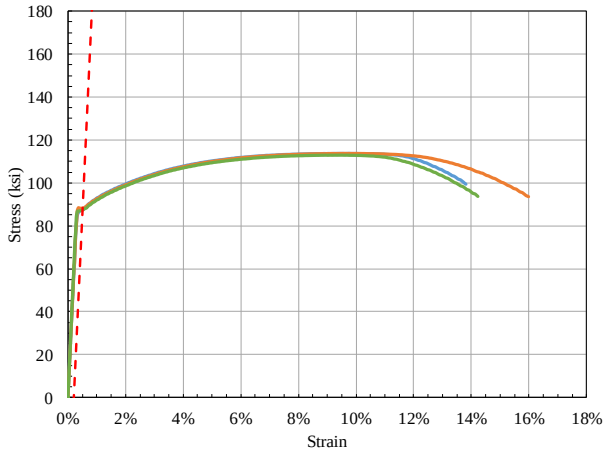

Figure 4-7: Stress-strain curves from monotonic tension tests of from M1-B5-80-#8

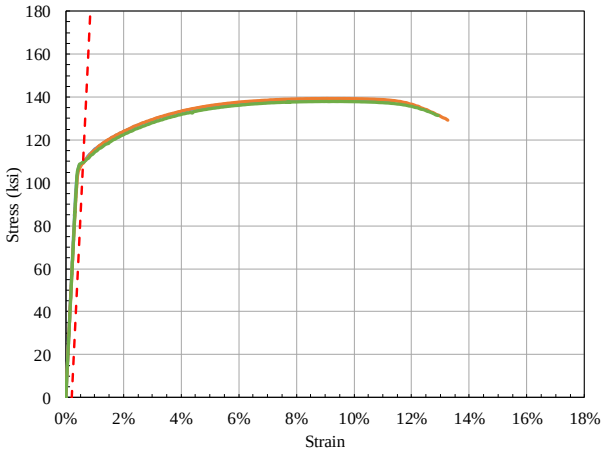

Figure 4-8: Stress-strain curves from monotonic tension tests of from M1-B2-100-#8

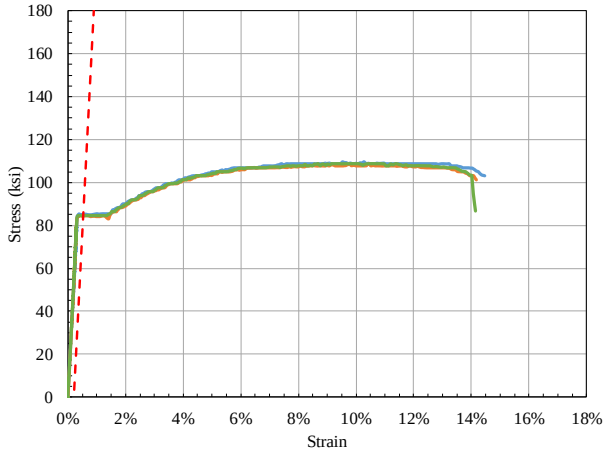

Figure 4-9: Stress-strain curves from monotonic tension tests of from M2-B1-80-#5

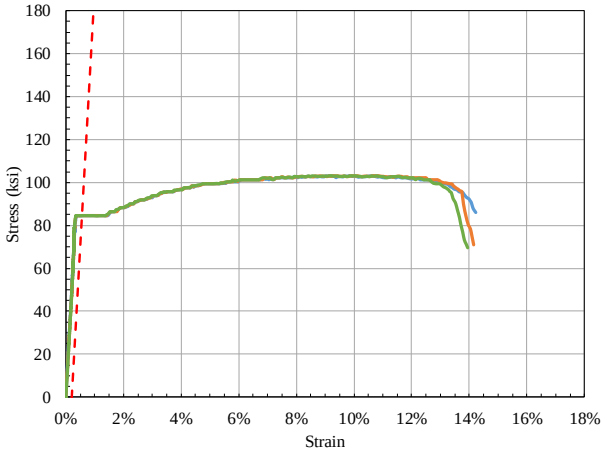

Figure 4-10: Stress-strain curves from monotonic tension tests of from M2-B2-80-#5

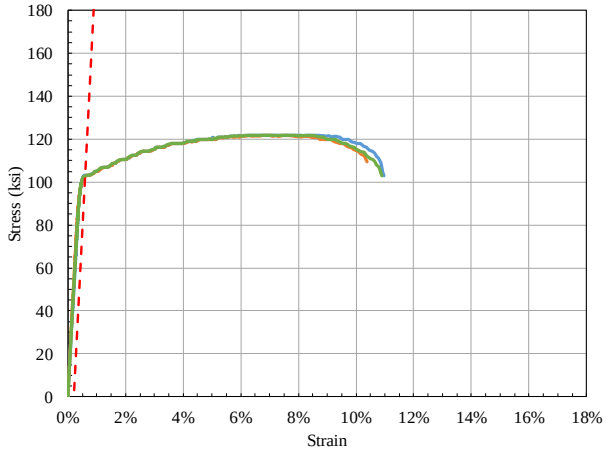

Figure 4-11: Stress-strain curves from monotonic tension tests of from M2-B1-100-#5

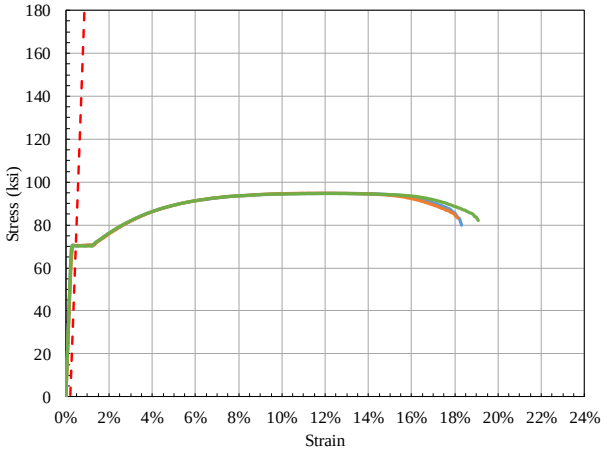

Figure 4-12: Stress-strain curves from monotonic tension tests of from M2-B3-60-#8

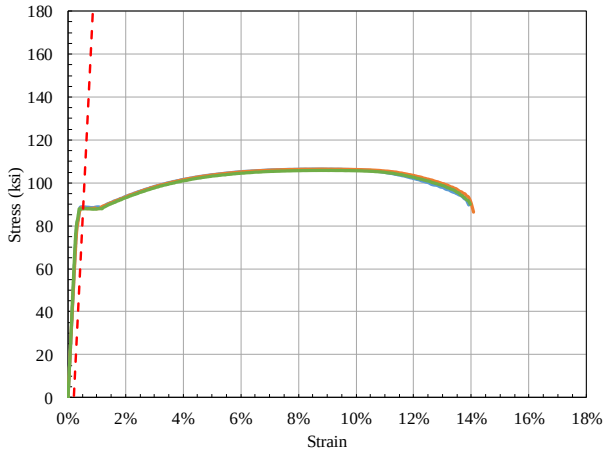

Figure 4-13: Stress-strain curves from monotonic tension tests of from M2-B1-80-#8

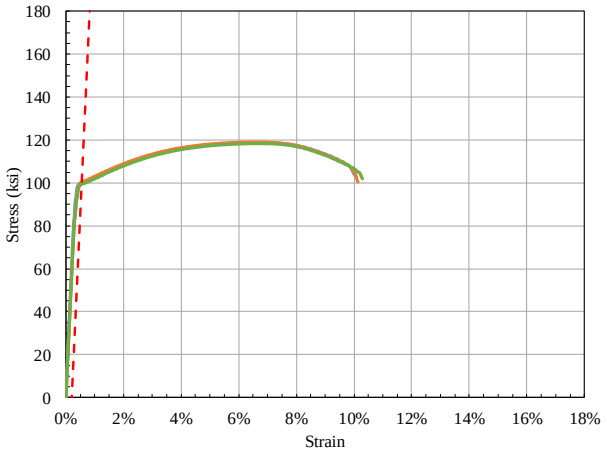

Figure 4-14: Stress-strain curves from monotonic tension tests of from M2-B3-80-#8

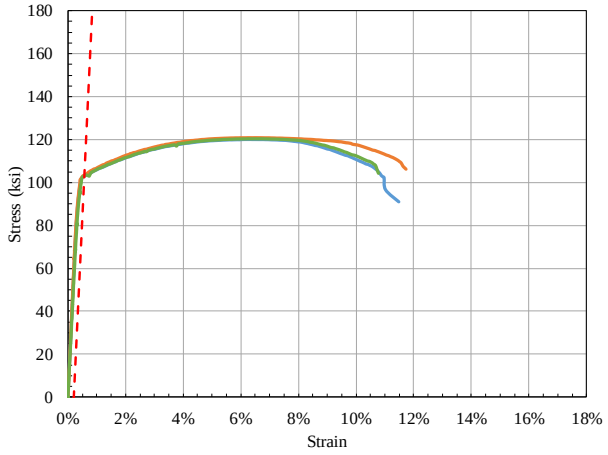

Figure 4-15: Stress-strain curves from monotonic tension tests of from M2-B1-100-#8

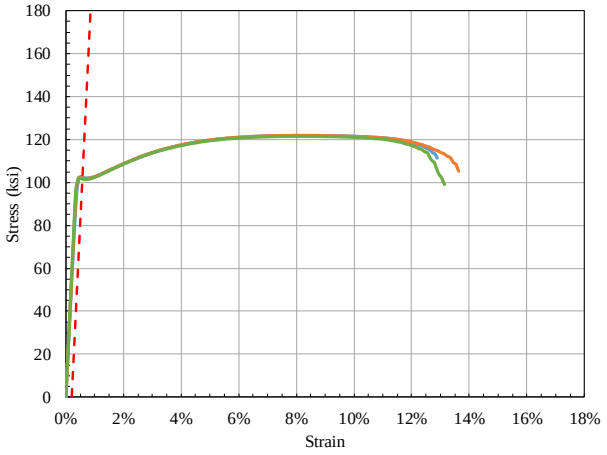

Figure 4-16: Stress-strain curves from monotonic tension tests of from M2-B3-100-#8

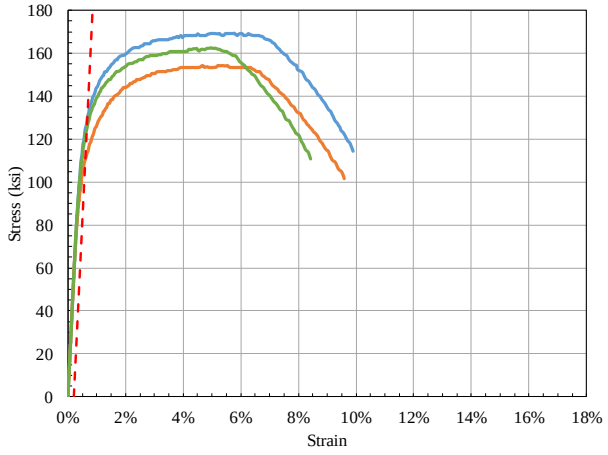

Figure 4-17: Stress-strain curves from monotonic tension tests of from M3-B1-100-#5

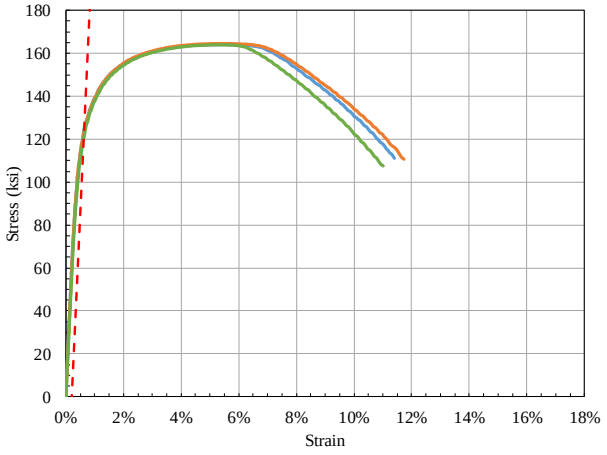

Figure 4-18: Stress-strain curves from monotonic tension tests of from M3-B1-100-#8

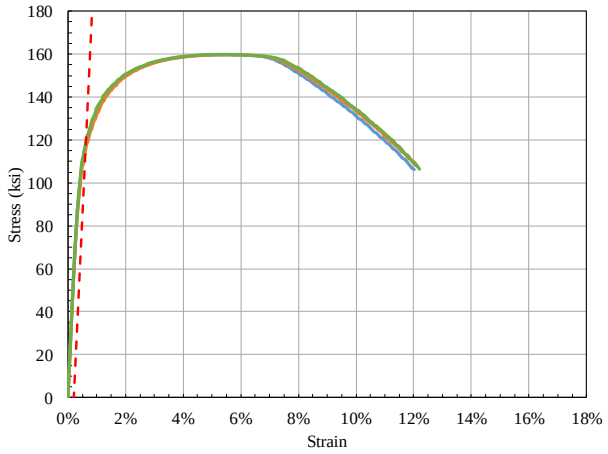

Figure 4-19: Stress-strain curves from monotonic tension tests of from M3-B2-100-#8

4.1.1 Observations from Monotonic Tests of Manufacturer 1 Bars

In general, manufacturer 1 bars exhibited only minor variability in stress-strain relations between specimens of the same batch, size, and grade. Batch 2 grade 60 #8 bars by manufacturer 1 (M1) demonstrated little variability between specimens prior to reaching uniform strain, but deviated from one another beyond that strain. The grade 80 #5 bars produced by manufacturer 1 exhibited a relatively long yield plateau, along with a uniform strain that is closer to the fracture strain than the yield strain, which corresponded with a smaller loss of strength before fracture. All five batches of grade 80 #8 bars from M1 tested in this study exhibited comparable monotonic properties, with a relatively short yield plateau and T/Y ratios that are approximately equivalent, with the exception of a single specimen from batch 2. Any variability between specimens of each batch occurred after uniform strain. The grade 100 #8 bars from batch 2 exhibited almost no deviation in stress-strain relations between specimens, even past the uniform strain.

4.1.2 Observations from Monotonic Tests of Manufacturer 2 Bars

The grade 60 #8 bars from manufacturer 2 (M2) showed little variation between specimens and had a yield strength that is approximately 10ksi higher than the specified 60ksi minimum. Both batches of grade 80 #5 bars from manufacturer 2 produced monotonic properties that are nearly equivalent with the exception of the elastic moduli and T/Y ratios. Batch 1 grade 80 #5 bars had higher elastic moduli and T/Y ratios than batch 2 grade 80 #5 bars. Batches 1 and 2 of the grade 80 #5 bars displayed a distinguished yield plateau with a length that is typical of grade 60 reinforcement. Batches 1 and 3 of the grade 80 #8 bars had significant differences in mechanical properties and stress-strain relations. Batch 3 grade 80 #8 bars had yield strengths close to 100ksi and lower uniform and fracture elongations when compared to batch 1 bars. Batch 1 bars had a distinguished yield plateau that is similar to that found in the grade 60 bars from batch 3, while batch 3 grade 80 #8 bars exhibited a distinct yielding point with little to no yield plateau. Batch 1 grade 100 #5 bars from M2 had lower T/Y ratios and ductilities when compared to grade 80 bars. In addition, the grade 100 bars from M2 had a smaller yield plateau than bars of other grades. Batch 1 and batch 3 of the grade 100 #8 bars had nearly equivalent stress-strain properties, with the largest difference being in the length of the yield plateau.

4.1.3 Observations from Monotonic Tests of Manufacturer 3 Bars

The grade 100 bars produced by manufacturer 3 (M3) satisfied the ASTM A1035 specifications and lacked a clear yield point. The bars exhibited significantly higher yield and tensile strengths than other grade 100 bars tested in this study. The ratio of tensile strength to yield strength of these bars was, however comparable to those of other grade 100 bars tested in this study. All bar sizes lost significant strength prior to fracture, up to 60ksi, after reaching

uniform elongation, which corresponded with a relatively high ratio of fracture to uniform elongation and a significant reduction in cross sectional area or necking prior to fracture. The #5 bars from M3 exhibited significant variability between specimens of the same batch at all stages of the monotonic test; with yield strengths differing by 20ksi between specimens and tensile strength varying by 15ksi.

4.1.4 Comparison of Mechanical Properties to Previous Study

The percent differences between each mechanical property of batch 0 bars tested by Ghannoum and Slavin (2016) and the batches tested in this study that are presented in Table 4-4 and Table 4-5 were calculated as follows:

$$\text{Percent Difference} = \frac{\text{Current Study Value - Previous Study Value}}{\text{Previous Study Value}}$$

Equation 4-1: Percent difference formula for monotonic properties

4.1.4.1 Manufacturer 1

The largest different between batches of grade 60 #8 bars was seen in the uniform and fracture strains. However, both batches 0 and 2 grade 60 #8 bars maintained a nearly identical ratio of fracture to uniform strain.

The M1 grade 80 #5 bars from the current study had slightly different but comparable mechanical properties than those from the previous study. Batch 1 showed increases in both yield strength and tensile strength and associated decreases in uniform and fracture elongation compared with batch 0 grade 80 #5 bars. There is a considerable difference in the shape of the stress-strain curves of batch 0 and batch 1 grade 80 #5 bars, with batch 0 bars showing a clear yield plateau before strain hardening and batch 1 lacking a definitive yield plateau.

All five batches of M1 grade 80 #8 bars tested in this study exhibited mechanical properties that are comparable to batch 0 equivalent bars, with the most significant differences

seen in the uniform and fracture strains. All grade 80 #8 bars of this study exhibited a decrease in uniform and fracture strain compared with batch 0 equivalent bars, with the exception of batch 2 bars that had higher uniform strains on average.

Bar Size	Grade	Batch	Yield Strength	Tensile Strength	T/Y Ratio	Elastic Modulus	Uniform Strain	Fracture Strain	Fracture Strain / Uniform Strain
#5	80	1	5.3%	10.0%	4.9%	-2.6%	-3.8%	-13.9%	-10.5%
#8	60	2	1.3%	-4.8%	-5.9%	3.3%	11.7%	10.9%	-0.8%
	80	1	4.5%	4.2%	-0.3%	0.4%	-6.5%	-9.5%	-3.2%
		2	1.5%	-0.7%	-2.1%	2.2%	6.2%	-4.0%	-9.6%
		3	1.4%	6.7%	5.3%	6.2%	-8.7%	-17.2%	-9.2%
		4	4.7%	3.3%	-1.3%	6.2%	-2.0%	-3.3%	-1.3%
		5	9.2%	3.2%	-5.5%	5.1%	-6.7%	-12.1%	-5.8%
	100	2	7.8%	8.0%	-0.2%	-7.3%	12.0%	7.5%	-4.1%

Table 4-4: Percent difference in mechanical properties from monotonic tension tests between batches of this study and batch 0 equivalent bars for manufacturer 1

4.1.4.2 Manufacturer 2

The grade 60 bars from the current study exhibited significantly different mechanical properties than those from batch 0 grade 60 bars. The bars from the current study showed an increase of approximately 14% in yield strength, but a decrease of 20% in T/Y ratio. Both the uniform and fracture strains increased by over 25% from batch 0 to batch 1 grade 60 bars, but maintained a similar ratio of fracture to uniform strain.

All of the mechanical properties of batch 1 M2 grade 80 #5 bars were within 5% of the properties of batch 0 equivalent bars, as was the majority of the mechanical properties from batch 2 grade 80 #5 bars.

Compared with batch 0 grade 100 #5 bars, batch 1 equivalent bars showed slightly lower mechanical properties with the exception of an increase in the ratio of fracture to uniform strain. The properties of both batches of grade 100 #8 bars were approximately equal to those of equivalent batch 0 bars, and both showed a decrease in the elastic modulus of over 10%. Batch 1

grade 100 #8 bars showed a slightly higher uniform strain, a significantly higher fracture strain, and therefore an 11% increase in the ratio between the two strains. Batch 3 grade 100 #8 bars showed a significant, but equivalent increase in both uniform and fracture strains compared with equivalent batch 0 bars.

Bar Size	Grade	Batch	Yield Strength	Tensile Strength	T/Y Ratio	Elastic Modulus	Uniform Strain	Fracture Strain	Fracture Strain / Uniform Strain
#5	80	1	1.3%	3.9%	2.2%	-3.3%	-0.5%	2.6%	3.2%
		2	1.1%	-1.8%	-3.2%	-11.2%	-5.5%	1.5%	7.5%
	100	1	-3.8%	-4.6%	-1.2%	-6.8%	-6.5%	-0.5%	6.4%
#8	60	3	14.4%	-8.1%	-19.8%	6.2%	26.0%	27.6%	1.3%
	80	1	-	-	-	-	-	-	-
		3	-	-	-	-	-	-	-
	100	1	-1.4%	-2.7%	-1.1%	-10.2%	4.2%	15.6%	11.0%
		3	-2.4%	-1.6%	1.1%	-12.1%	34.2%	34.9%	0.6%

Table 4-5: Percent difference in mechanical properties from monotonic tension tests between batches of this study and batch 0 equivalent bars for manufacturer 2

4.2 LOW-CYCLE FATIGUE TESTS

4.2.1 General Behavior

A total of 227 fatigue tests were conducted in this study. All tests started by pulling a bar coupon to its peak target tension strain before reversing loading direction to the opposite target peak strain. A positive strain reported in this study implies a tensile strain measured from face to face of clear gripping span. A negative strain indicates a compressive strain. Bars were loaded cyclically using strain control and experienced varying levels of strength degradation during the cycles. Buckling and cracking of the bars contributed mainly to cyclic strength degradation. Cyclic strength degradation varied considerably with clear gripping span and between manufacturers.

Typically, bars gripped at longer clear spans and sustaining greater lateral buckling amplitudes experienced more pronounced cyclic strength degradation than the equivalent bars

tested at a tighter clear span. Figure 4-20, Figure 4-24, and Figure 4-29 overlay the stress-strain response for different clear spans for each manufacturer. Figure 4-21, Figure 4-25, Figure 4-30 plot the progression of tension and compression peak stresses per cycle normalized by the first cycle peak tensile stress. It can be seen in these figures that as clear gripping span increases, the compressive capacity of the bar decreases.

At a gripping span of $4d_b$, limited bar buckling was typically observed, while at $6d_b$ and $8d_b$ clear spans, significant buckling could be observed for all grades and manufacturers. Figure 4-22, Figure 4-23, Figure 4-26, Figure 4-27, Figure 4-28, Figure 4-31, Figure 4-32 contrast the buckling amplitude at the final compression cycle for different clear spans for each manufacturer.

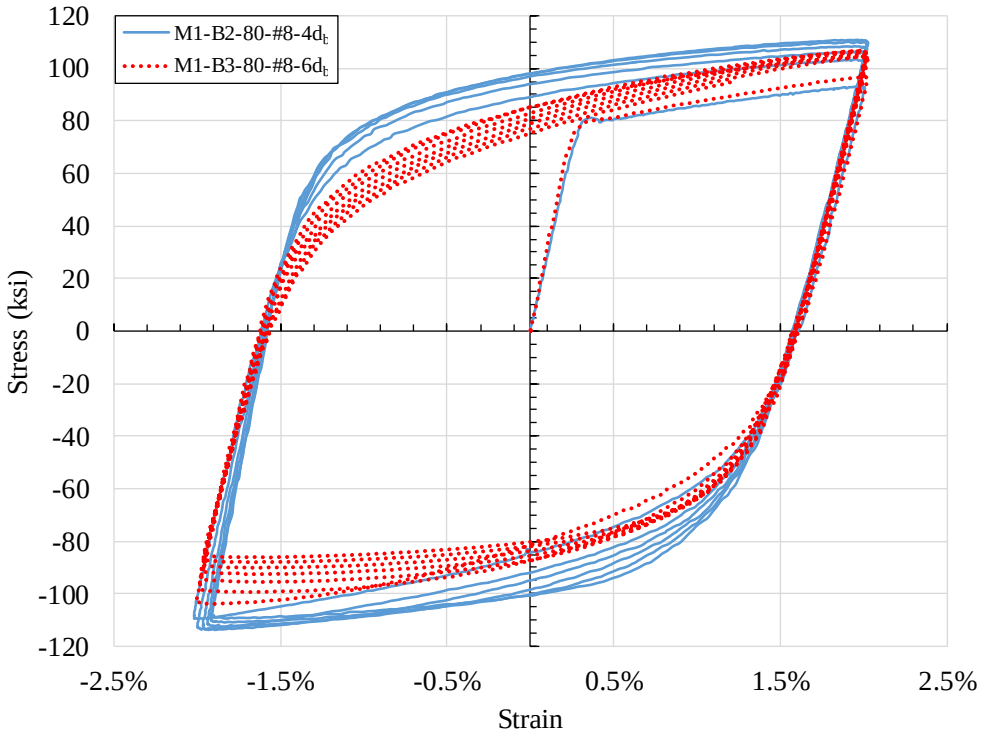

Figure 4-20: Cyclic strength degradation comparison for #8 bars from manufacturer 1 tested at different clear spans

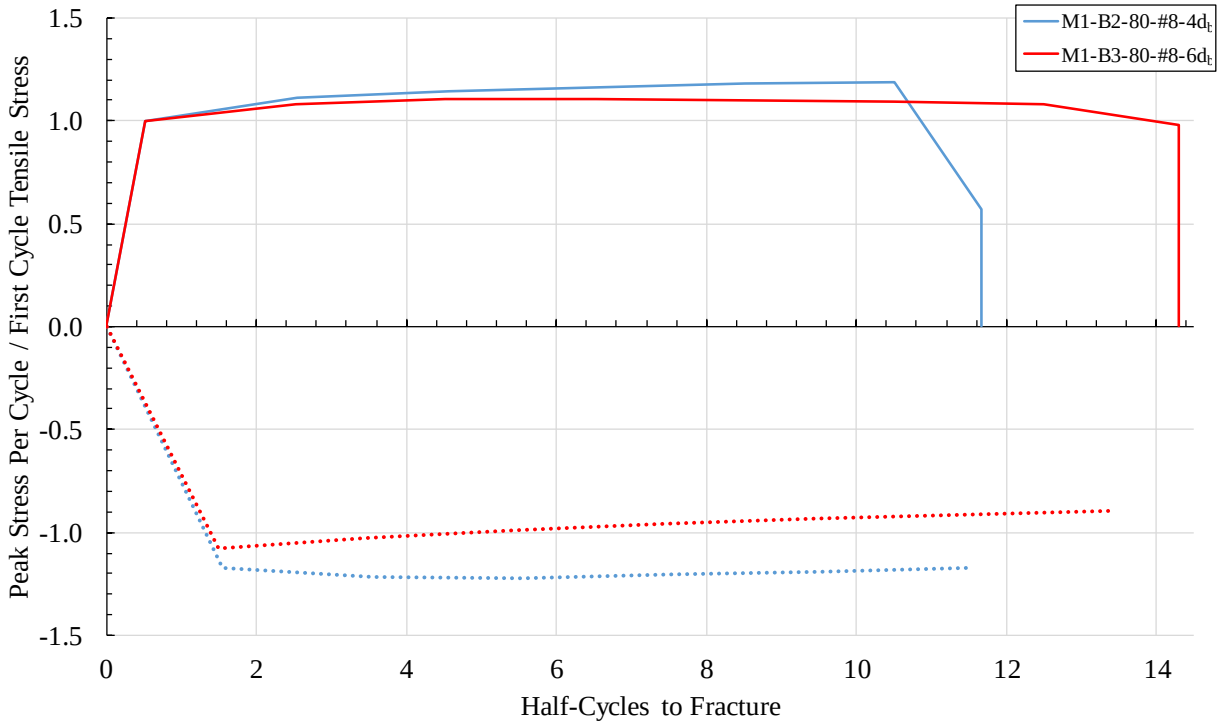

Figure 4-21: Progression of peak stresses per cycle for #8 bars from manufacturer 1 tested at different clear spans

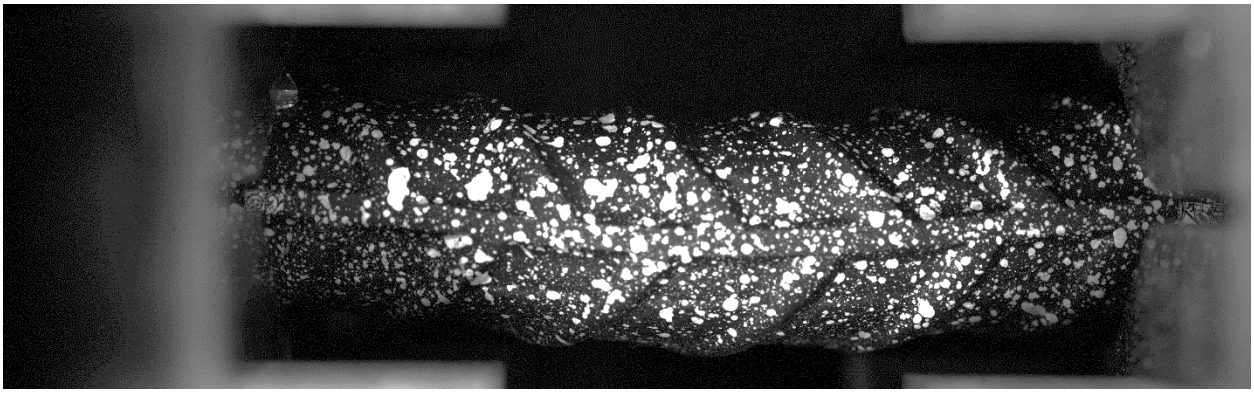

Figure 4-22: Final compression cycle for a M1-B2-80-#8-4d_b specimen under the +2% to -2% strain protocol

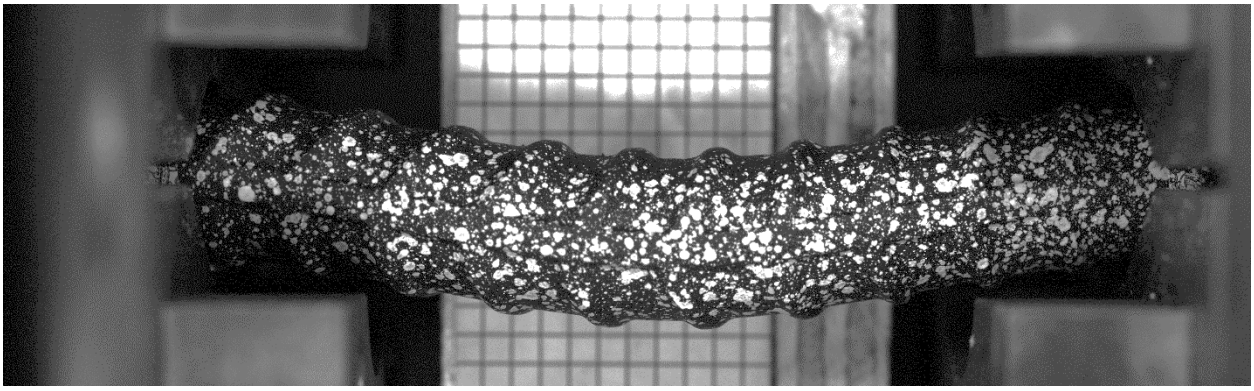

Figure 4-23: Final compression cycle for a M1-B3-80-#8-6d_b specimen under the +2% to -2% strain protocol

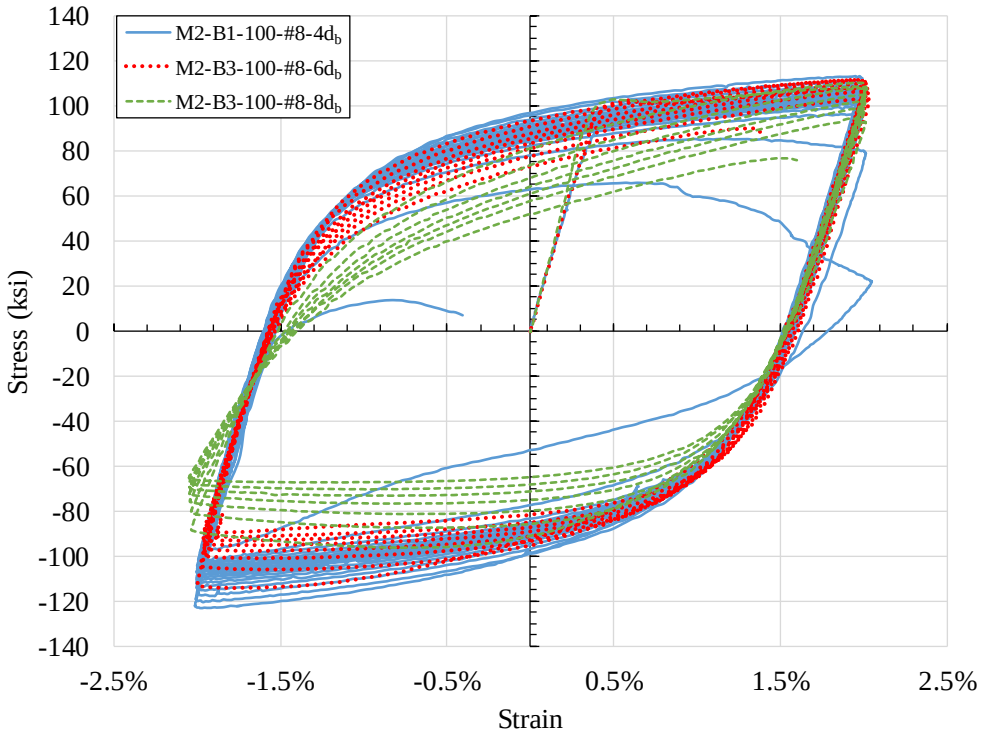

Figure 4-24: Progression of peak stresses per cycle for #8 bars from manufacturer 2 tested at different clear spans

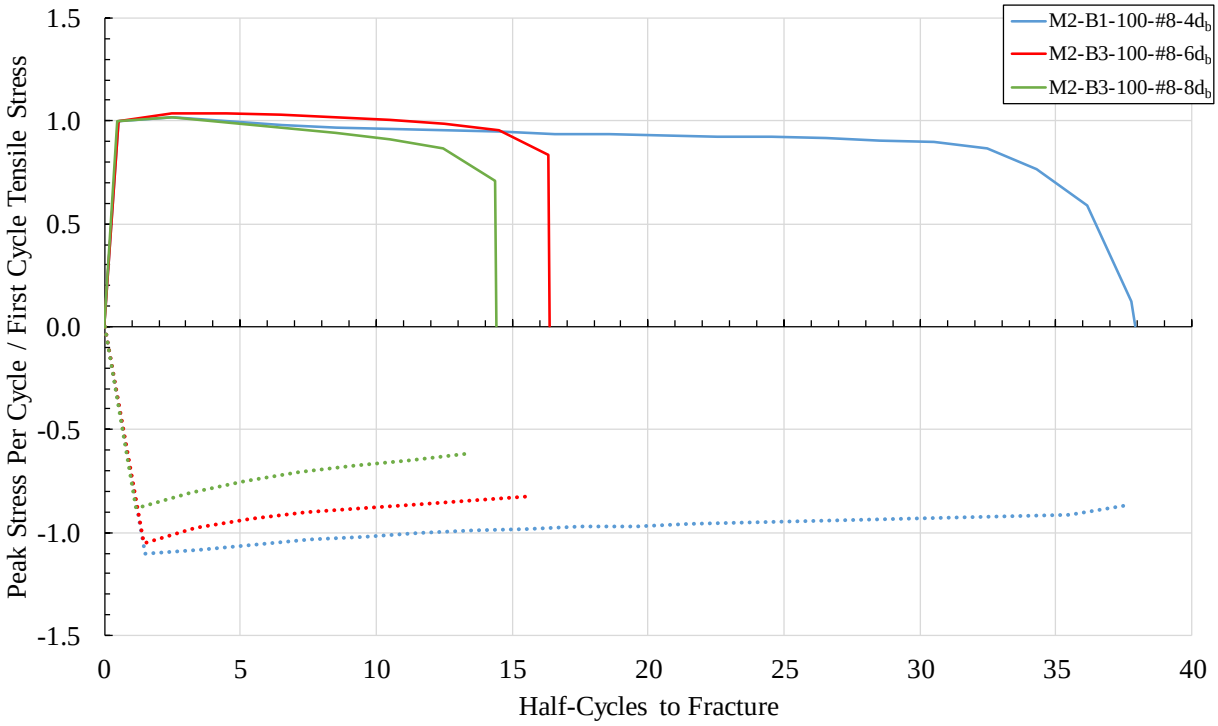

Figure 4-25: Progression of peak stresses per cycle for #8 bars from manufacturer 2 tested at different clear spans

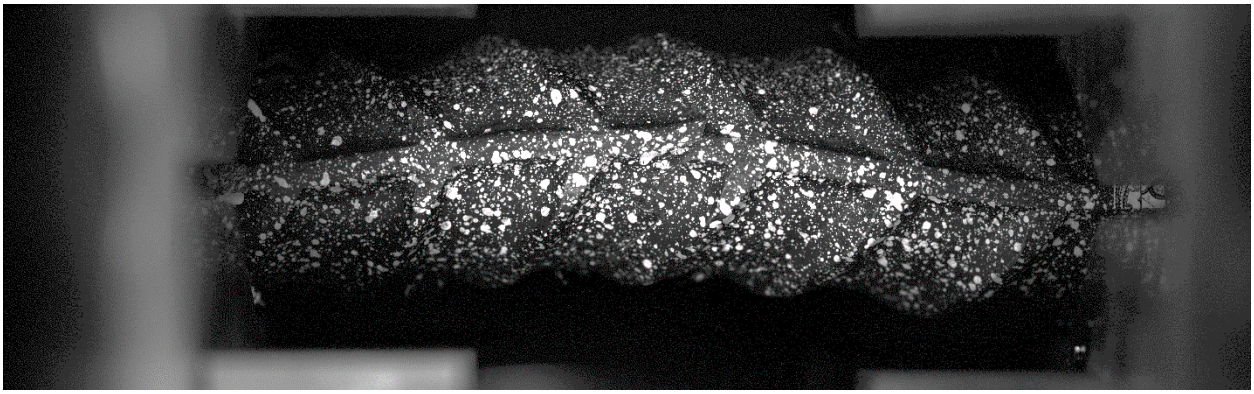

Figure 4-26: Final compression cycle for a M2-B1-100-#8-4d_b specimen under the +2% to -2% strain protocol

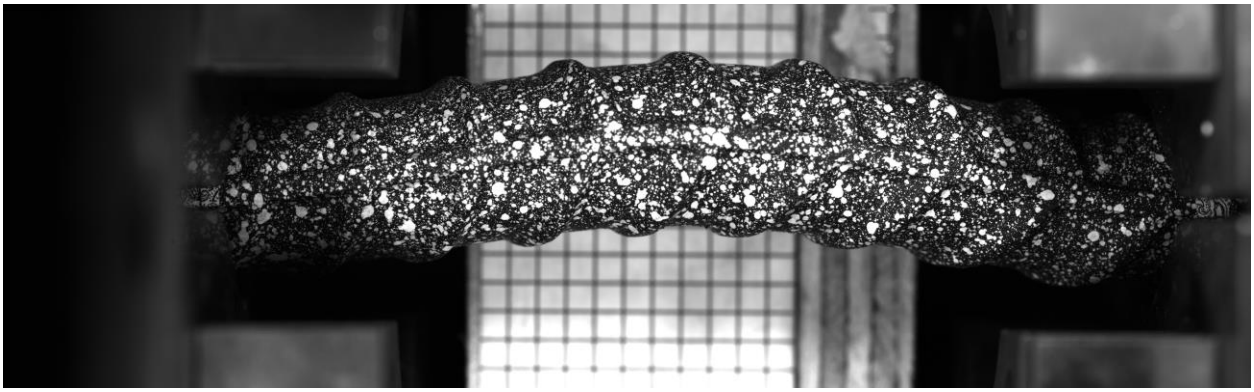

Figure 4-27: Final compression cycle for a M2-B3-100-#8-6d_b specimen under the +2% to -2% strain protocol

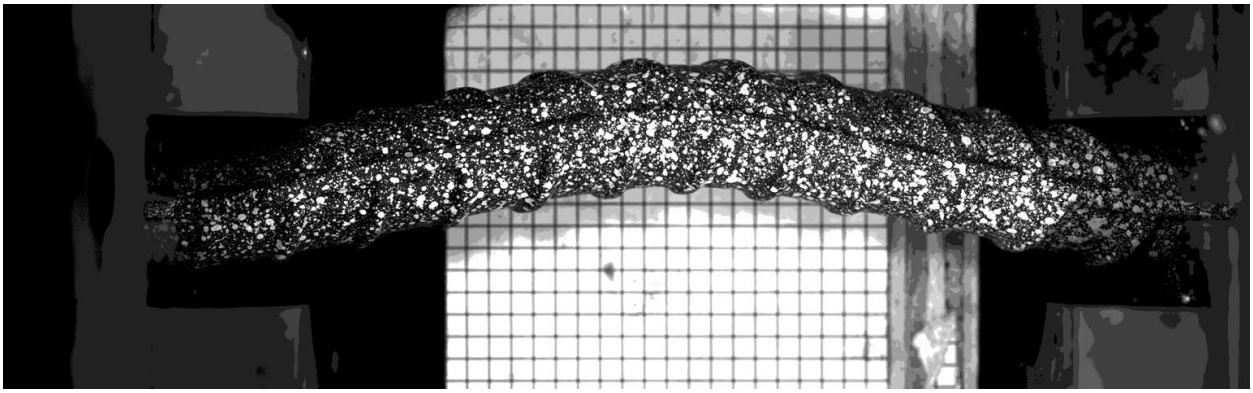

Figure 4-28: Final compression cycle for a M2-B3-100-#8-8d_b specimen under the +2% to -2% strain protocol

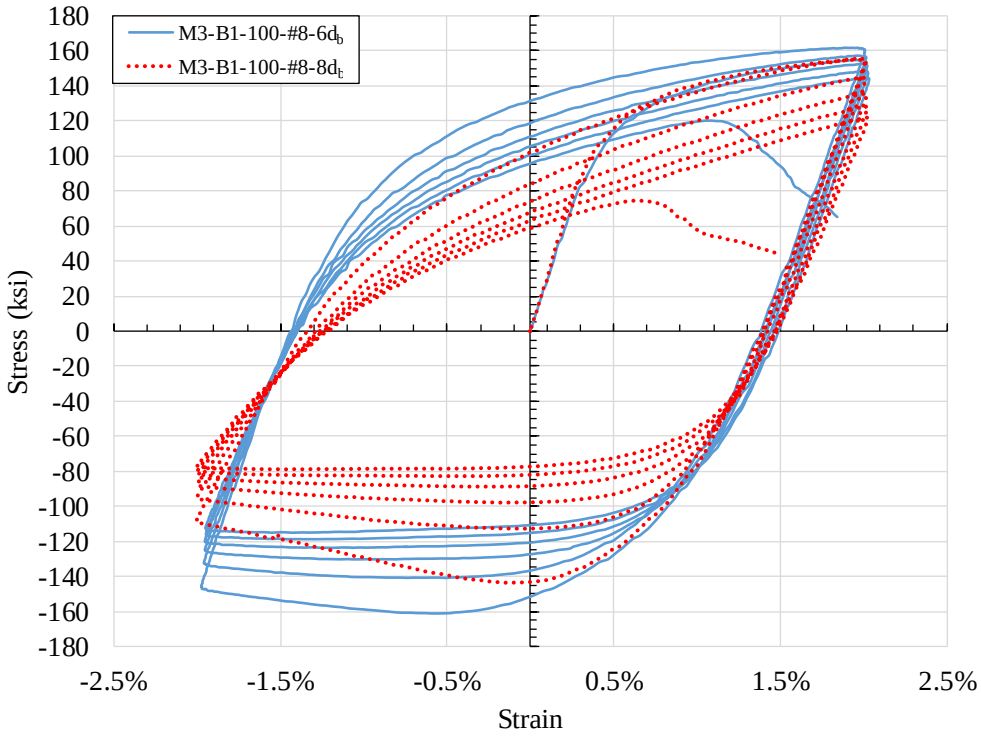

Figure 4-29: Progression of peak stresses per cycle for #8 bars from manufacturer 3 tested at different clear spans

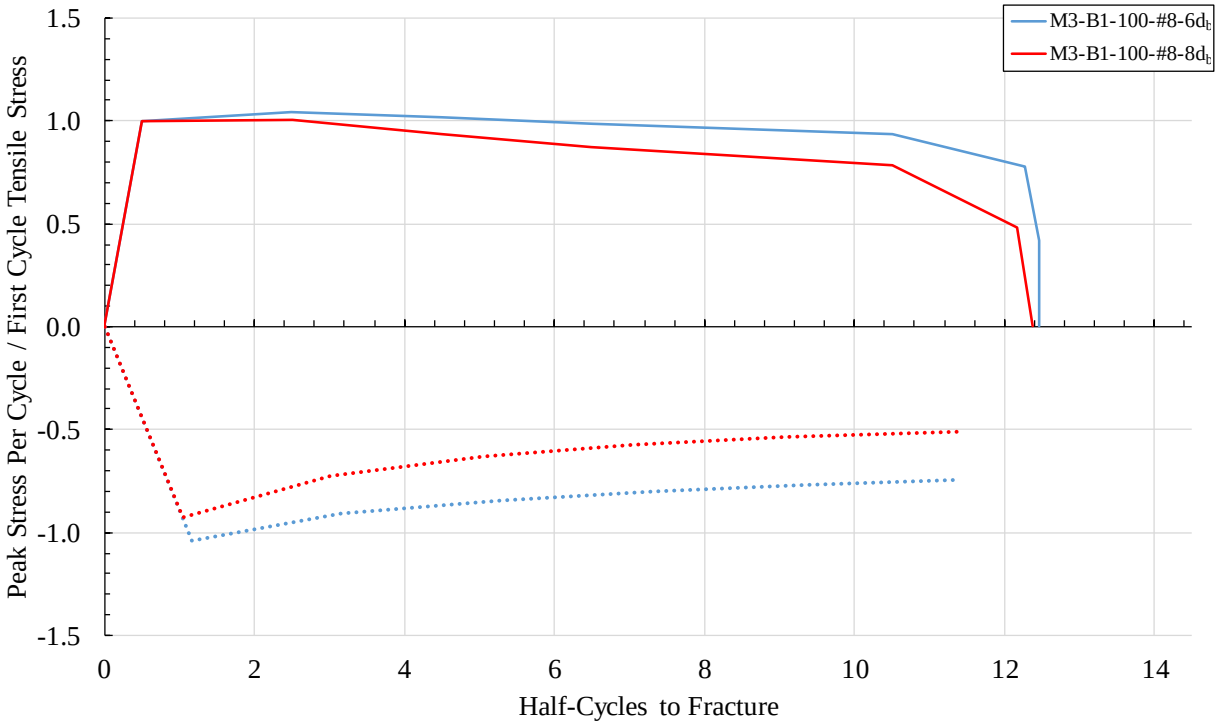

Figure 4-30: Progression of peak stresses per cycle for #8 bars from manufacturer 3 tested at different clear spans

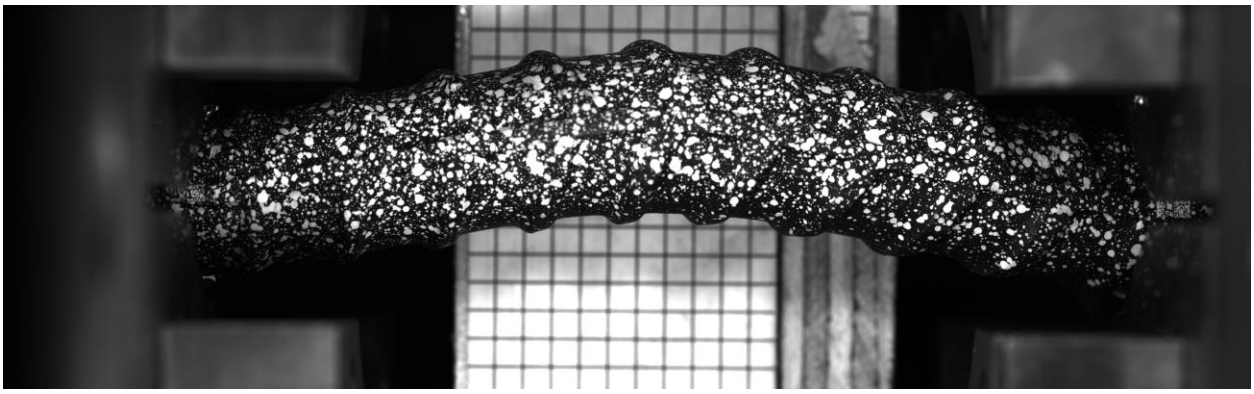

Figure 4-31: Final compression cycle for a M3-B1-100-#8-6d_b specimen under the +2% to -2% strain protocol

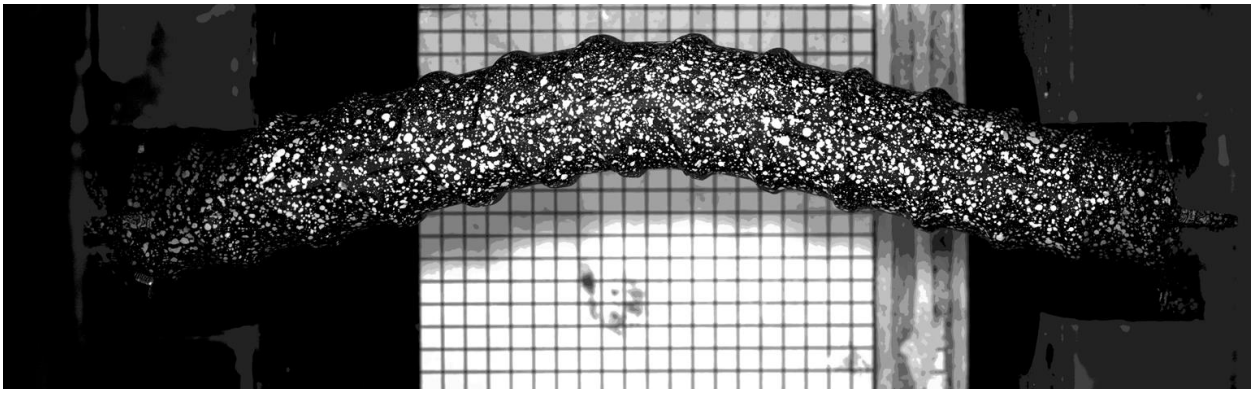

Figure 4-32: Final compression cycle for a M3-B1-100-#8-8d_b specimen under the +2% to -2% strain protocol

Figure 4-33, Figure 4-34, and Figure 4-35 contrast the stress-strain response of two grade 80 #8 bars from manufacturers 1 and 2, as well as a grade 100 bar from manufacturer 3 tested under the same clear span of 6d_b and loading strain protocol of +4% to -1%. The dashed line in the figures denotes 80% of the tensile strength reached when the bars reached their peak tensile strain of +4% strain for the first time. The trends in the plots discussed herein are typical for each manufacturer and relatively insensitive to bar grade, which indicates larger dependency of the stress-strain relations on the manufacturing process. As can be seen in Table 4-13 and Table 4-14, the grade 80 bars produced by manufacturer 1 typically sustained relatively low cyclic strength degradation before a sudden brittle fracture occurs. On the other hand, the grade 80 bars produced by manufacturer 2 exhibited similar strength degradation as bars from manufacturer 1 in the initial cycles but did not typically sustain a sudden fracture. M2 bars generally experienced

larger numbers of cycles to fracture than M1 bars, and sustained gradually widening fatigue cracks that resulted in significant strength degradation before fracture occurred. The final tensile strength just prior to fracture can be seen to drop to approximately 60% of the initial tensile capacity of the M2 bar.

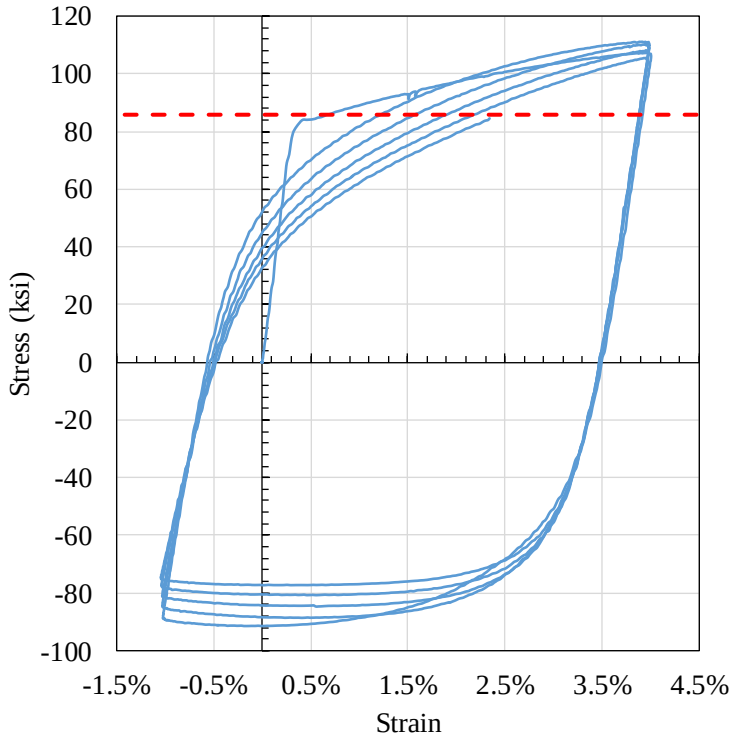

Figure 4-33: Stress-Strain plot for a M1-B1-80-#8-6d_b bar under the +4% to -1% strain protocol (10.47 half-cycles to fracture)

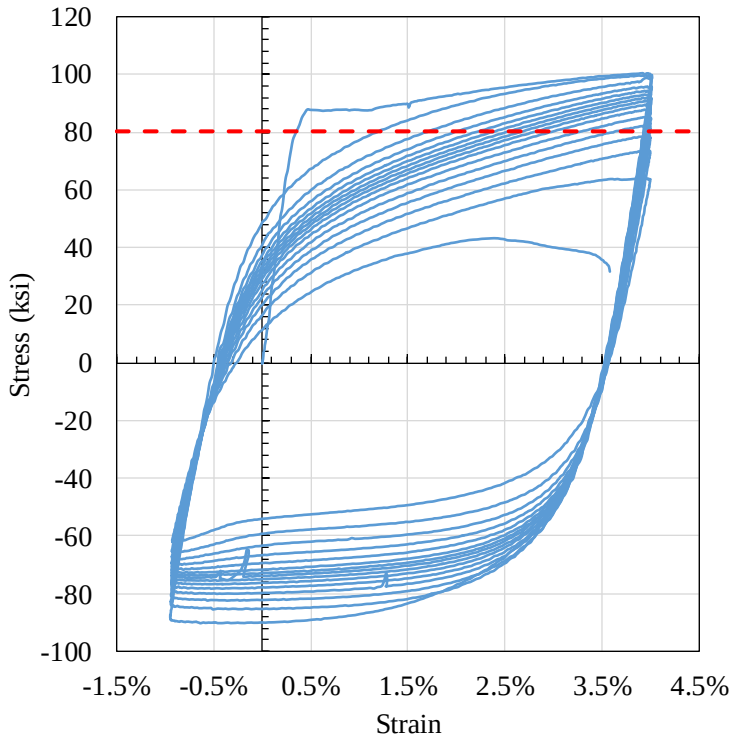

Figure 4-34: Stress-Strain plot for a M2-B1-80-#8-6d_b bar under the +4% to -1% strain protocol (30.72 half-cycles to fracture, 23.80 half-cycles to 80% capacity)

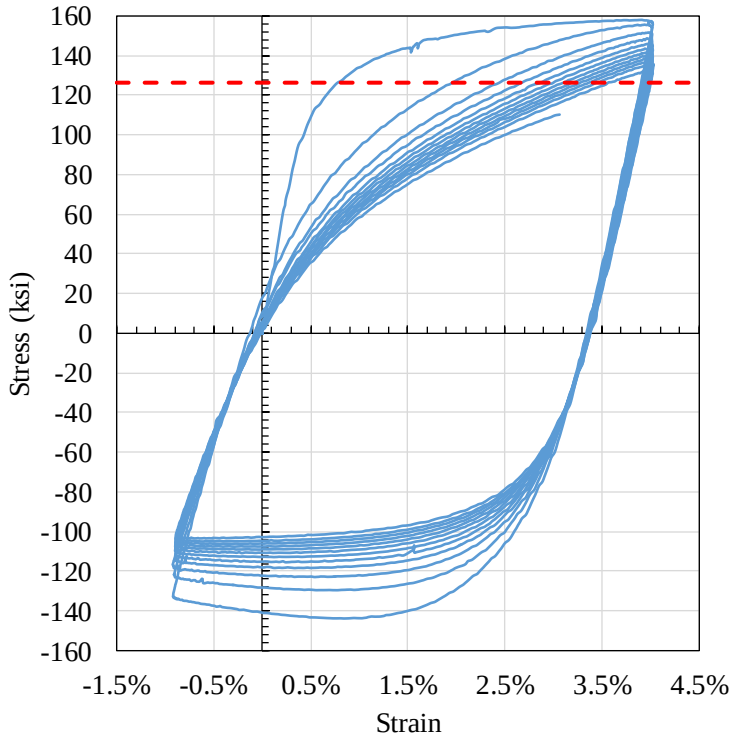

Figure 4-35: Stress-Strain plot for a M3-B2-100-#8-6d_b bar under the +4% to -1% strain protocol (24.61 half-cycles to fracture)

For M1 bars, a crack would initiate around midspan and propagate rapidly through the cross section of the bar as seen in Figure 4-36. In contrast, bars from M2 saw cracks initiating on the compression side of buckling that ran along the transverse deformations and gradually increased in length and width until full fracture occurred. Figure 4-37 shows the fracture planes of a typical M2-B1-80-#8-6d_b bar. A typical fracture plane of a bar from M3 can be seen in Figure 4-38.

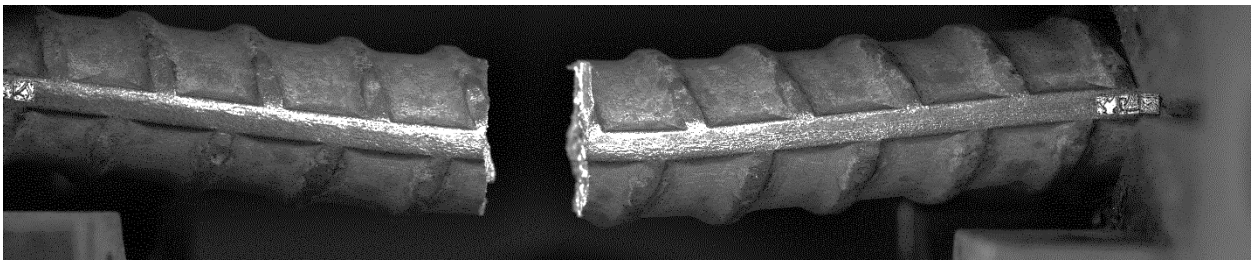

Figure 4-36: Fracture profile typical of a M1-B1-80-#8-6d_b bar under the +4% to -1% strain protocol

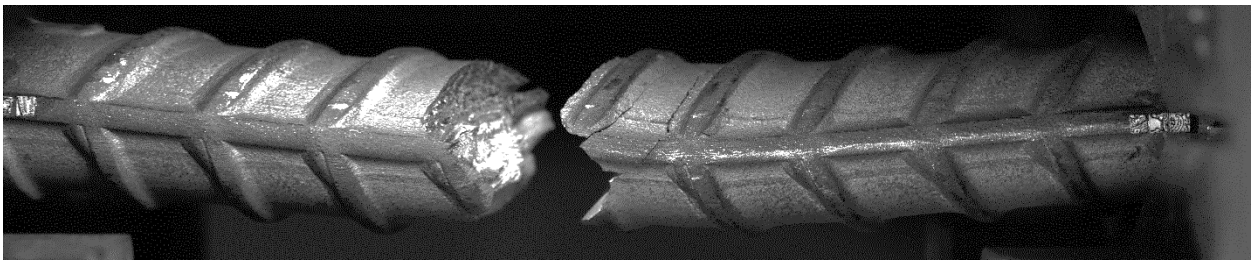

Figure 4-37: Fracture profile typical of a M2-B1-80-#8-6d_b bar under the +4% to -1% strain protocol

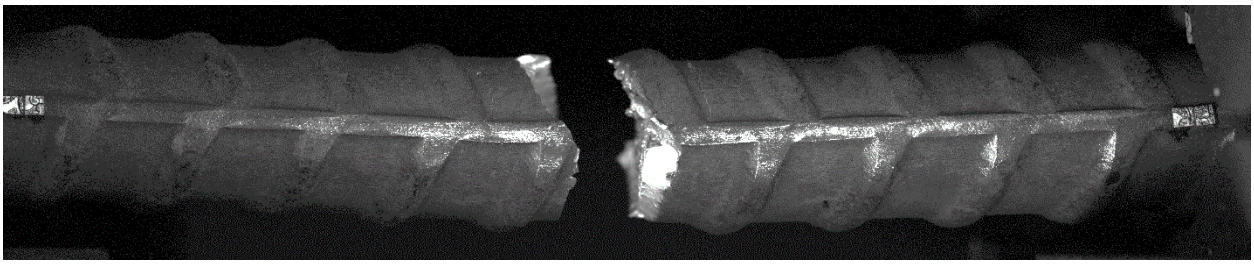

Figure 4-38: Fracture profile typical of a M3-B2-100-#8-6d_b bar under the +4% to -1% strain protocol

Along with a reduction in capacity, bars from M2-B1-80-#8 typically experienced a reduction in stiffness as cracks begin to propagate through the cross section. During compression cycles, this reduction in stiffness causes the bars to reach increased buckling amplitudes. Figure

4-39 and Figure 4-40 contrast the first compression cycle and the last compression cycle before fracture for the M2-B1-80-#8 specimen from Figure 4-34. It can be clearly seen that the buckling amplitude in the last compression cycle is significantly greater than the amplitude experienced during the first compression cycle.

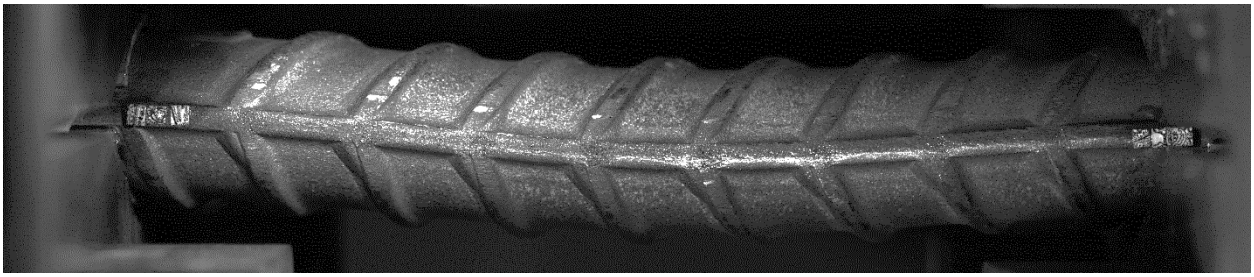

Figure 4-39: First compression cycle for a M2-B1-80-#8-6d_b specimen under the +4% to -1% strain protocol

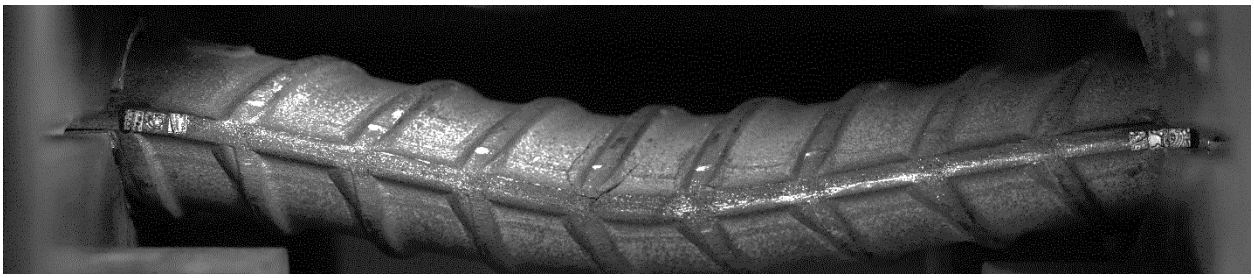

Figure 4-40: Final compression cycle for a M2-B1-80-#8-6d_b specimen under the +4% to -1% strain protocol

Figure 4-41 through Figure 4-46 show the crack development and growth during the peaks of the final tensile half-cycles prior to bar fracture for a typical M2-B1-80-#8-6d_b bar. In Figure 4-41, cracks are visible but the specimen is only experiencing a 13% reduction in strength from its initial tensile capacity. Figure 4-42 and Figure 4-43 show the formation of additional fatigue cracks in the same direction as the transverse ribs as well as the widening of existing cracks. The tensile stress achieved by the bar at peak tensile strain is slightly above the 80% threshold at this stage. In Figure 4-44, the cracks begin to cut across the longitudinal rib. After this half-cycle, the reduction in tensile strength from cycle to cycle starts to increase. By Figure 4-45, the crack widths are substantially larger than four half-cycles prior and the bar experiences

a reduction of capacity of 27%. Figure 4-46 shows the state of the bar in the final complete tensile half-cycle before fracture occurs.

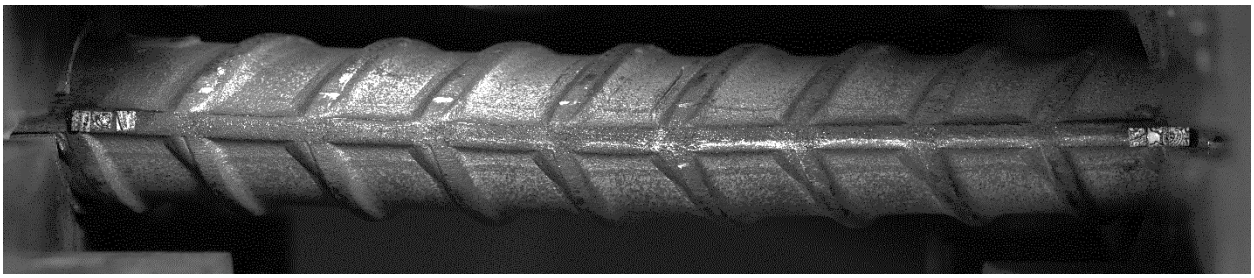

Figure 4-41: Crack growth for a M2-B1-80-#8-6d_b bar under the +4% to -1% strain protocol at half-cycle 18.8 and 87% of tensile capacity (30.72 half-cycles to fracture)

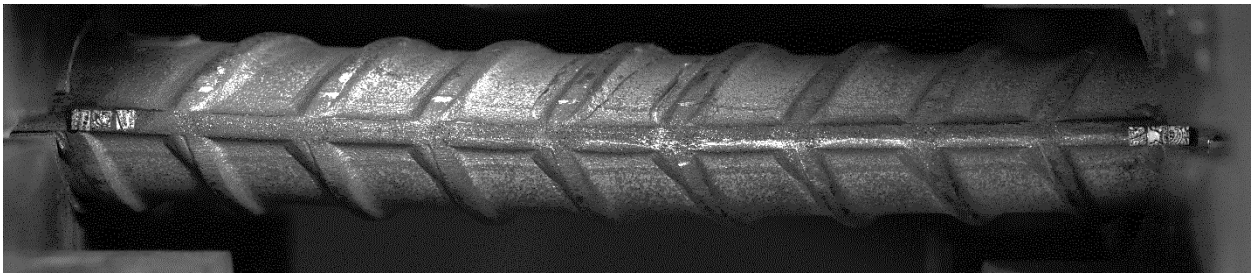

Figure 4-42: Crack growth for a M2-B1-80-#8-6d_b bar under the +4% to -1% strain protocol at half-cycle 20.8 and 85% of tensile capacity (30.72 half-cycles to fracture)

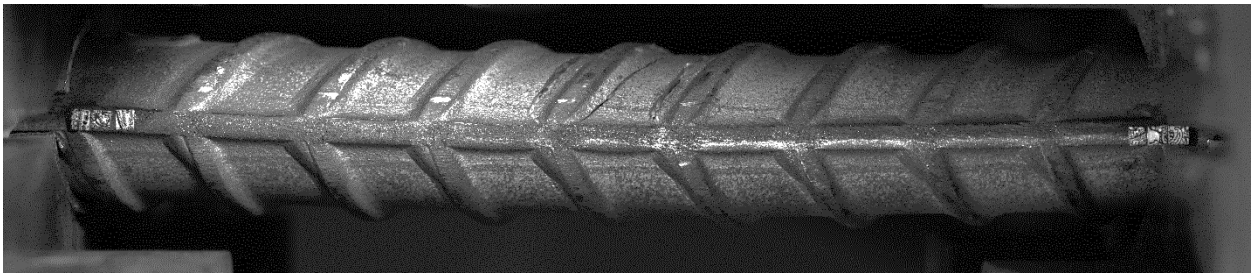

Figure 4-43: Crack growth for a M2-B1-80-#8-6d_b bar under the +4% to -1% strain protocol at half-cycle 22.8 and 82% of tensile capacity (30.72 half-cycles to fracture)

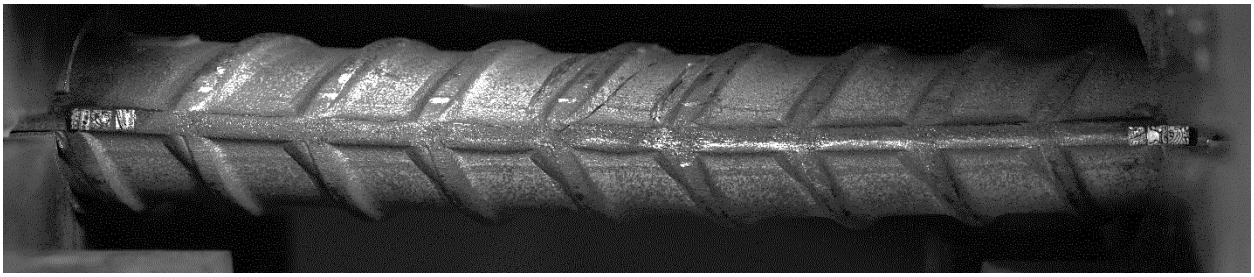

Figure 4-44: Crack growth for a M2-B1-80-#8-6d_b bar under the +4% to -1% strain protocol at half-cycle 24.8 and 78% of tensile capacity (30.72 half-cycles to fracture)

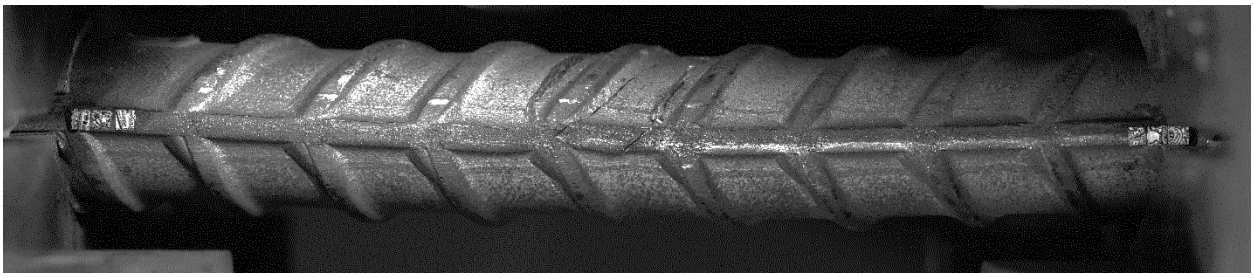

Figure 4-45: Crack growth for a M2-B1-80-#8-6d_b bar under the +4% to -1% strain protocol at half-cycle 26.8 and 73% of tensile capacity (30.72 half-cycles to fracture)

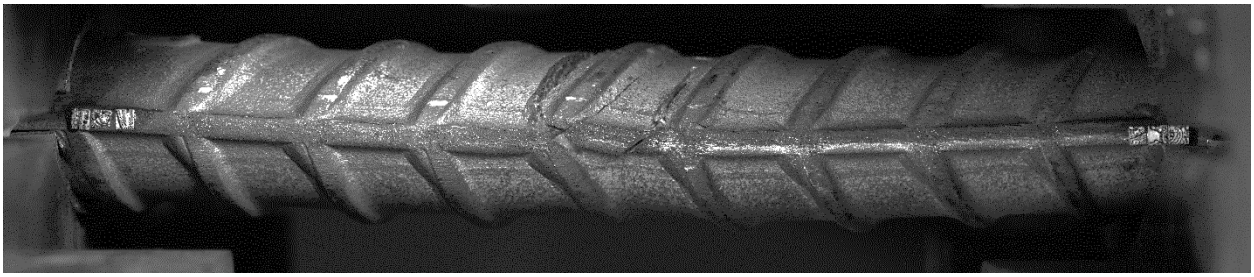

Figure 4-46: Crack growth for a M2-B1-80-#8-6d_b bar under the +4% to -1% strain protocol at half-cycle 28.8 and 63% of tensile capacity (30.72 half-cycles to fracture)

4.2.2 Summary of Test Results

The number of half-cycles of loading was evaluated starting from the onset of loading up until fracture and accounted for partial half-cycles imposed at the beginning and end of a test. For strain protocols in which the peak strain generating compressive stresses was less than 0%, the first partial half-cycle imposed on a bar was included in the reported numbers of half-cycles to failure. Specimens that fractured at the grips of the test machine were generally treated as unsuccessful and discarded. The mean number of half-cycles to fracture for #5 and #8 bars tested under the primary strain protocols, the coefficient of variation (COV) for the values, and the number of tests from which the mean and COV values were obtained are presented in Table 4-6, Table 4-7, Table 4-8, and Table 4-9. The tables break down the values for each manufacturer, strain protocol, and clear gripping span. Table 4-10 and Table 4-11 provide the same information for #8 bars tested under the secondary strain protocols. From these tables, it can be seen that

there is a significant amount of variability in the fatigue performance even amongst bars from the same batch tested under the same strain protocol.

Loading Protocol			+4% to 0%
Mfr	Grade	Batch	$6d_b$
1	80	1	33.3 (4)
2	80	1	47.7 (6)
		2	48.0 (6)
	100	1	74.9 (4)
3	100	1	15.8 (4)

Table 4-6: Mean number of half-cycles to fracture for #5 bars tested under primary strain protocols with number of samples in parenthesis

Loading Protocol			+4% to 0%
Mfr	Grade	Batch	$6d_b$
1	80	1	0.252
2	80	1	0.411
		2	0.569
	100	1	0.113
3	100	1	0.299

Table 4-7: COV of half-cycles to fracture for #5 bars tested under primary strain protocols

Loading Protocol			+2% to -2%			+4% to -1%	
Mfr	Grade	Batch	$4d_b$	$6d_b$	$8d_b$	$4d_b$	$6d_b$
1	60	2	27.9 (3)	-	-	15.2 (3)	-
	80	1	-	12.2 (5)	-	-	11.7 (6)
		2	11.4 (3)	-	-	8.1 (3)	-
		3	-	16.8 (4)	-	-	-
		4	-	13.6 (4)	-	-	-
		5	-	12.4 (4)	-	-	-
	100	2	8.7 (6)	-	-	6.7 (6)	-
2	60	3	-	24.2 (3)	24.8 (3)	-	-
	80	1	38.7 (4)	39.8 (4)	-	-	25.2 (4)
		3	-	20.9 (3)	15.7 (3)	-	-
	100	1	40.1 (4)	-	-	-	18.9 (4)
		3	-	17.6 (3)	15.7 (3)	-	-
3	100	1	-	9.8 (4)	13.4 (4)	-	-
		2	-	33.6 (4)	-	-	23.6 (4)

Table 4-8: Mean number of half-cycles to fracture for #8 bars tested under primary strain protocols with number of samples in parenthesis

Loading Protocol			+2% to -2%			+4% to -1%	
Mfr	Grade	Batch	$4d_b$	$6d_b$	$8d_b$	$4d_b$	$6d_b$
1	60	2	0.136	-	-	0.207	-
	80	1	-	0.210	-	-	0.271
		2	0.287	-	-	0.453	-
		3	-	0.317	-	-	-
		4	-	0.130	-	-	-
		5	-	0.318	-	-	-
	100	2	0.310	-	-	0.486	-
2	60	3	-	0.150	0.161	-	-
	80	1	0.553	0.430	-	-	0.285
		3	-	0.239	0.196	-	-
	100	1	0.135	-	-	-	0.215
		3	-	0.240	0.147	-	-
3	100	1	-	0.311	0.356	-	-
		2	-	0.050	-	-	0.197

Table 4-9: COV of half-cycles to fracture for #8 bars tested under primary strain protocols

Loading Protocol			+4% to 0%			+4% to -2%			+6% to 0%		
Mfr	Grade	Batch	$4d_b$	$6d_b$	$8d_b$	$4d_b$	$6d_b$	$8d_b$	$4d_b$	$6d_b$	$8d_b$
1	60	2	33.2 (3)	-	-	-	-	-	10.8 (3)	-	-
2	60	3	-	38.6 (3)	25.5 (3)	-	-	-	-	16.8 (3)	11.2 (3)
	80	1	32.9 (4)	-	-	13.8 (4)	-	-	19.1 (4)	-	-
		3	-	16.0 (3)	18.1 (3)	-	-	-	-	9.3 (3)	8.6 (3)
	100	1	34.4 (4)	-	-	17.8 (4)	-	-	16.3 (4)	-	-
		3	-	18.8 (3)	13.5 (3)	-	-	-	-	7.5 (3)	6.9 (3)
3	100	1	-	18.3 (4)	14.5 (4)	-	13.5 (4)	7.9 (4)	-	7.3 (4)	9.9 (4)

Table 4-10: Mean number of half-cycles to fracture for #8 bars tested under secondary strain protocols with number of samples in parenthesis

Loading Protocol			+4% to 0%			+4% to -2%			+6% to 0%		
Mfr	Grade	Batch	$4d_b$	$6d_b$	$8d_b$	$4d_b$	$6d_b$	$8d_b$	$4d_b$	$6d_b$	$8d_b$
1	60	2	0.398	-	-	-	-	-	0.174	-	-
2	60	3	-	0.142	0.251	-	-	-	-	0.204	0.204
	80	1	0.113	-	-	0.603	-	-	0.566	-	-
		3	-	0.085	0.245	-	-	-	-	0.158	0.028
	100	1	0.238	-	-	0.426	-	-	0.461	-	-
		3	-	0.096	0.226	-	-	-	-	0.175	0.280
3	100	1	-	0.695	0.412	-	0.095	0.297	-	0.325	0.113

Table 4-11: COV of half-cycles to fracture for #8 bars tested under secondary strain protocols

The number of half-cycles until the bar stress at peak tensile strain dropped to 80% of the tensile stress measured during the first excursion to the peak tensile strain (NH80) was extracted from test data. Table 4-12, Table 4-13, and Table 4-14 present the ratio between the number of half-cycles to 80% of initial tensile capacity (NH80) to the number of half-cycles to fracture (NHF), as defined by Equation 4-2. Bars that maintained a tensile strength above 80% of the initial cycle strength before fracture occurred are marked as 100%.

$$\text{Ratio}_{NH80} = \frac{\text{Number of Half-Cycles to 80\% of Initial Capacity}}{\text{Number of Half-Cycles to Fracture}}$$

Equation 4-2: Ratio of cycles to 80% capacity

Loading Protocol			+4% to 0%
Mfr	Grade	Batch	$6d_b$
1	80	1	100.00%
2	80	1	83.83%
		2	74.31%
	100	1	77.48%
3	100	1	87.03%

Table 4-12: Ratio of half-cycles to 80% capacity to half-cycles to fracture for #5 bars tested under primary strain protocols

Loading Protocol			+2% to -2%			+4% to -1%	
Mfr	Grade	Batch	$4d_b$	$6d_b$	$8d_b$	$4d_b$	$6d_b$
1	60	2	93.66%	-	-	100.00%	-
	80	1	-	100.00%	-	-	100.00%
		2	100.00%	-	-	100.00%	-
		3	-	100.00%	-	-	-
		4	-	100.00%	-	-	-
		5	-	100.00%	-	-	-
	100	2	100.00%	-	-	100.00%	-
2	60	3	-	88.87%	73.29%	-	-
	80	1	89.18%	86.78%	-	-	78.50%
		3	-	91.51%	81.93%	-	-
	100	1	87.27%	-	-	-	86.43%
		3	-	100.00%	100.00%	-	-
3	100	1	-	100.00%	78.64%	-	-
		2	-	94.16%	-	-	100.00%

Table 4-13: Ratio of half-cycles to 80% capacity to half-cycles to fracture for #8 bars tested under primary strain protocols

Loading Protocol			+4% to 0%			+4% to -2%			+6% to 0%		
Mfr	Grade	Batch	$4d_b$	$6d_b$	$8d_b$	$4d_b$	$6d_b$	$8d_b$	$4d_b$	$6d_b$	$8d_b$
1	60	2	92.39%	-	-	-	-	-	100.00%	-	-
2	60	3	-	91.55%	62.64%	-	-	-	-	89.34%	53.70%
	80	1	88.21%	-	-	82.43%	-	-	76.87%	-	-
		3	-	89.69%	81.23%	-	-	-	-	100.00%	70.02%
	100	1	87.25%	-	-	86.65%	-	-	79.87%	-	-
		3	-	100.00%	100.00%	-	-	-	-	100.00%	100.00%
3	100	1	-	92.50%	69.19%	-	100.00%	63.18%	-	100.00%	50.70%

Table 4-14: Ratio of half-cycles to 80% capacity to half-cycles to fracture for #8 bars tested under secondary strain protocols

As can be seen in Table 4-12, Table 4-13, and Table 4-14 bars from manufacturer 1 tend to maintain a tensile strength larger than 80% of the initial cycle strength up to fracture. This is not typically the case for bars from manufacturers 2 and 3, which generally experienced more gradual strength loss prior to fracture across all grades. Values in the tables also indicate that the ratio of NH80 to NHF only drops slightly with increasing gripping span. This indicates that inherent bar properties such as microstructure and bar deformations may play a more prominent role than gripping span in determining this ratio.

4.2.3 Effects of Primary Variables on Fatigue Life of Bars

In this section, figures are presented that show the effects of steel grade on the fatigue life with filled markers indicating the mean value of half-cycles to fracture (NHF) and error bars indicating the maximum and minimum values of the NHF. Where applicable, black X's mark the mean number of half-cycles to a strength drop below 80% of the initial-cycle tensile strength (NH80). In the figures, the shape of the filled markers at the mean value of NHF indicate the bar grade, with a tringle marker denoting grade 60 bars, a square marker denoting grade 80 bars, and a diamond marker denoting grade 100 bars. The color distinguishes between manufacturers and batches, with lighter colors representing lower grade bars and darker colors indication higher grade bars. For manufacturer 1, the blue color palette is used for results from Ghannoum and Slavin (2016), batch 0, and the purple palette is used for specimens in this study. For manufacturer 2, the red palette is used for batch 0 results and the orange palette for results from this study. The green palette for manufacturer 3. If multiple batches of the same size, grade and manufacturers are plotted, additional markers are overlaid inside of the NHF marker.

As this study is part of an ongoing research project, the test matrix is not yet completed. Only test data where comparable tests are available were considered in the following discussions.

4.2.3.1 Effects of Varying Production Techniques across Batches

Manufacturer 1

As described in more detail in section 3.1, except for batch 2 bars, M1 grade 80 batches varied only in chemical composition, had similar deformation geometries, and were produced using the same processes and in the same mill. Notably, the chemical variations attempted by manufacturer 1 included modifying the source of the Vanadium used in the micro-alloying process, as well as adjusting the equivalent carbon content. M1 batch 2 bars were produced in a different mill owned by the manufacturer, but still using similar production processes. The main difference between batch 2 bars and other batch bars was the deformation geometry (Section 3.6).

#5 Bars

The #5 grade 80 bars from batch 1 produced by manufacturer 1 and tested in this study (M1-B1-80-#5-6d_b) showed an improvement in fatigue life to fracture of 108% on average when compared to the M1-B0-80-#5-6d_b bars tested in the previous study by Ghannoum and Slavin (2016) (Figure 4-47). The mean fatigue life to fracture of the M1-B1-80-#5-6d_b bars was close to, but did not surpass that of the baseline grade 60 #5 bars or that of the grade 100 bars produced by the same manufacturer (Figure 4-48). In addition to the increased fatigue performance, the variability in fatigue life to fracture of M1-B1-80-#5 bars decreased from that of batch 0 equivalent bars (Figure 4-48). Table 4-15 tracks the fatigue life to fracture for each batch of #5 bars produced by manufacturer 1 and tested to the +4% to 0% strain protocol.

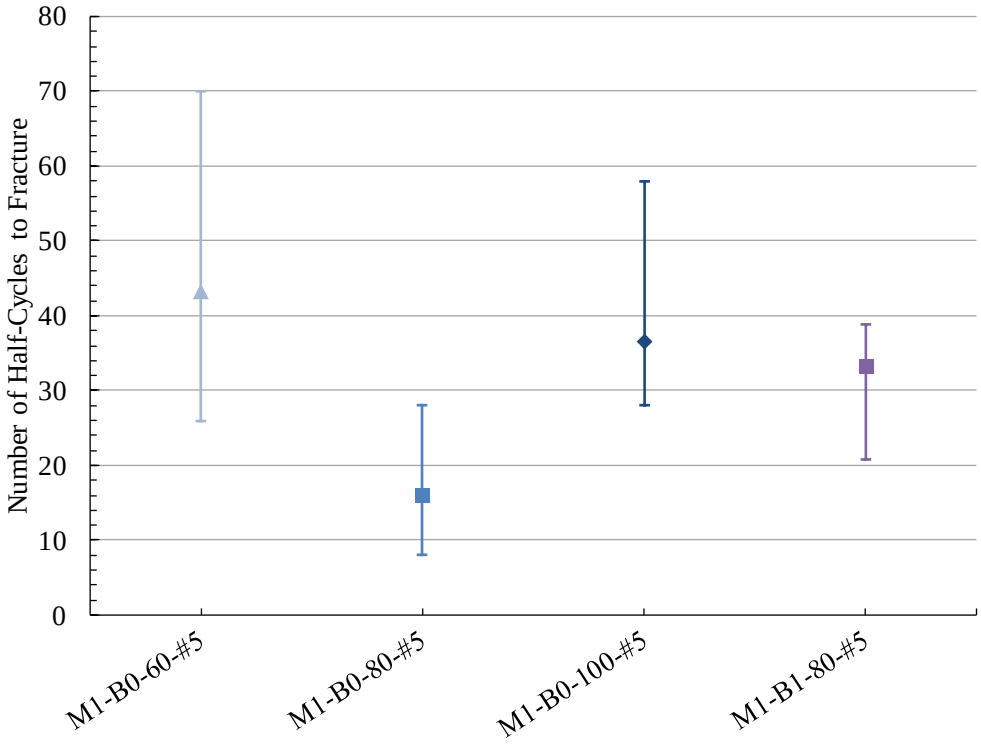

Figure 4-47: Half-cycles to fracture for #5 bars tested under the +4% to 0% strain protocol with a clear span of $6d_b$ produced by manufacturer 1

Loading Protocol		+4% to 0%		
Clear Span		$6d_b$		
Grade	Batch	Half-Cycles to Fracture	Percent Difference from B0	Percent Difference from B0-60
60	0	43.20	-	-
80	0	16.00	-	-63.0%
	1	33.33	108.3%	-22.8%
100	0	36.50	-	-15.5%

Table 4-15: Percent difference in fatigue life to fracture from batch 0 for #5 bars produced by manufacturer 1 under the +4% to 0% strain protocol

#8 Bars

M1 #8 bars tested in this study exhibited consistent fatigue results compared with those of equivalent batch 0 bars tested in the previous study, with the exception of all bars from batch 2 (Figure 4-48 to Figure 4-51, Table 4-16 and Table 4-17). As described in section 3.6, batch 2

bars had differing surface deformation geometries from other M1 batches. With all other parameters being approximately equivalent in batch 2 bars compared with other bars from M1, the changes in deformation geometry appear to have significantly decreased the fatigue life to fracture for batch 2 bars (Figure 4-48 and Figure 4-50). While none of the grade 80 #8 bars tested in the current study were able to match the fatigue life of the baseline grade 60 measurements, the results from batches 1, 3, 4, and 5 were consistent with previous batch 0 grade 80 results. This indicates that the chemical modifications attempted for the various batches tested in this study (Section 3.1) did not yield significantly different fatigue life to fracture.

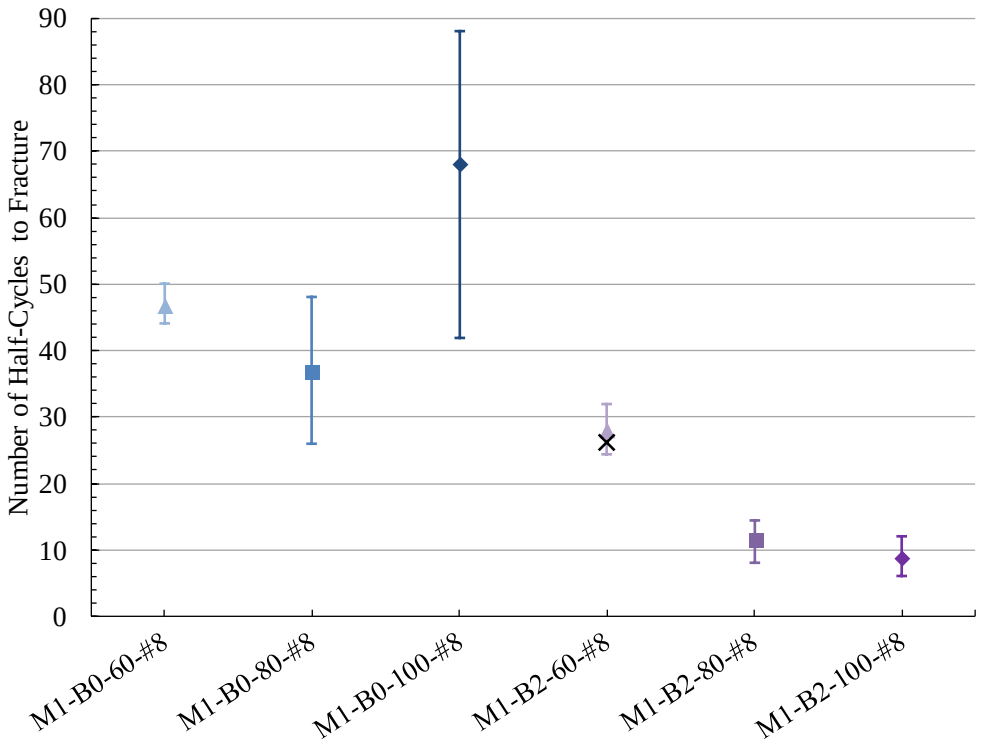

Figure 4-48: Number of half-cycles to fracture (NHF) for #8 bars tested under the +2% to -2% strain protocol with a clear span of $4d_b$ produced by manufacturer 1; the X markers indicate the mean NH80 values where applicable

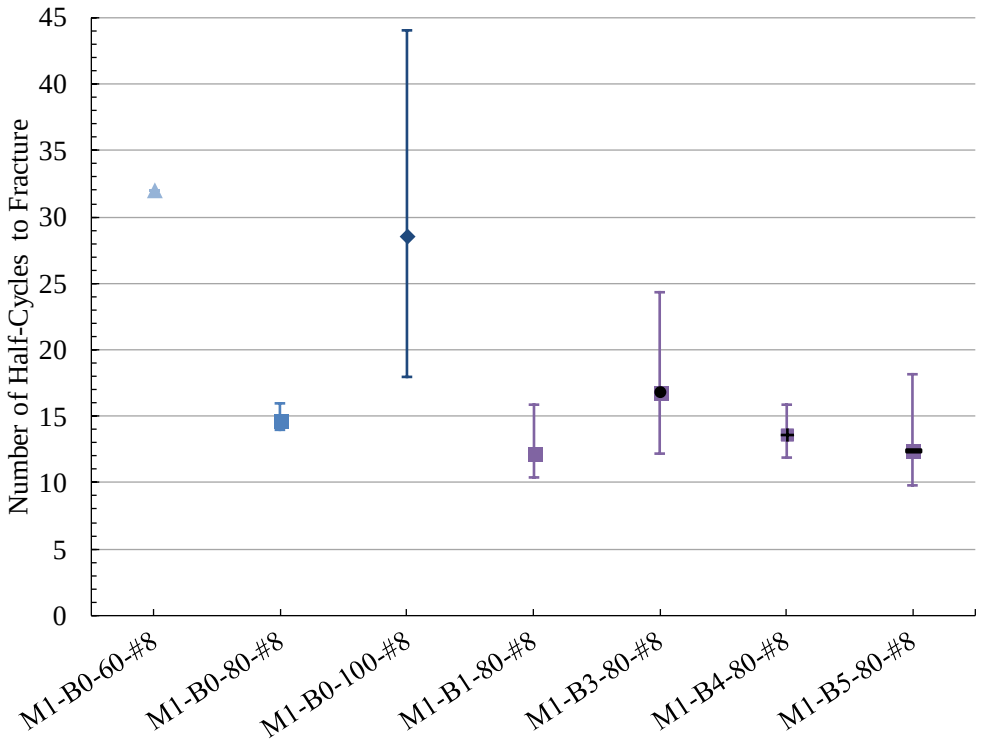

Figure 4-49: Half-cycles to fracture for #8 bars tested under the +2% to -2% strain protocol with a clear span of $6d_b$ produced by manufacturer 1

Loading Protocol		+2% to -2%					
Clear Span		$4d_b$			$6d_b$		
Grade	Batch	Half-Cycles to Fracture	Percent Difference from B0	Percent Difference from B0-60	Half-Cycles to Fracture	Percent Difference from B0	Percent Difference from B0-60
60	0	46.67	-	-	32.00	-	-
	2	27.94	-40.1%	-40.1%	-	-	-
80	0	36.67	-	-21.4%	14.67	-	-54.2%
	1	-	-	-	12.21	-16.8%	-61.9%
	2	11.37	-69.0%	-75.6%	-	-	-
	3	-	-	-	16.78	14.4%	-47.5%
	4	-	-	-	13.56	-7.5%	-57.6%
	5	-	-	-	12.42	-15.3%	-61.2%
100	0	68.00	-	45.7%	28.50	-	-10.9%
	2	8.69	-87.2%	-81.4%	-	-	-

Table 4-16: Percent difference in fatigue life to fracture from batch 0 for #8 bars produced by manufacturer 1 under the +2% to -2% strain protocol

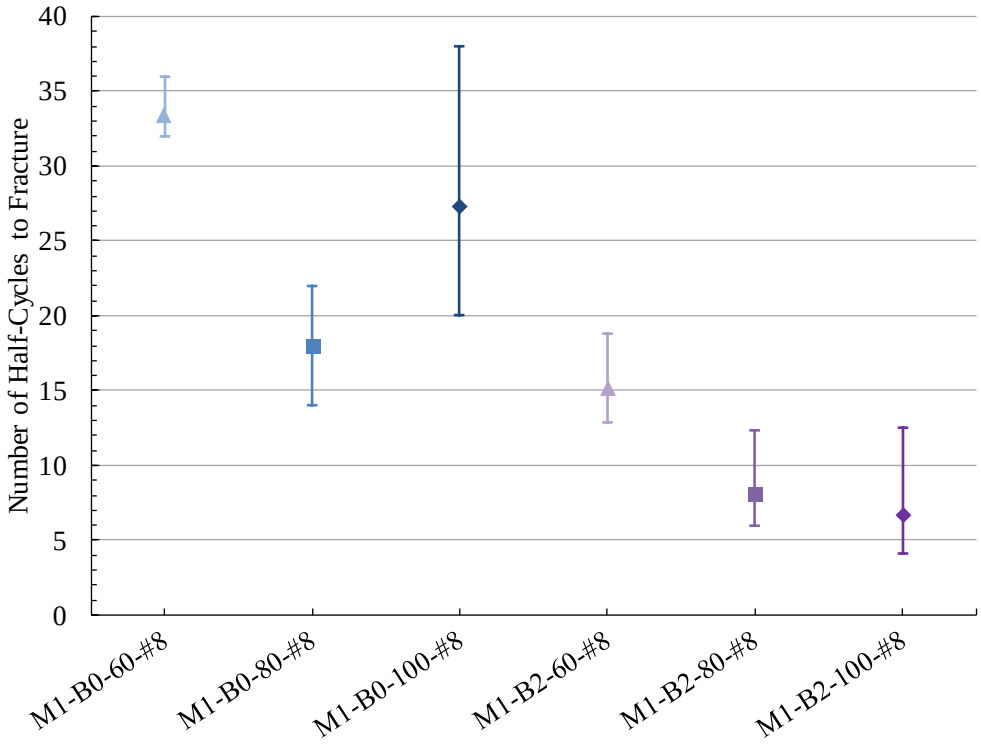

Figure 4-50: Half-cycles to fracture for #8 bars tested under the +4% to -1% strain protocol with a clear span of $4d_b$ produced by manufacturer 1

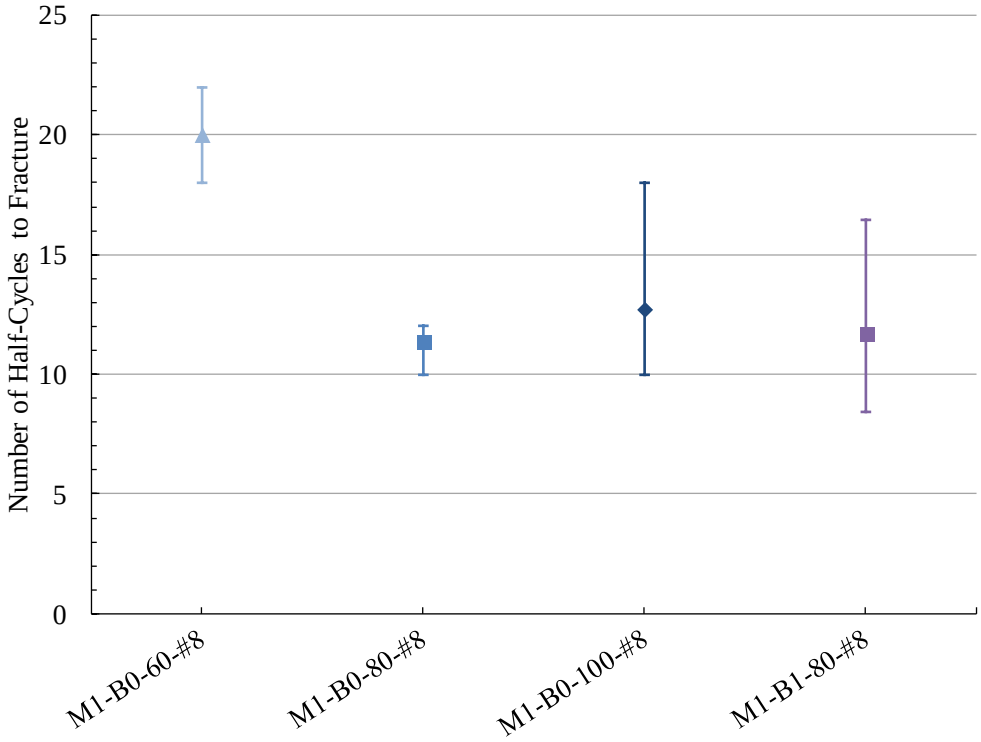

Figure 4-51: Half-cycles to fracture for #8 bars tested under the +4% to -1% strain protocol with a clear span of $6d_b$ produced by manufacturer 1

Loading Protocol		+4% to -1%					
Clear Span		$4d_b$			$6d_b$		
Grade	Batch	Half-Cycles to Fracture	Percent Difference from B0	Percent Difference from B0-60	Half-Cycles to Fracture	Percent Difference from B0	Percent Difference from B0-60
60	0	33.33	-	-	20.00	-	-
	2	15.21	-54.4%	-54.4%	-	-	-
80	0	18.00	-	-46.0%	11.33	-	-43.3%
	1	-	-	-	11.72	3.4%	-41.4%
	2	8.09	-55.1%	-75.7%	-	-	-
100	0	27.33	-	-18.0%	12.67	-	-36.7%
	2	6.69	-75.5%	-79.9%	-	-	-

Table 4-17: Percent difference in fatigue life to fracture from batch 0 for #8 bars produced by manufacturer 1 under the +4% to -1% strain protocol

Conclusions

Overall, with the exception of batch 2, grade 80 bars produced by M1 did not show significant differences in their NHF across batches. Grade 80 bars did however exhibit significantly lower NHF compared with equivalently tested grade 60 bars. These reductions in number of half-cycles to fractures ranged from more than 75% to under 20%. Except for batch 2 bars, grade 80 M1 batches varied only in chemical composition, had similar deformation geometries, and were produced using the same processes and in the same mill. Test results therefore indicate that the chemical modifications attempted for the various grade 80 batches did not yield significantly different fatigue life to fracture.

The only grade 100 bars tested in this study from M1 were from batch 2. These grade 100 bars as well as grade 80 bars from batch 2 saw drastically fewer NHF compared with equivalently tested grade 60 bars. Batch 2 bars are however atypical of M1 production due to their bar deformation patterns, but highlight the importance of controlling bar deformations in ASTM specifications if reliable fatigue life is to be achieved.

Manufacturer 2

As described in more detail in section 3.1, M2 batches 1 and 2 and M2-B0-80-#5 bars varied from other batch 0 bars in the sharpness of the radius at the base of their deformations. In the latter batches, the deformation base radius was softened in an attempt to improve fatigue performance of the bars (Table 3-6).

#5 Bars

Both batches of M2 grade 80 #5 bars (M2-B1,2-80-6d_b) tested in this study displayed comparable but highly variable fatigue life to fracture (Figure 4-52 and Table 4-6). Both batches sustained similar minimum NHF of around 20 under the +4% to 0% strain protocol, similar maximum NHF of approximately 75, and a mean number of half-cycles to fracture that is within 1% of one another (Table 4-6). However, when examining the Coefficient of Variation (COV) for NHF, batch 1 results produced a COV of 0.411 and batch 2 results a COV of 0.569 (Table 4-7), implying that batch 1 results are more centrally distributed around the mean, though significant variability is still present. For M2-B2-80-6d_b bars, the distribution of fatigue life to fracture of specimens was bi-polar, with about half the specimens having a fatigue life to fracture around 25 half-cycles and the other half around 70 half-cycles. Neither batch 1 or 2 bars were able to reach the fatigue life of the batch 0 grade 80 bars, even though all these bars had comparable base deformation radii. However, both batch 1 and 2 bars still showed a significant increase in NHF over the baseline batch 0 grade 60 #5 bars (Figure 4-52, Table 4-18), which had sharper base deformation radii (Table 3-7).

Batch 1 of the grade 100 #5 bars produced by manufacturer 2 had the smallest variation of any #5 bars tested in this study, with a COV of 0.113 (Table 4-7). M2-B1-100-#5-6d_b bars

produced 125% higher NHF than M2-B0-100-6d_b bars, and close to 300% higher NHF than the baseline B0 grade 60 tests under the +4% to 0% strain protocol. M2-B0-100-#5-6d_b did not reach the NHF of the grade 80 #5 bars from batch 0, but had a significantly lower variability in results. It is noteworthy that the grade 100 #5 bars tested in this study (M2-B1-100-#5-6d_b) showed an increase of 56% in NHF compared with that of both batches of grade 80 #5 bars tested in the same manner (Table 4-18).

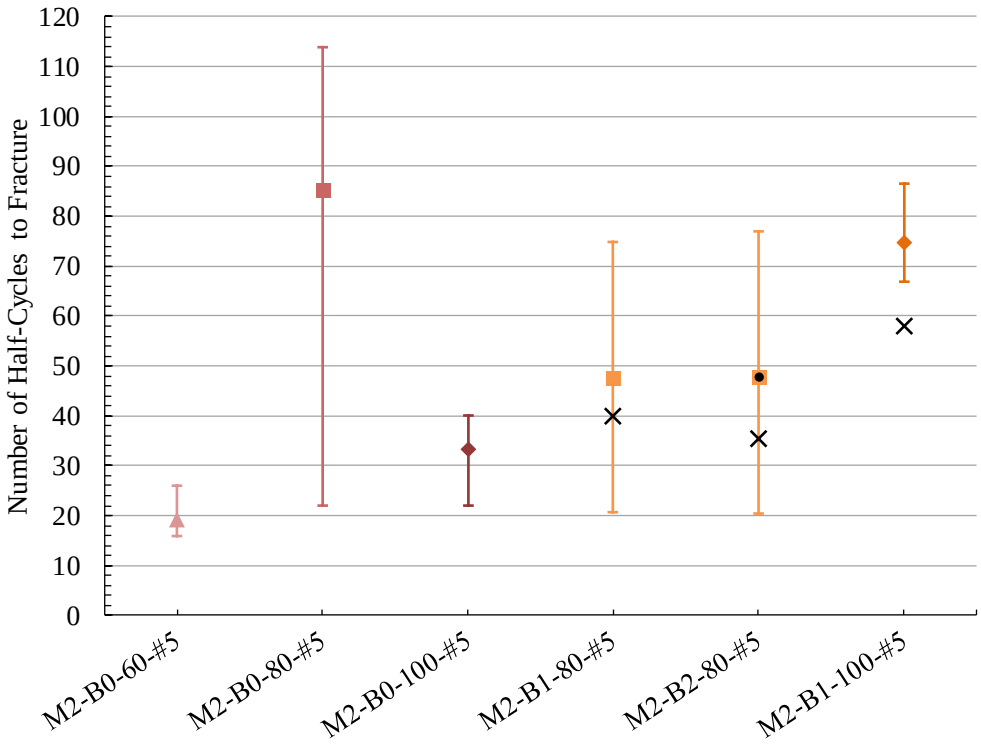

Figure 4-52: Number of half-cycles to fracture (NHF) for #5 bars tested under the +4% to 0% strain protocol with a clear span of 6d_b produced by manufacturer 2; the X markers indicate the mean NH80 values where applicable

Loading Protocol		+4% to 0%		
Clear Span		$6d_b$		
Grade	Batch	Half-Cycles to Fracture	Percent Difference from B0	Percent Difference from B0-60
60	0	19.33	-	-
80	0	85.50	-	342.2%
	1	47.71	-44.2%	146.8%
	2	48.00	-43.9%	148.3%
100	0	33.33	-	72.4%
	1	74.86	124.6%	287.2%

Table 4-18: Percent difference in fatigue life to fracture from batch 0 for #5 bars produced by manufacturer 2 under the +4% to 0% strain protocol

#8 Bars

As no grade 80 #8 bars were tested in batch 0, no direct comparison to prior grade 80 results can be made for M2. However, it can be seen that batch 1 grade 80 bars exhibited a 44% decrease in fatigue performance from equivalent batch 0 grade 60 bars tested under the +2% to -2% strain protocol and a clear span of $4d_b$ (Figure 4-53, Table 4-19). When the clear span is increased to $6d_b$, batch 1 grade 80 bars were observed to sustain 66% and 72% increases in NHF over the baseline batch 0 grade 60 bars for the +2% to -2% and +4% to -1% strain protocols, respectively (Figure 4-54, Table 4-19, Figure 4-55, Table 4-20). Additionally, for the +2% to -2% tests conducted at $4d_b$, the data point with highest NHF falls 1.5 standard deviations outside of the mean, contributing to a higher mean fatigue life, while for both of the strain protocols conducted at $6d_b$, one specimen fell significantly below the mean forcing the average fatigue life to be lower. Similar to the grade 80 results, batch 1 of the grade 100 bars, compared to equivalent grade 60 bars of batch 0, showed a decrease in fatigue performance when tested under the +2% to -2% strain protocol at $4d_b$, but an increase in fatigue performance under the +4% to -1% strain protocol at $6d_b$.

It appears that the higher grade bars exhibit improved fracture fatigue life compared to grade 60 bars when significant bar buckling is experienced but not when buckling was limited at a clear span of $4d_b$. Notably, the grade 80 bars of batch 1 experienced nearly the same NHF in the +2% to -2% strain protocol at both the $4d_b$ and $6d_b$ clear spacing (Figure 4-53, Figure 4-54). Grade 60 bars on the other hand saw a significant drop in NHF when tested at a $6d_b$ clear span as opposed to a $4d_b$ clear span. It is possible the increased hardness of the outer shell of the higher grade bars as a result of the quenching process contributed to the improved toughness when buckling concentrates the highest strain demands at the bar outer layers. The differences between grade 60 batch 0 bars and higher grade bars of batch 1 in terms of number of half-cycles to 80% peak strength (NH80) are less significant as can be seen in Figure 4-54 and Figure 4-55. This indicates that while the quenching process is extending the number of cycles to bar fracture, the gradual increase in crack length and width in the higher-grade bars limits the contribution of these bars to member strength in the latter cycles.

Limited comparisons between batch 3 and the results from the previous study can be made as there is only a single overlapping clear span and strain protocol. Grade 60 #8 bars from batch 0 had slightly sharper deformation radii than batch 3 grade 60 bars (Table 3-6) which manifested itself in limited change in NHF under the +2% to -2% strain protocol and a clear span of $4d_b$ (Table 4-19). Grade 80 and 100 #8 bars from batch 3 showed a small decrease in NHF compared to the baseline grade 60 results and to the results of higher grade bars from batch 1.

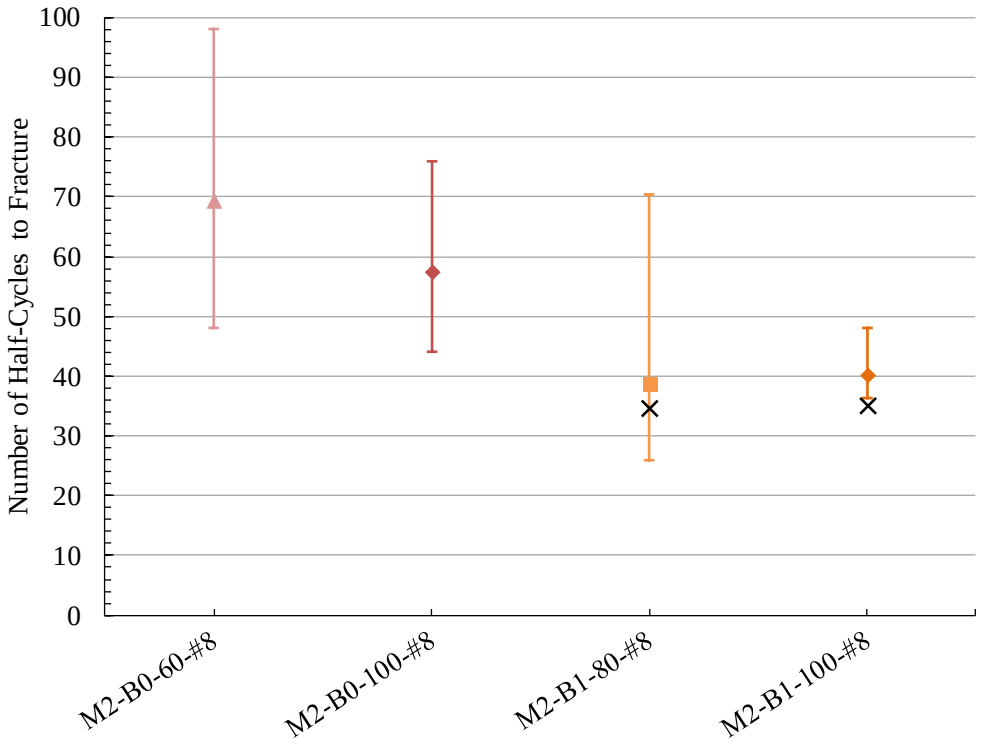

Figure 4-53: Number of half-cycles to fracture (NHF) for #8 bars tested under the +2% to -2% strain protocol with a clear span of $4d_b$ produced by manufacturer 2; the X markers indicate the mean NH80 values where applicable

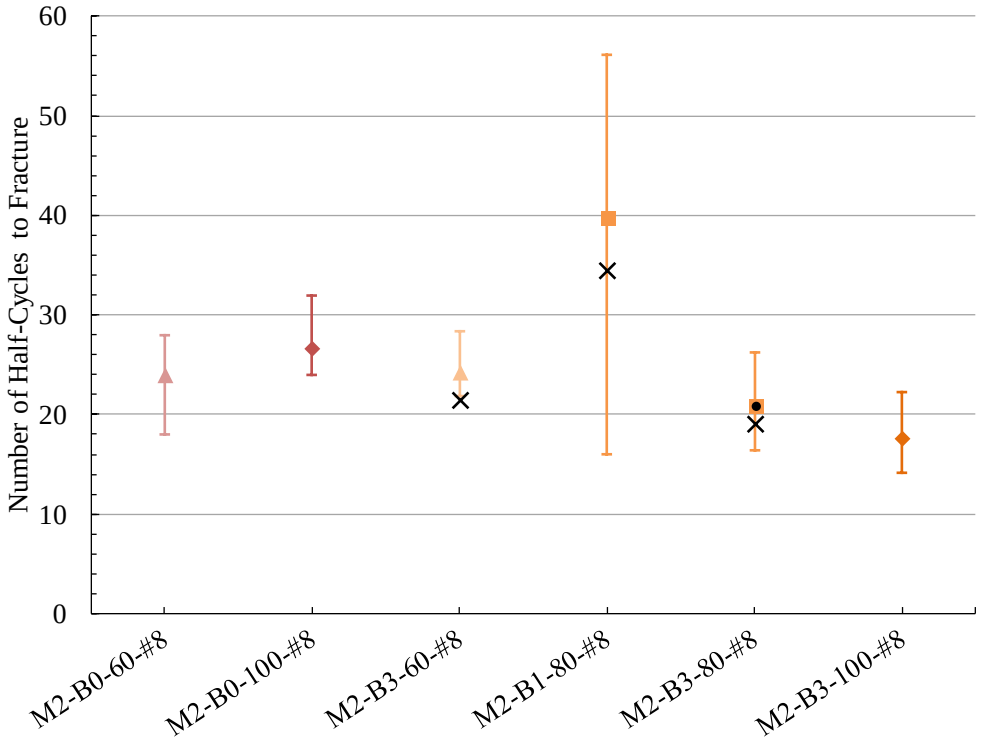

Figure 4-54: Number of half-cycles to fracture (NHF) for #8 bars tested under the +2% to -2% strain protocol with a clear span of $6d_b$ produced by manufacturer 2; the X markers indicate the mean NH80 values where applicable

Loading Protocol		+2% to -2%					
Clear Span		$4d_b$			$6d_b$		
Grade	Batch	Half-Cycles to Fracture	Percent Difference from B0	Percent Difference from B0-60	Half-Cycles to Fracture	Percent Difference from B0	Percent Difference from B0-60
60	0	69.33	-	-	24.00	-	-
	3	-	-	-	24.19	0.8%	0.8%
80	1	38.68	-	-44.2%	39.76	-	65.7%
	3	-	-	-	20.89	-	-13.0%
100	0	57.33	-	-17.3%	26.67	-	11.1%
	1	40.11	-30.0%	-42.2%	-	-	-
	3	-	-	-	17.57	-34.1%	-26.8%

Table 4-19: Percent difference in fatigue life to fracture from batch 0 for #8 bars produced by manufacturer 2 under the +2% to -2% strain protocol

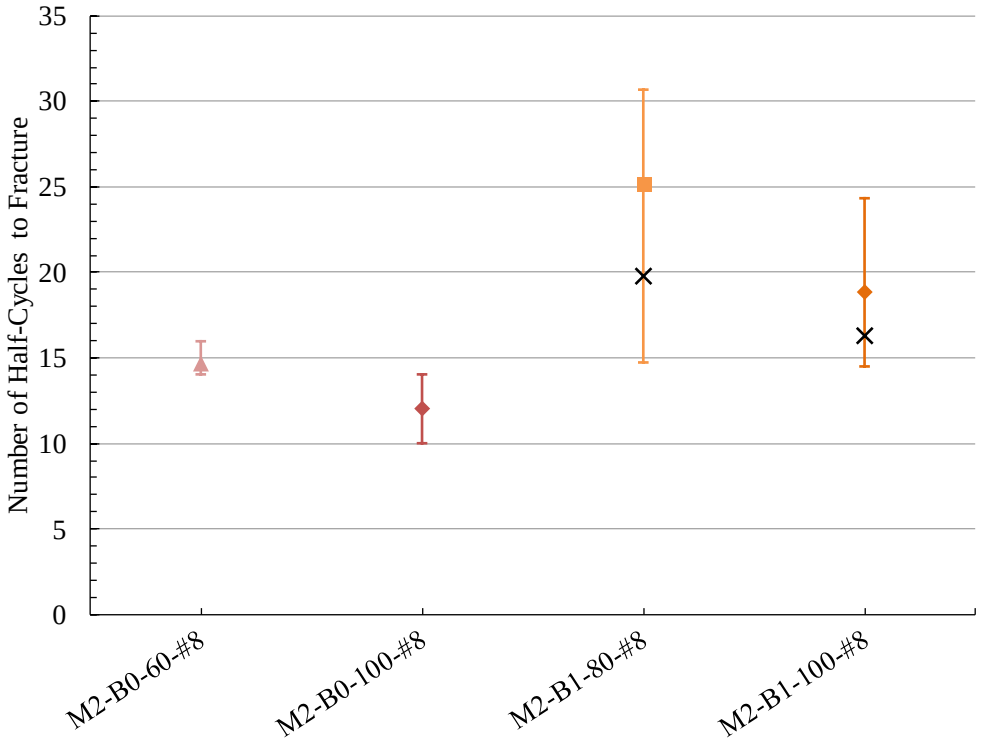

Figure 4-55: Number of half-cycles to fracture (NHF) for #8 bars tested under the +4% to -1% strain protocol with a clear span of $6d_b$ produced by manufacturer 2; the X markers indicate the mean NH80 values where applicable

Loading Protocol		+4% to -1%					
Clear Span		$4d_b$			$6d_b$		
Grade	Batch	Half-Cycles to Fracture	Percent Difference from B0	Percent Difference from B0-60	Half-Cycles to Fracture	Percent Difference from B0	Percent Difference from B0-60
60	0	25.33	-	-	14.67	-	-
80	1	-	-	-	25.22	-	72.0%
100	0	28.50	-	12.5%	12.00	-	-18.2%
	1	-	-	-	18.86	57.2%	28.6%

Table 4-20: Percent difference in fatigue life to fracture from batch 0 for #8 bars produced by manufacturer 2 under the +4% to -1% strain protocol

Conclusions

Results from manufacturer 2 varied across bar size and grade. Neither batch of grade 80 #5 bars tested in this study were able to match previous grade 80 results, but still surpassed the fatigue life of grade 60 bars. The grade 100 #5 bars showed a dramatic improvement in fatigue life for the batches tested in this study, more than doubling the recorded fatigue life to fracture from batch 0. The #8 bars showed mixed results. For a clear span of $4d_b$, the #8 high-strength bars tested were unable to match the fatigue performance of grade 60 bars, with the grade 100 batch 1 bars lagging in fatigue life from batch 0 bars. At a clear span of $6d_b$, the results were mixed for #8 bars, with several batches of HSRB meeting or surpassing the fatigue life to fracture of comparable grade 60 bars and others showing worse performance. In general, the bars produced by manufacturer 2 showed significant variation in fatigue life.

4.2.3.2 Effects of Bar Grade

Figure 4-56 provides the number of half-cycles to fracture (NHF), number of half-cycles to 80% of the tensile strength at the initial cycle (NH80), and the maximum and minimum values of NHF for each batch of #5 bars tested under the +4% to 0% strain protocol with a clear span of $6d_b$. As can be seen in the figure, a significant amount of variability in results exists per bar type

and across all grades and manufacturers. For manufacturer 1, the grade 60 batch 0 bars had the best fatigue performance, while the grade 80 and grade 100 bars performed comparably at approximately 20% reduction in NHF compared with grade 60 batch 0 bars. Manufacturer 2 bars trended in the opposite direction with grade 60 batch 0 bars performing significantly worse than both grade 80 and grade 100 bars from batches 0 and 1. This may be due to the tighter deformation-base radii of the grade 60 bars of batch 0. The batches of grade 80 #5 bars from manufacturer 2 consistently had the highest variability of all #5 tests. The grade 100 #5 bars produced by manufacturer 3 in batch 1 exhibit a fatigue life that is well below that of grade 100 bars produced by other manufacturers as well as all batches of grade 60 and grade 80 bars from manufacturer 1 and 2, with the exception of M1-B0-80-#5 bars. M3-B1-100-#5 bars had significantly flatter bar deformations and larger deformation base radii compared with other bars from M3 as well as other manufactures (Table 3-7). These deformation properties are not typical of M3 production and may be due to a production anomaly. However, here again, the data suggests that stricter limits on bar deformations are needed to ensure adequate fatigue life in reinforcing bars.

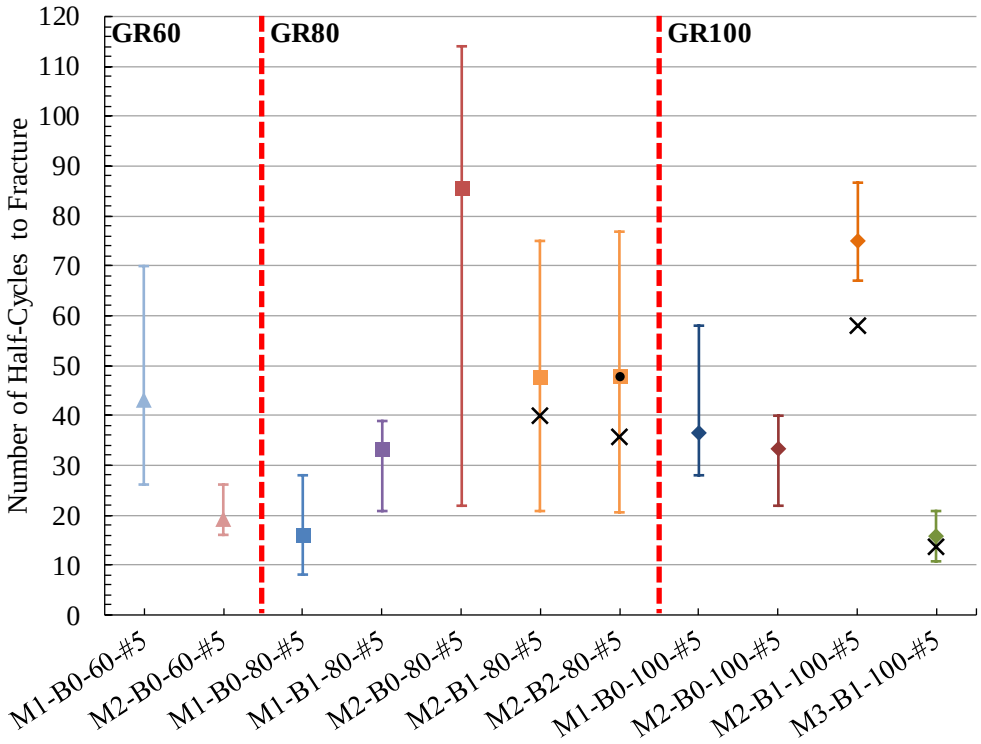

Figure 4-56: Number of half-cycles to fracture (NHF) for #5 bars tested under the +4% to 0% strain protocol with a clear span of $6d_b$; the X markers indicate the mean NH80 values where applicable

Figure 4-57 and Figure 4-58 provide the number of half-cycles to fracture (NHF), number of half-cycles to 80% of the tensile strength at the initial cycle (NH80), and the maximum and minimum values of NHF for each batch of #8 bars +2% to -2% strain protocol with a clear spans of $4d_b$ and $6d_b$, respectively. As can be seen in the figures, the M1-B2 bars of grades 80 and 100 performed significantly worse than all other bars. This was attributed to their non-conventional bar deformation geometries. In the following comparisons, these bars will not be considered. For a clear span of $4d_b$, grade 80 bars exhibited a fatigue life that is less than that of grade 60 bars for both manufacturers 1 and 2. The grade 100 bars showed significant scatter in their results, with those produced by manufacturer 1 performing better than their grade 60 and 80 counterparts and those from manufacturer 2 besting grade 80 performance but unable to reach the fatigue life of grade 60 counterparts from the same manufacturer.

Consistent with the $4d_b$ results, at a clear span of $6d_b$, grade 80 bars were unable to meet the performance of grade 60 bars, with the exception of batch 1 bars produced by manufacturer 2. However, it can be noted that due to the large variation in results between specimens for that batch, some tests failed at values lower than those of comparable grade 60 bars. Again, significant scatter in results occurred with grade 100 bars, with several batches surpassing the benchmark grade 60 results while others did not. Grade 100 bar fatigue lives, however, exceeded those of grade 80 bars in some cases. Two nominally identical batches of grade 100 bars from manufacturer 3 showed the second highest and the lowest fatigue performance under the clear span and strain protocol represented in Figure 4-58. It is not clear why the bars from manufacturer 3 show such variability in their response at this stage.

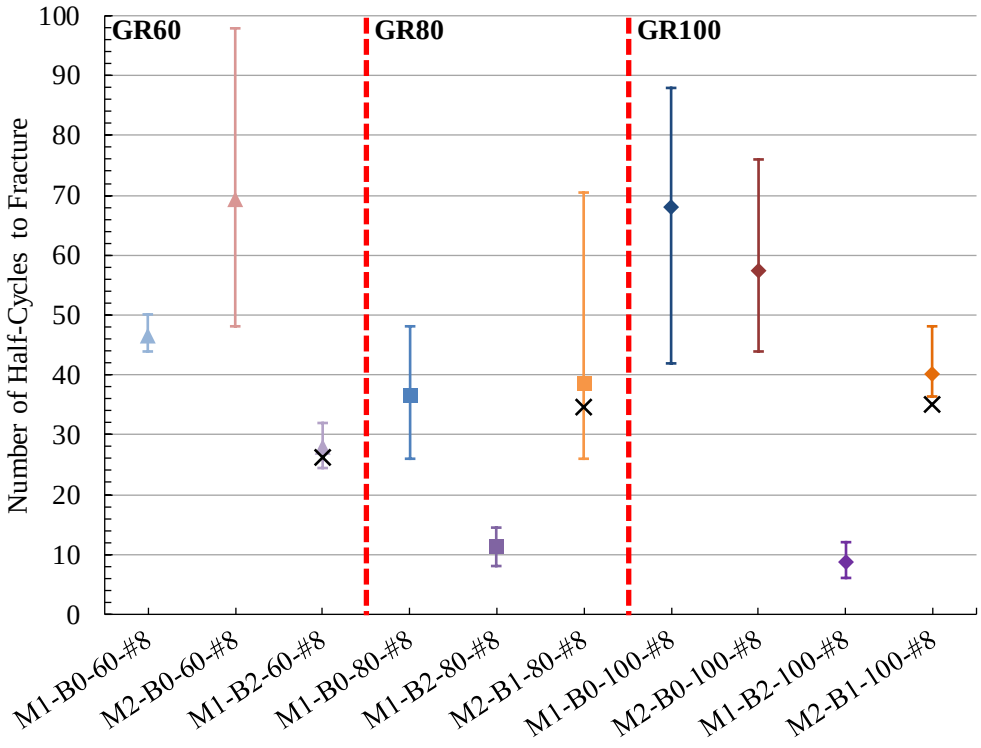

Figure 4-57: Number of half-cycles to fracture (NHF) for #8 bars tested under the +2% to -2% strain protocol with a clear span of $4d_b$; the X markers indicate the mean NH80 values where applicable

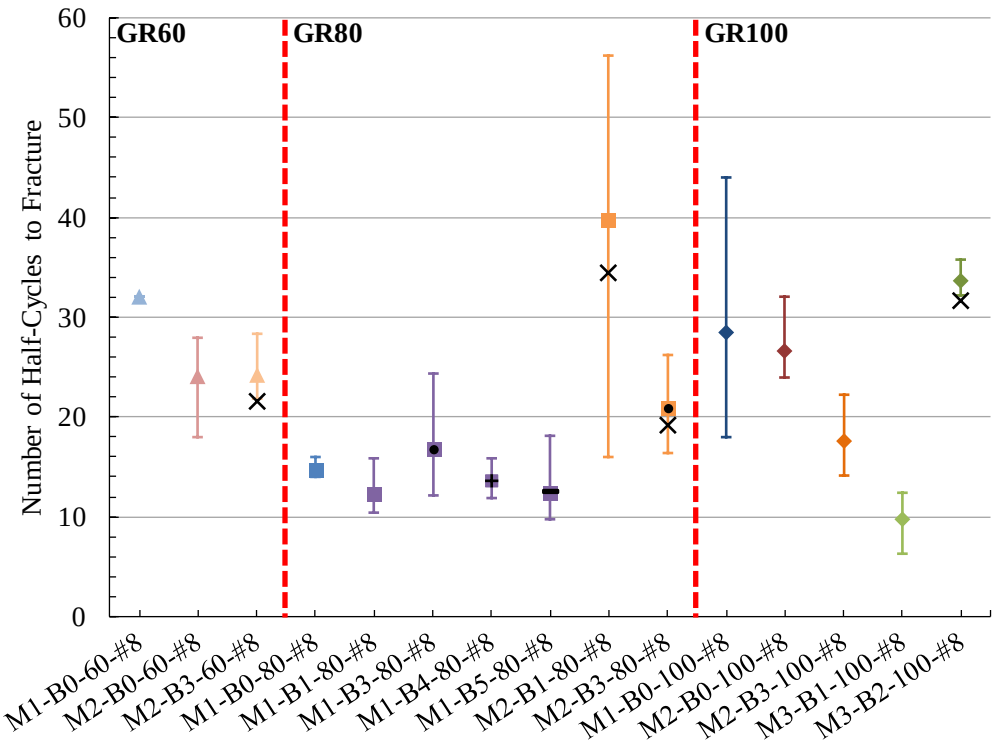

Figure 4-58: Number of half-cycles to fracture (NHF) for #8 bars tested under the +2% to -2% strain protocol with a clear span of $6d_b$; the X markers indicate the mean NH80 values where applicable

Bars tested at a clear span of $6d_b$ under the +4% to -1% strain protocol yielded similar trends to those tested under +2% to -2% strain at the same clear span (Figure 4-59). M1 grade 80 bars were unable to meet the performance of grade 60 bars from the same manufacturer. Batch 1 grade 80 bars produced by manufacturer 2 had higher NHF values compared with their grade 60 counterparts. Grade 100 bars from M1 exhibited comparable fatigue life to grade 80 bars from M1 and lower than that of the grade 60 bar counterparts. Batch 0 grade 100 bars from M2 exhibited lower fatigue life than comparable grade 60 bars but batch 1 grade 100 bars saw larger NHF and NH80 values than their grade 60 counterparts.

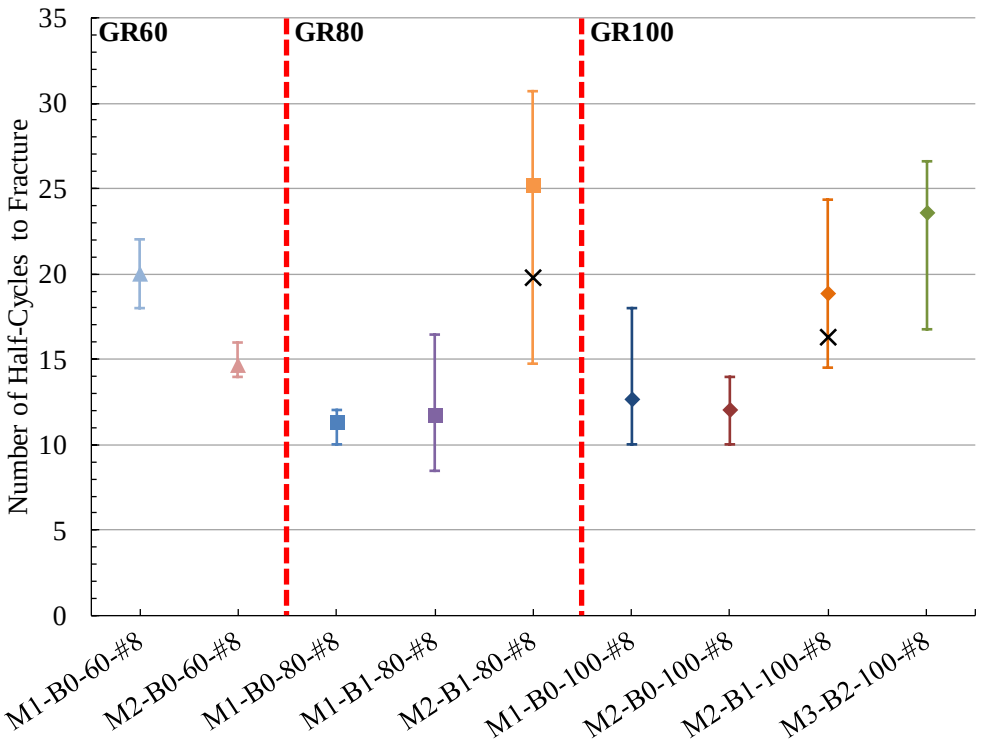

Figure 4-59: Number of half-cycles to fracture (NHF) for #8 bars tested under the +4% to -1% strain protocol with a clear span of $6d_b$; the X markers indicate the mean NH80 values where applicable

4.2.3.3 Effects of Clear Span

Previous research by Ghannoum and Slavin (2016) focused on clear spans of between $4d_b$ and $6d_b$, however, in this study tests at $8d_b$ were conducted to evaluate the effects of clear span and buckling on bar fatigue life. Only bars that were tested using the same strain protocol at multiple clear spans are included in this discussion. Consequently, this section deals primarily with #8 bars from manufacturer 2. Previous research by Ghannoum and Slavin (2016) indicated a strong inverse relationship between clear span and fatigue life namely an increase in clear span causes a decrease in the number of half-cycles to fracture (NHF). In the current study, a clear span of $8d_b$ was added to further explore this behavior.

Figure 4-60, Figure 4-61, and Figure 4-62 show the fatigue performance of #8 bars produced by manufacturer 2 under a +2% to -2% strain protocol and multiple clear spans.

Although each plot contains results from a single bar type but multiple batches, a clear trend emerges. The decrease in fatigue performance caused by increasing clear span appears to level off after $6d_b$, that is, increasing the clear span to $8d_b$ did not appear to reduce the NHF significantly from the $6d_b$ values. Additionally, the variability in test results from samples of the same batch and bar type is observed to decrease substantially as the clear span increases. The grade 60 #8 bars saw a decrease of nearly 50 half-cycles when tested at a clear span of $6d_b$ instead of $4d_b$ (Figure 4-60). However, the same bars had equivalent NHF at clear spans of $6d_b$ and $8d_b$ (Figure 4-60). The same trend was observed for the grade 100 bars (Figure 4-62). The grade 80 bars on the other hand, showed large variabilities in their NHF results both within a batch and between batches. However, a similar trends of equivalent NHF at clear spans of $6d_b$ and $8d_b$ can be seen for the grade 80 bars of batch 3 (Figure 4-61).

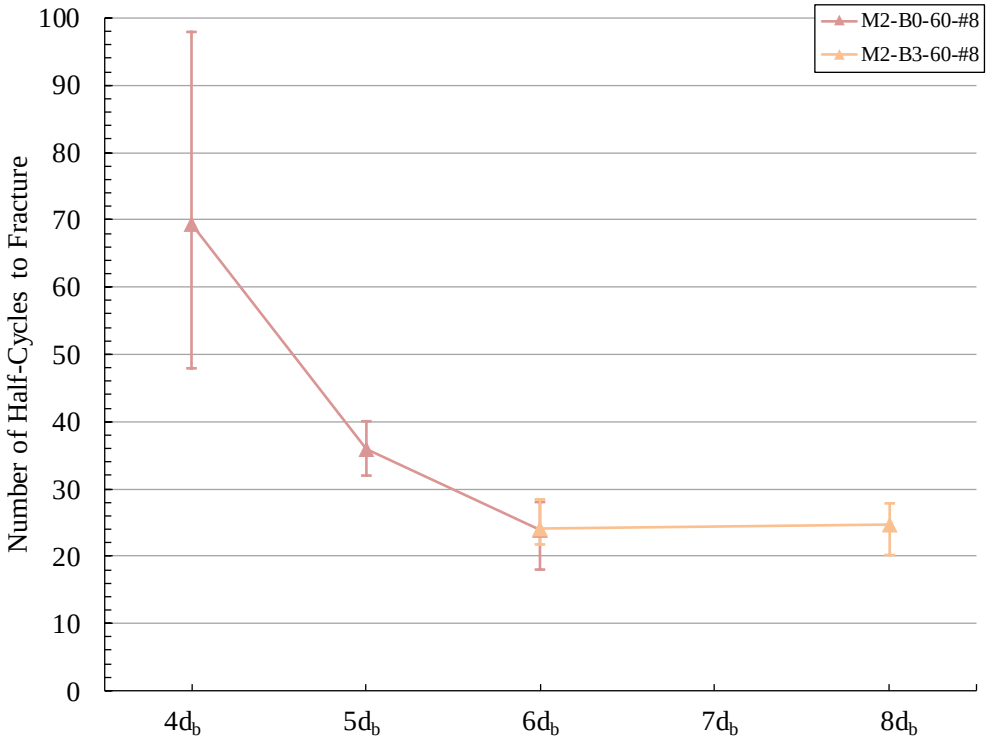

Figure 4-60: Half-cycles to fracture for grade 60 #8 bars from manufacturer 2 tested under the +2% to -2% strain protocol under multiple clear spans

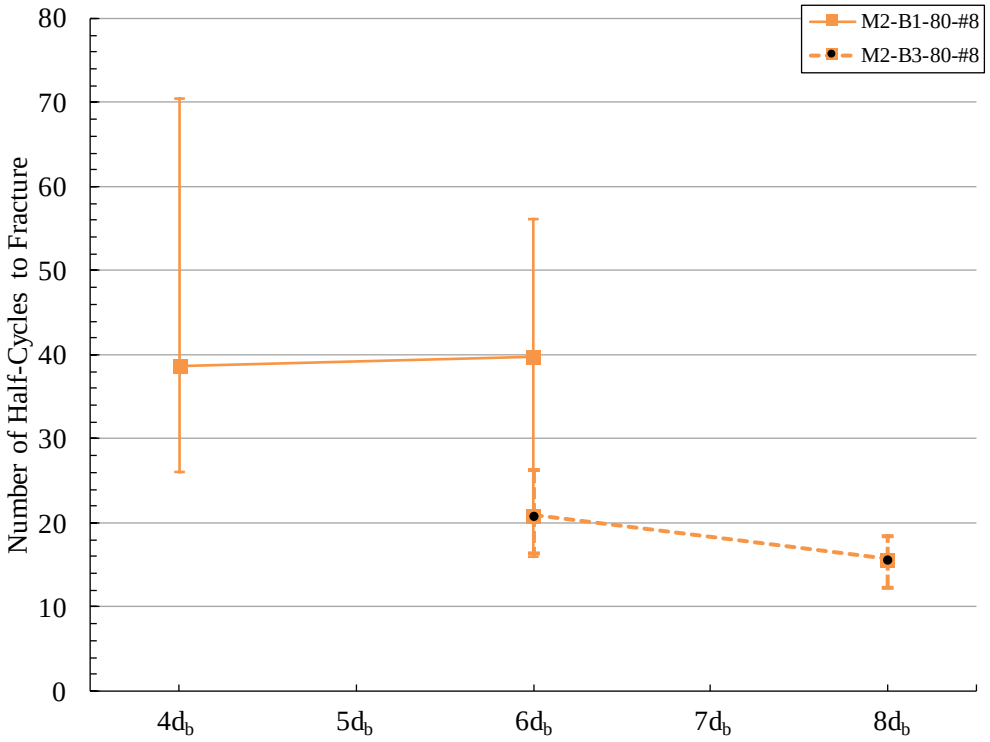

Figure 4-61: Half-cycles to fracture for grade 80 #8 bars from manufacturer 2 tested under the +2% to -2% strain protocol under multiple clear spans

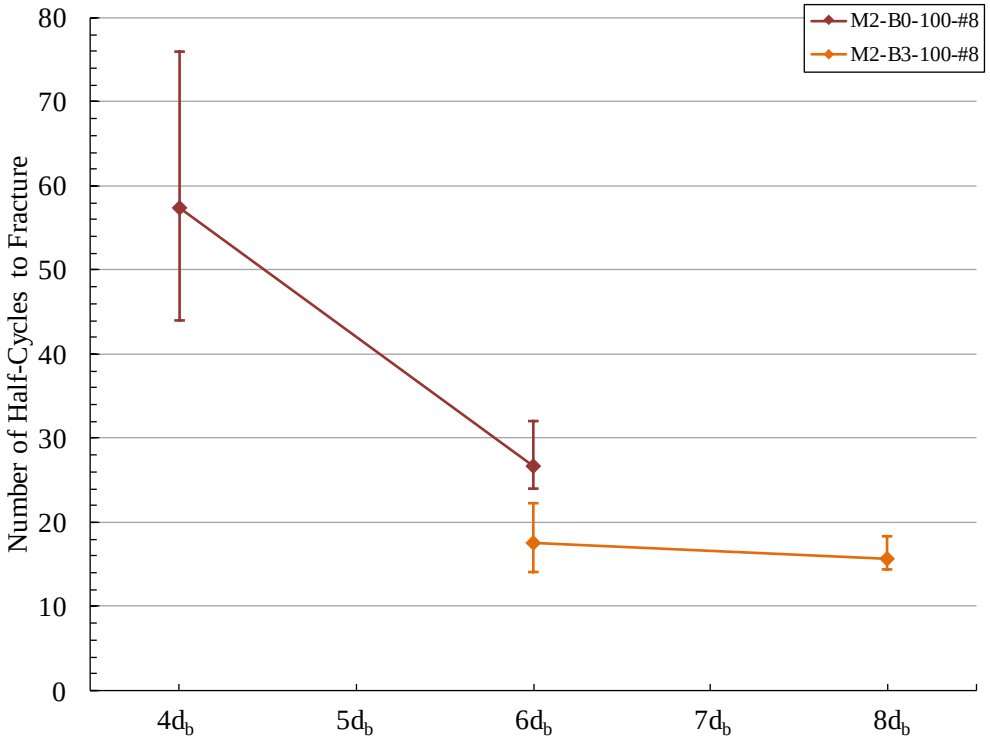

Figure 4-62: Half-cycles to fracture for grade 100 #8 bars from manufacturer 2 tested under the +2% to -2% strain protocol under multiple clear spans

Figure 4-63 and Figure 4-64 plot the results of the #8 bars from batch 3 produced by manufacturer 2 under two additional strain protocols (+4% to 0% and +6% to 0%). For both strain protocols, the grade 60 bars resisted significantly fewer half-cycles to fracture at a clear span of $8d_b$ compared to $6d_b$, which is different to the behavior of grade 60 bars under the +2% to -2% strain protocol. The grade 80 and 100 bars on the other hand sustained similar NHF at the clear spans of $6d_b$ and $8d_b$. It is not clear why the grade 60 bars showed different trends at the different strain protocols at this stage. As the test matrix of the overall project becomes more complete, these trends will be investigated in more detail.

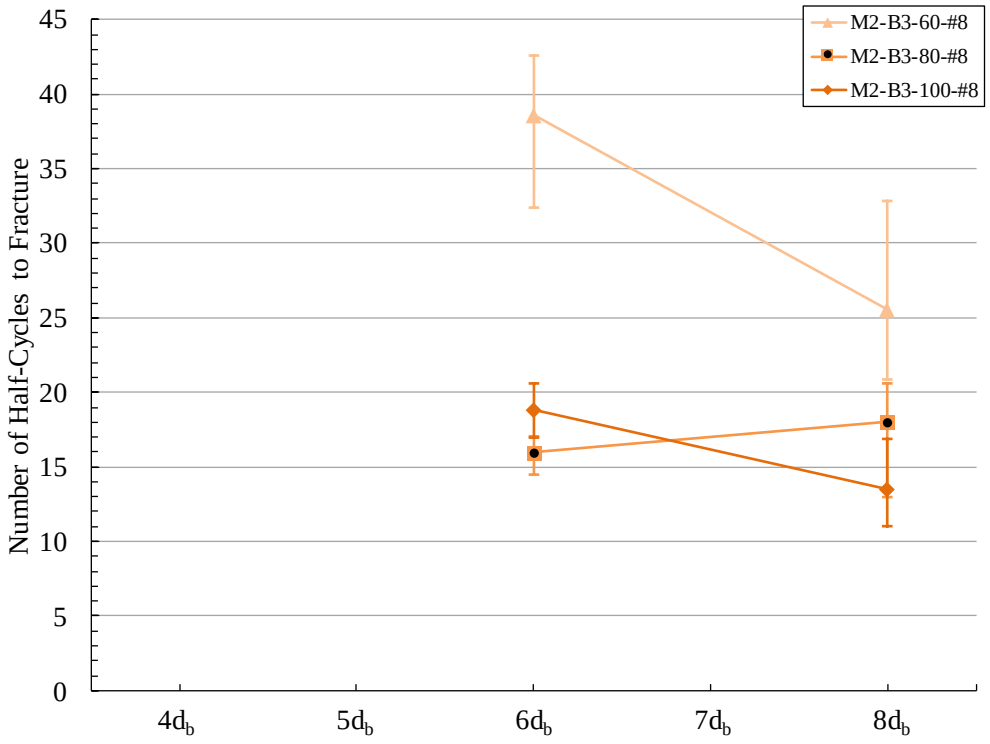

Figure 4-63: Half-cycles to fracture for batch 3 of #8 bars from manufacturer 2 tested under the +4% to 0% strain protocol under multiple clear spans

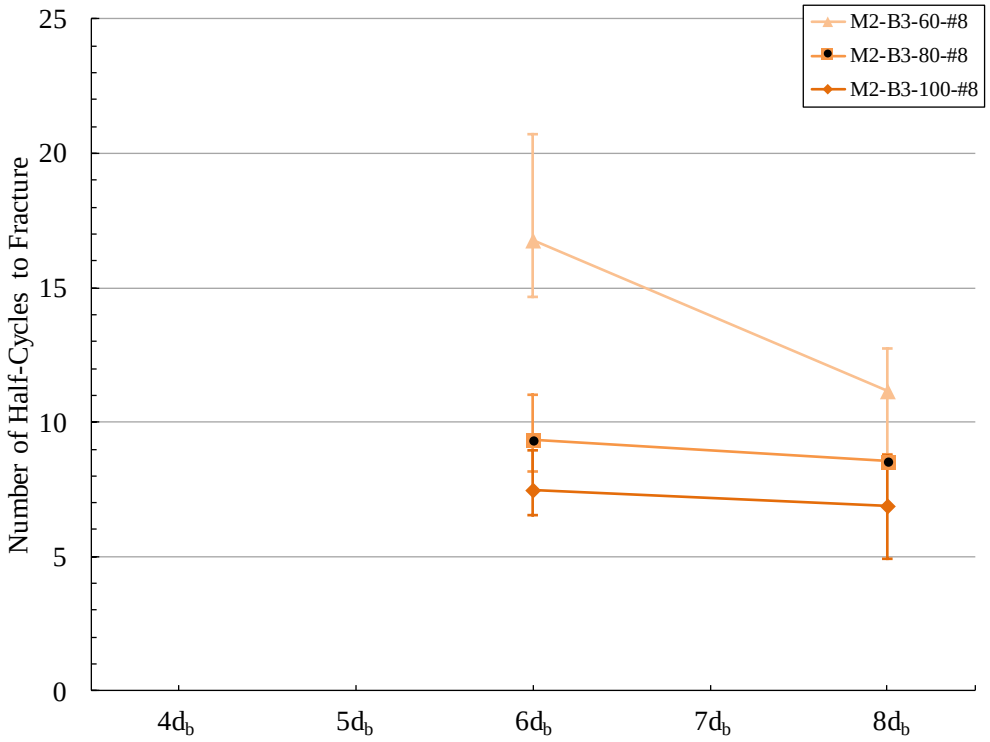

Figure 4-64: Half-cycles to fracture for batch 3 of #8 bars from manufacturer 2 tested under the +6% to 0% strain protocol under multiple clear spans

4.2.3.4 Effects of Strain Protocol

Only bars that were tested using multiple strain protocols at the same clear spans are included in the following discussion. Figure 4-65, Figure 4-66, and Figure 4-67 plot the number of half-cycles to failure against the strain protocol for bars tested at a clear span of $4d_b$. As demonstrated in previous research, it can be seen in the figures that an increase in total strain amplitude causes a decrease in fatigue life. The +2% to -2% and +4% to 0% (4% total strain amplitude) tests showed consistently higher fatigue performance than the +4% to -1% (5% total strain amplitude) tests and the +4% to -2% and +6% to 0% (6% total strain amplitude) tests. Additionally as the applied cyclic strain amplitude increased, the variability in the results decreased. As these tests were conducted at a clear span of $4d_b$, buckling effects were reduced.

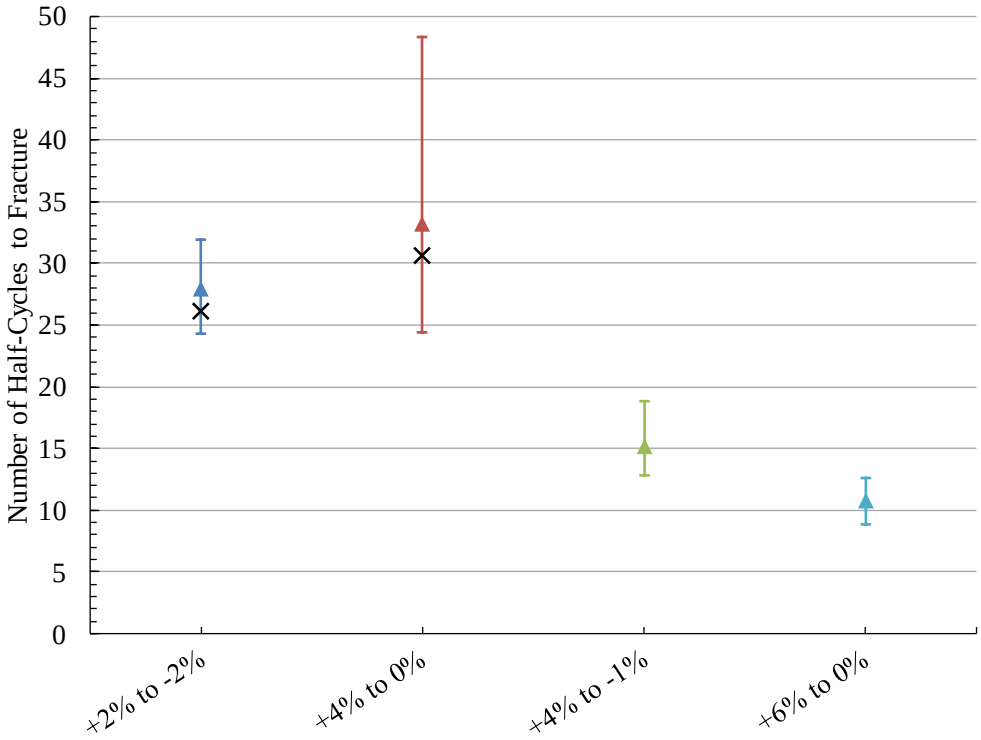

Figure 4-65: Half-cycles to fracture for M1-B2-60-#8 tested under multiple strain protocols at $4d_b$

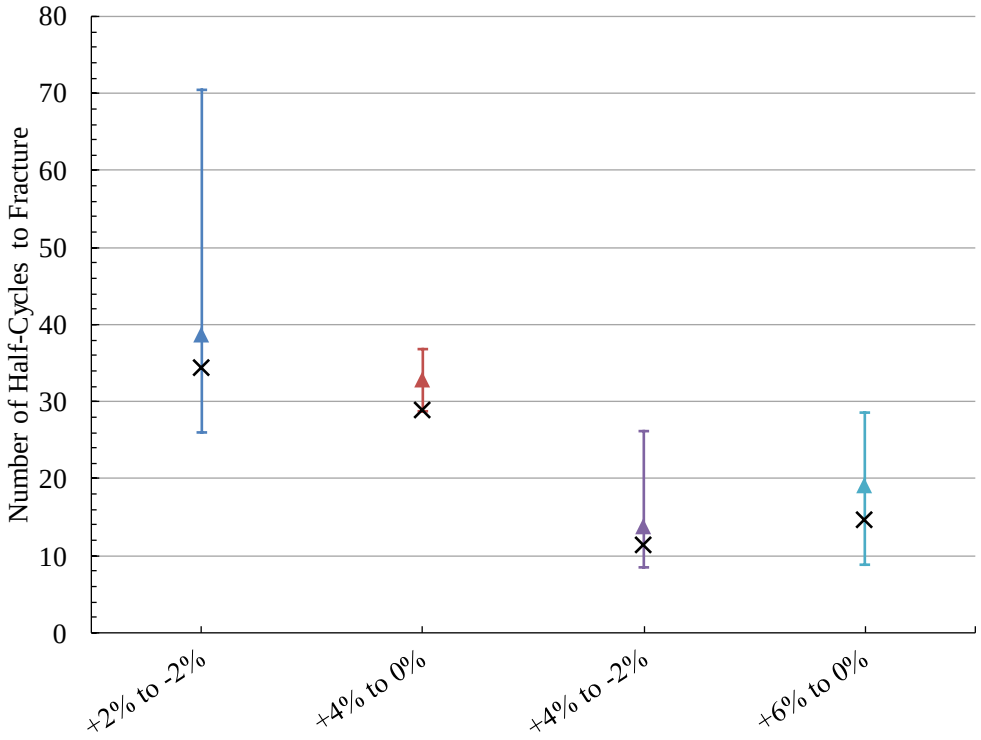

Figure 4-66: Half-cycles to fracture for M2-B1-80-#8 tested under multiple strain protocols at $4d_b$

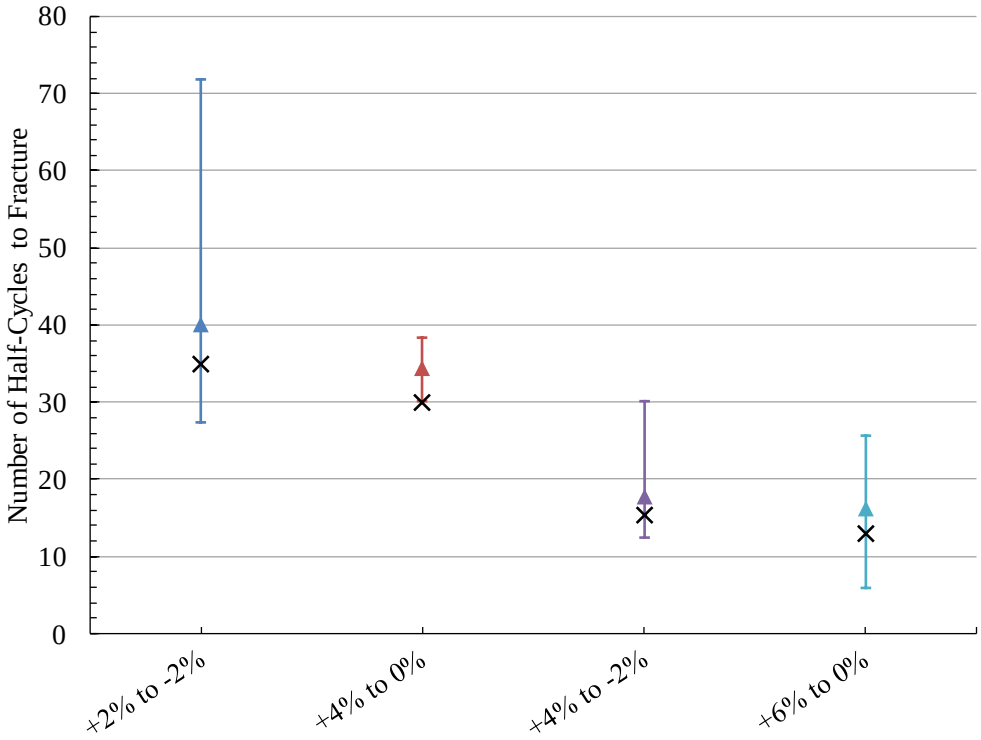

Figure 4-67: Half-cycles to fracture for M2-B1-100-#8 tested under multiple strain protocols at $4d_b$

Figure 4-68, Figure 4-69, and Figure 4-70 show the number of half-cycles to failure for 3 different strain protocols and 2 clear spans for #8 bars from batch 3 produced by manufacturer 2. Except for the grade 60 bars tested under the +2% to -2% strain protocols, these bars exhibited significant reductions in NHF when tested at a clear span of $8d_b$ compared to $6d_b$. The grade 100 bars showed similar but smaller reductions in NHF when tested at a clear span of $8d_b$ compared to $6d_b$, with almost no reduction under the strain protocol of +6% to 0%. The grade 80 bars instead showed mixed results that indicate limited changes within the scatter of the data in the NHF across all strain protocols when changing the clear span.

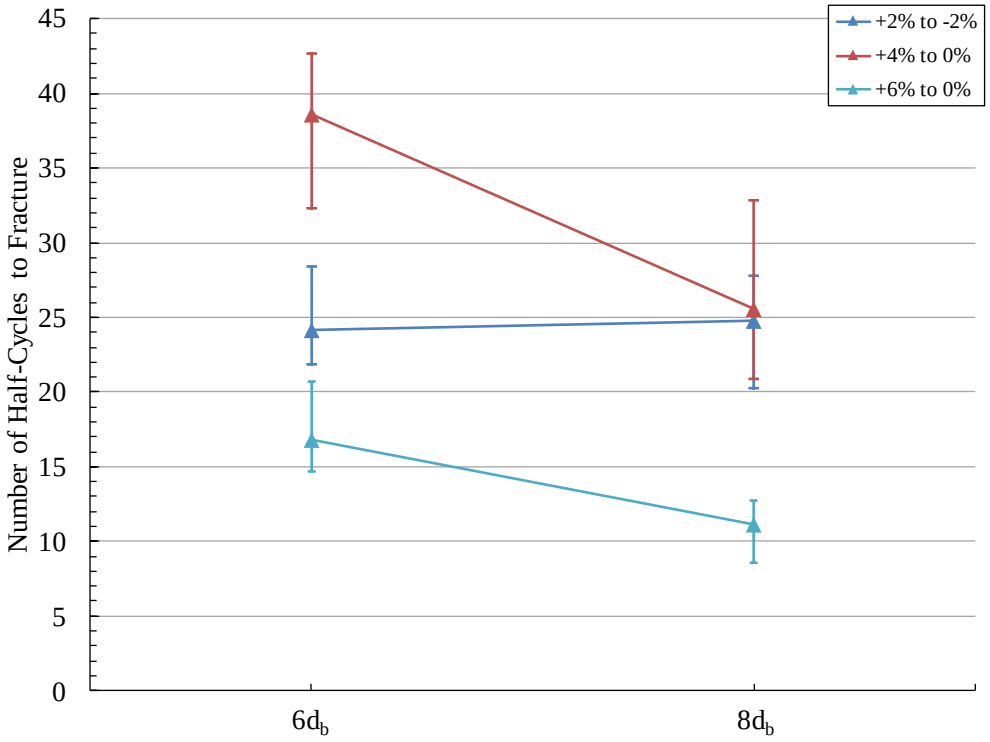

Figure 4-68: Half-cycles to fracture for M2-B3-60-#8 tested under multiple strain protocols

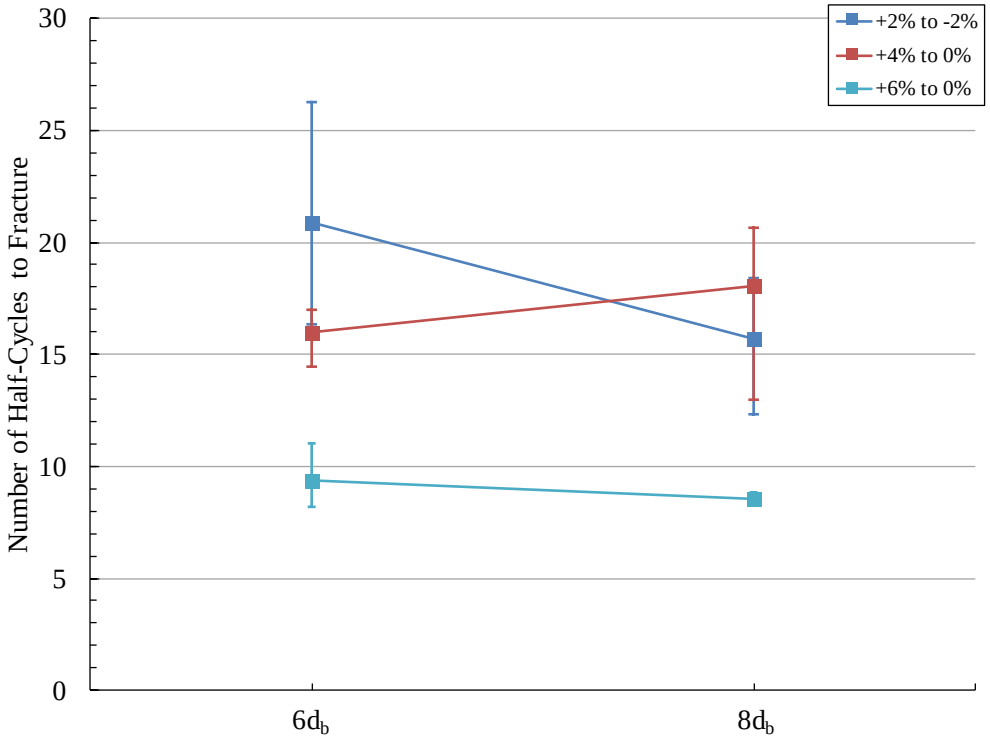

Figure 4-69: Half-cycles to fracture for M2-B3-80-#8 tested under multiple strain protocols

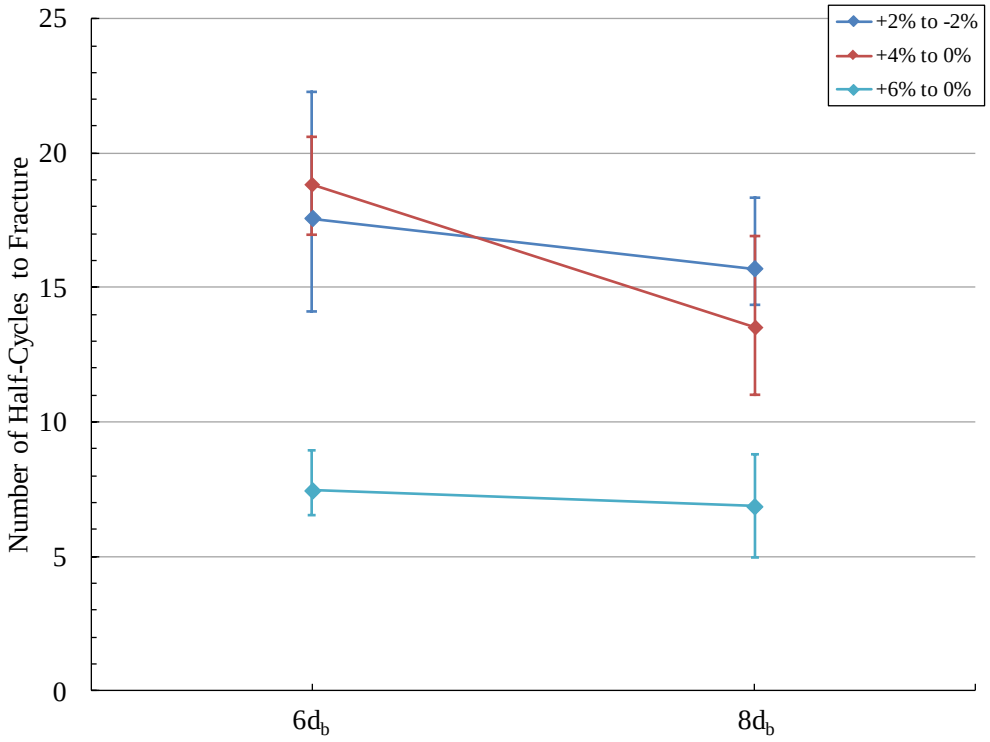

Figure 4-70: Half-cycles to fracture for M2-B3-100-#8 tested under multiple strain protocols

Figure 4-71 plots the fatigue life of #8 bars from batch 1 produced by manufacturer 3 and tested with four different loading protocols and two clear spans. As can be seen in the figure, mixed results were observed that indicate limited changes within the scatter of the data in the NHF across all strain protocols when changing the clear span from $6d_b$ to $8d_b$.

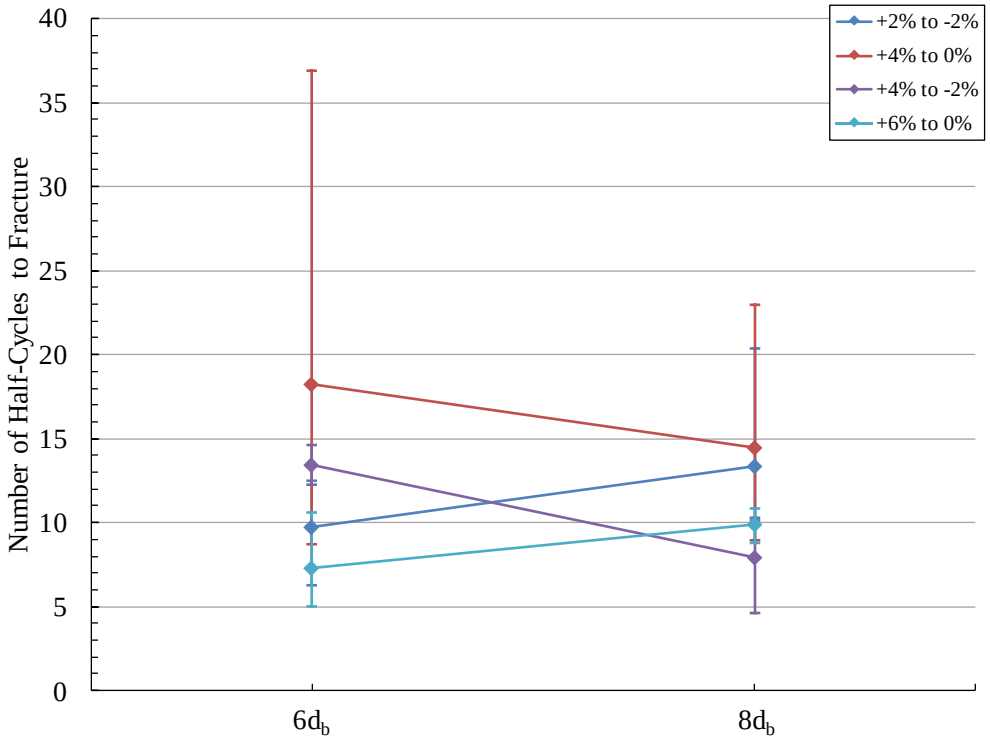

Figure 4-71: Half-cycles to fracture for M3-B1-100-#8 tested under multiple strain protocols

4.2.3.5 Effects of Manufacturing Process

Only bars of the same grade that were tested using the same strain protocols and at the same clear span are included in this discussion. Figure 4-72 and Figure 4-73 plot the results from grade 80 tests conducted at a clear span of $6d_b$ under two different strain protocols. At both protocols, the bars produced by manufacturer 2 have a higher number of half-cycles to fracture than those produced by manufacturer 1. Specimens from manufacturer 1 were able to maintain a tension strength above 80% of the first cycle strength up until failure, while those from manufacturer 2 saw significant strength reduction before fracture occurs. Even when this is considered, bars from manufacturer 2 still had higher NH80 values than the NHF values of bars from manufacturer 1. The bars produced by manufacturer 1 exhibit a lower amount of variability in their results than the bars produced by manufacturer 2.

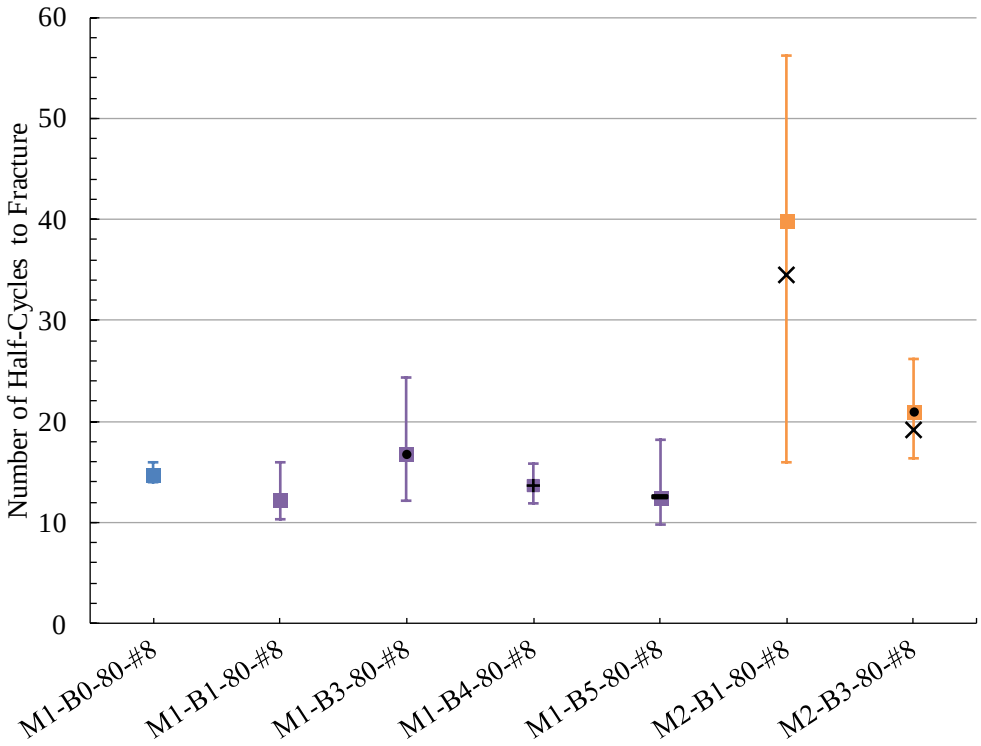

Figure 4-72: Half-cycles to fracture for grade 80 #8 bars under a +2% to -2% strain protocol at a clear span of $6d_b$

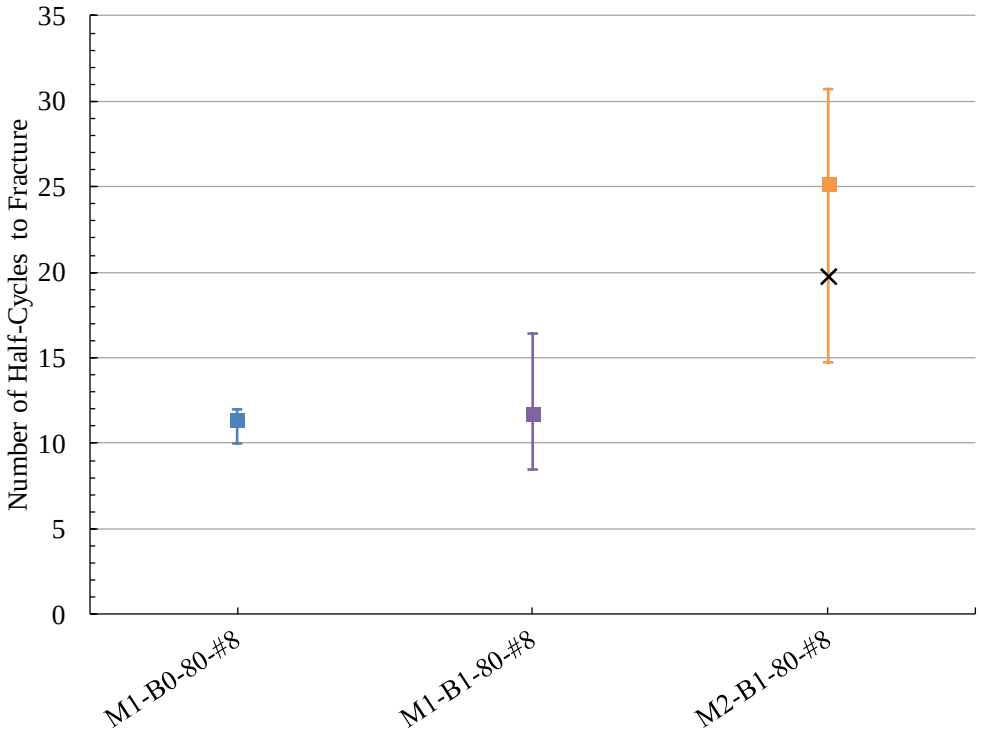

Figure 4-73: Half-cycles to fracture for grade 80 #8 bars under a +4% to -1% strain protocol at a clear span of $6d_b$

Figure 4-74 and Figure 4-75 plot the results from grade 100 tests from all three manufacturers that were conducted at a clear span of $6d_b$ and under two different strain protocols. Bars from different batches produced by manufacturer 2 and manufacturer 3 performed inconsistently compared to bars from manufacturer 1. For the +2% to -2% loading protocol, batch 3 from manufacturer 2 and batch 1 from manufacturer 3 had a fatigue life that is lower than those of bars from manufacturer 1. For the +4% to -1% loading protocol, batch 1 from manufacturer 2 and batch 2 from manufacturer 3 had a fatigue life that is higher than those of bars from manufacturer 1. Bars from batch 2 of manufacturer 3 had the highest fatigue life of any grade 100 #8 bars tested at these strain protocols and clear spans.

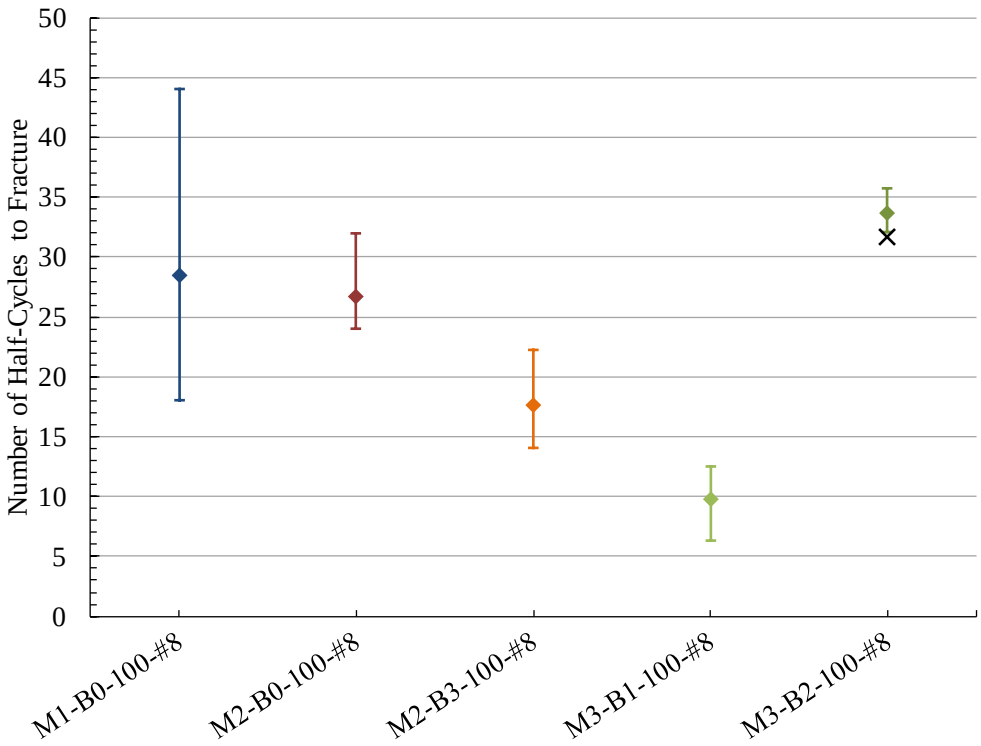

Figure 4-74: Half-cycles to fracture for grade 100 #8 bars under a +2% to -2% strain protocol at a clear span of $6d_b$

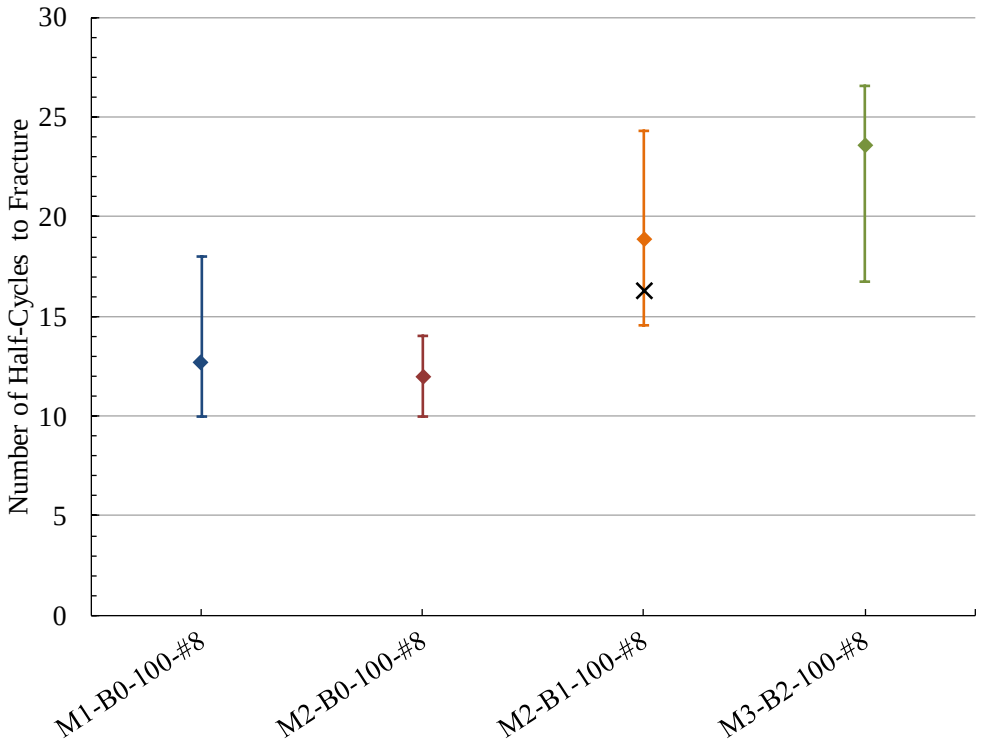

Figure 4-75: Half-cycles to fracture for grade 100 #8 bars under a +4% to -1% strain protocol at a clear span of $6d_b$

5. ANALYSIS OF TEST RESULTS AND CONCLUSIONS

5.1 FATIGUE LIFE MODELING

Several relationships for the prediction of fatigue life based on the strain amplitude have been proposed (Mander et al. 1994, Brown and Kunnath 2004, Hawileh et al. 2010, Ghannoum and Slavin, 2016). However, due to the recent developments in the production of HSRB, some of these relations no longer apply. Ghannoum and Slavin (2016) proposed a power function as previously discussed in section 2.2, where the coefficients of the equation are derived experimentally from low-cycle fatigue tests. This equation is reproduced below.

$$\text{Half-Cycles to Failure} = c*(\text{Total Strain Range})^{d}$$

Equation 2-1: Fatigue life modeling with fatigue life as the dependent variable

Using the combined results from the previous study and the current study, further calibration of the material constants was performed. Table 5-1 and Table 5-2 present the material coefficients derived from experimental data and the R^2 values for each curve fit. Only the coefficients that were updated are included below. Additionally, due to the geometric irregularities of batch 2 from manufacturer 1, they were not included in the coefficient calibration.

Clear Span		$4d_b$		$6d_b$		$8d_b$	
Mfr	**Grade**	**c**	**d**	**c**	**d**	**c**	**d**
1	80	7.71E-03	-2.59	2.54E-02	-1.97	-	-
2	60	6.16E-03	-2.83	1.62E-02	-2.32	1.76E-02	-2.25
	80	1.55E-03	-3.14	2.49E-03	-2.89	5.54E-03	-2.50
	100	5.50E-04	-3.53	1.96E-03	-2.91	4.68E-03	-2.50
3	100	-	-	3.98E-03	-2.68	6.52E-03	-2.43

Table 5-1: Summary of material coefficients derived from experimental analysis for #8 bars

Clear Span		$4d_b$	$6d_b$	$8d_b$
Mfr	Grade	R^2	R^2	R^2
1	80	0.979	0.966	-
2	60	0.971	0.957	0.975
	80	0.886	0.880	0.937
	100	0.927	0.940	0.947
3	100	-	0.783	0.892

Table 5-2: Coefficients of determination for the calibrated fatigue model

Figure 5-1 illustrates the fatigue model prediction for grade 80 #8 bars produced by manufacturer 1. Figure 5-2, Figure 5-3, and Figure 5-4 show the fatigue model prediction for grade 60, grade 80 and grade 100 #8 bars produced by manufacturer 2. Figure 5-5 shows the fatigue model prediction for grade 100 #8 bars produced by manufacturer 3.

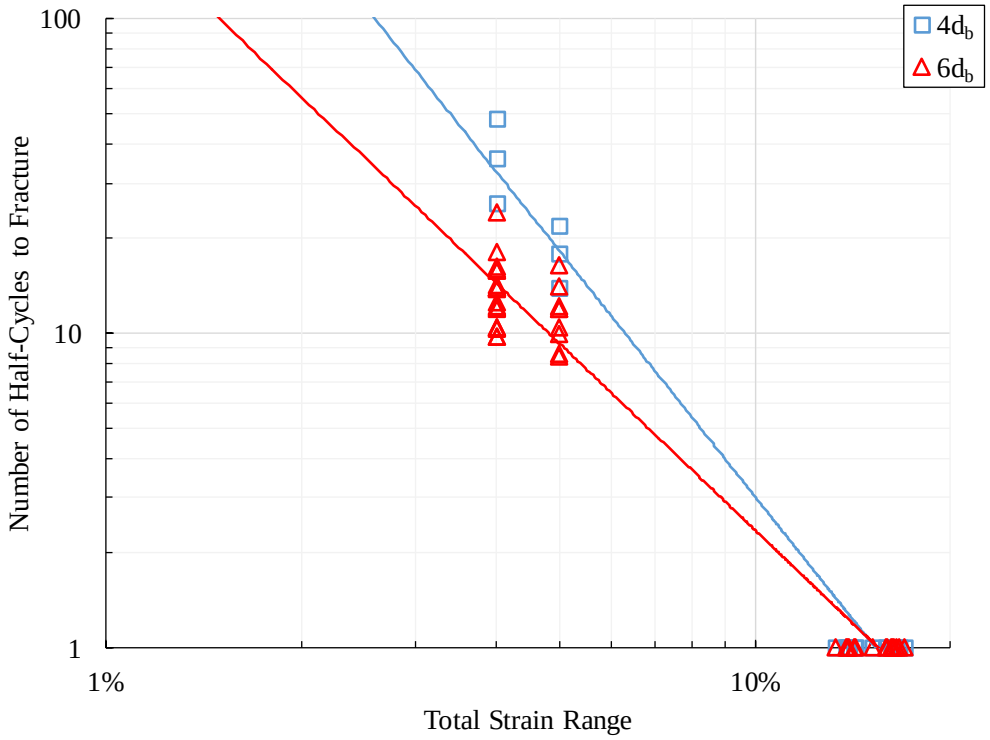

Figure 5-1: Relationship between half-cycles to fracture and total strain range for grade 80 #8 bars produced by manufacturer 1

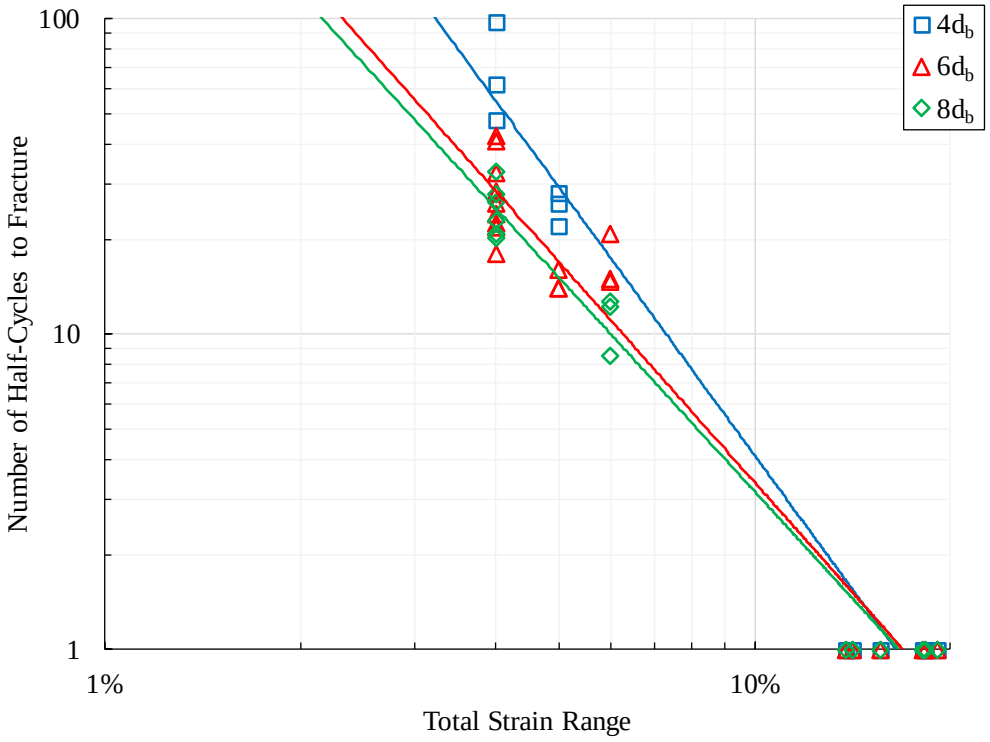

Figure 5-2: Relationship between half-cycles to fracture and total strain range for grade 60 #8 bars produced by manufacturer 2

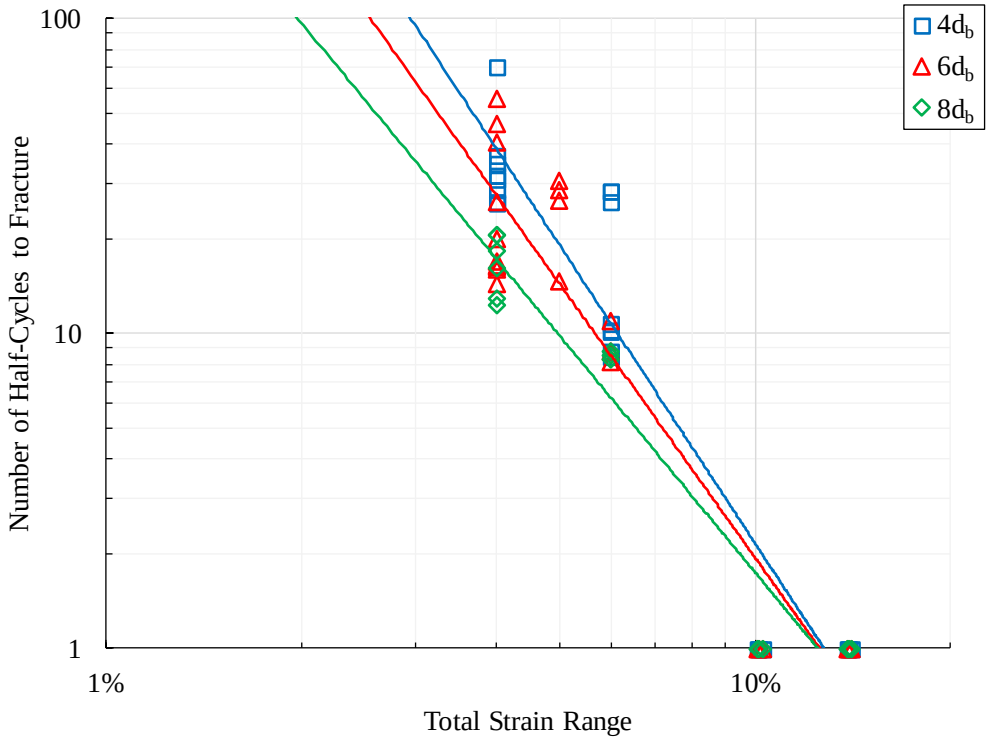

Figure 5-3: Relationship between half-cycles to fracture and total strain range for grade 80 #8 bars produced by manufacturer 2

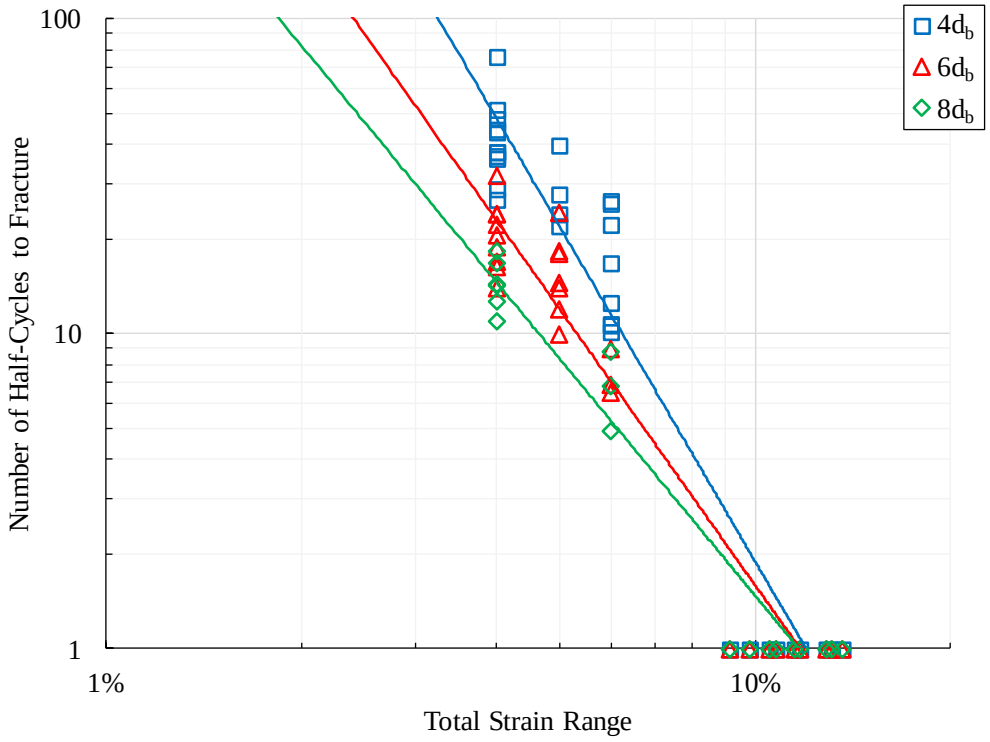

Figure 5-4: Relationship between half-cycles to fracture and total strain range for grade 100 #8 bars produced by manufacturer 2

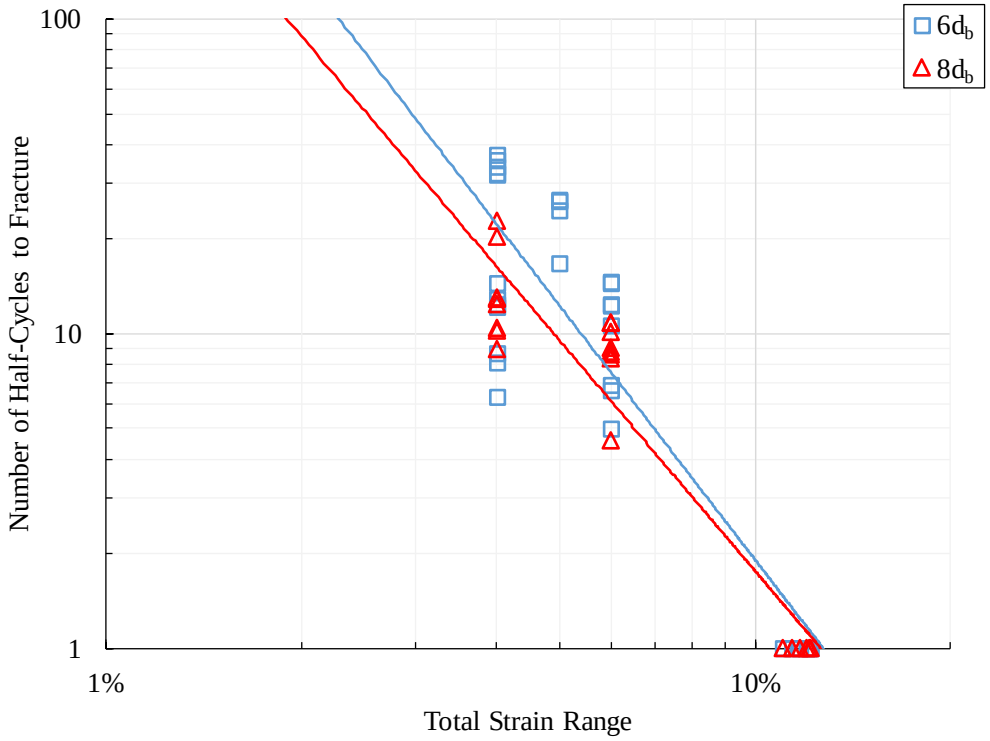

Figure 5-5: Relationship between half-cycles to fracture and total strain range for grade 100 #8 bars produced by manufacturer 3

6. SUMMARY AND CONCLUSIONS

6.1 SUMMARY

The allowance of high-strength reinforcing bars (HSRB) in reinforced concrete structures subjected to seismic loading has the potential to reduce reinforcement congestion, reduce costs, and allow for designs not currently possible using the existing design provisions. Recent fatigue testing of HSRB have revealed a high variability in the resistance to fatigue of HSRB being developed in the U.S., with some exhibiting much higher and others much lower fatigue lives than the benchmark grade 60 bars (Ghannoum and Slavin, 2016). This study is part of a broader project whose ultimate objectives are to evaluate any changes in bar fracture and seismic risk associated with switching to HSRB, and to define the acceptable mechanical properties for HSRB for use in seismic applications based on those risks.

As part of that effort, mechanical tests were conducted on bars produced by three different manufacturers to quantify the mechanical properties of experimental batches of high-strength bars and aid the development process of those new types of bars. Monotonic tension tests along with low-cycle fatigue tests were performed on grade 60 and high-strength reinforcing bars in order to evaluate their performance under simulated seismic conditions. Relationships for the prediction of fatigue life were updated. High-strength reinforcing bars produced using the three main manufacturing techniques in the United States. and produced by three different manufacturers were tested. Additionally, bar grade, up to grade 100, clear griping span, loading strain protocol, and geometric deformations were varied in the study. Bar testing is still ongoing as part of the broader project, which encompass steel from the main five manufacturers of reinforcing bars in the United States. Results of tests completed to date were presented.

6.2 CONCLUSIONS

6.2.1 Manufacturer 1

For manufacturer 1, this study focused on the grade 80 bars satisfying ASTM A706 specifications, as those bars were targeted for production adjustments. Limited tests were conducted on grade 100 bars from manufacturer 1. With the exception of batch 2, which had atypical geometric deformations, the grade 80 bars produced by manufacturer 1 did not exhibit significant differences in their fatigue life. The test results therefore indicate that the modifications attempted by manufacturer 1 to the bar chemical composition did not produce significant changes in their fatigue life to fracture. Batch 2 bars from manufacturer 1 exhibited substantially reduced fatigue lives compared with bars from other batches. The atypical geometry of the bars tested from batch 2 highlight the importance of introducing more stringent deformation specifications so more consistent reinforcing bar fatigue life can be achieved. Overall, the grade 80 bars from manufacturer 1 performed the worst in terms of number of half-cycles to fracture than other grades, with grade 100 bars having an intermediate fatigue performance and grade 60 bars have the best fatigue performance.

6.2.2 Manufacturer 2

Manufacturer 2 opted to soften the radii at the base of their bar's deformations in an attempt to improve fatigue performance. This study compared the fatigue performance of bars with both deformation geometries. Generally, the bars with the improved geometry saw substantial increases in their fatigue life both when considering fracture as the failure criteria and when considering loss of 20% of peak tensile strength as the failure criteria. Grade 60 bars benefitted the least from the improved geometry, while the smaller #5 bars appeared to benefit

the most. Bars from manufacturer 2, however, showed substantial variations and variability in fatigue performance across both bar size and bar grade. All HSRB #5 bar types from manufacturer 2 exhibited on average a significant increase in number of half-cycles to fracture over grade 60 counterparts. However, due to the high variability in fatigue life results, the error bars of #5 grade 60 and 80 bars overlapped significantly. The #8 bars from manufacturer 2 showed mixed results. In general, the HSRB from manufacturer 2 were unable to match the fatigue performance of grade 60 bars when tested at $4d_b$, but showed equivalent or improved performance at $6d_b$. This is due to the fatigue life to fracture of HSRB being relatively insensitive to the clear gripping span, while the grade 60 bars experienced marked drops in fatigue life as the clear span increased. It is possible that the hardened outer layer generated by the quenching process improved toughness of the higher-strength bars during buckling that generates the highest strain demands are in those outer layers.

6.2.3 Manufacturer 3

Results from manufacturer 3 were inconsistent. With one batch of #8 bars showing fatigue performance exceeding that of grade 60 bars from other manufacturers and another batch showing lower fatigue performance. It is not clear at this stage why bars from manufacturer 3 showed such variable performance.

6.2.4 Effects of Clear Span on Fatigue Life

Previous research from Ghannoum and Slavin (2016) indicated that with an increase in clear span, all bars experience a decrease in fatigue life. This study added an additional clear span of 8 bar diameters (d_b) to investigate this trend further. Generally, fatigue performance was observed to drop when the clear gripping span increased from 4 to 6 bar diameters (d_b).

However, the fatigue life to fracture tended to level off when increasing from $6d_b$ to $8d_b$, and an associated marked drop in variability in fatigue life within each bar and test type was also observed. These trends where however not uninform across grades. For several of the strain protocols tested, the grade 60 bars showed a measurable decrease in fatigue life when the clear gripping span was increased from $6d_b$ to $8d_b$, while the HSRB fatigue life tended to remain constant for both clear griping spans.

6.2.5 Effects of Deformation Geometry on Fatigue Life

The two lowest performing batches relative to other tests were bars from batch 2 from manufacture 1 (M1-B2) across all three grades and manufacturer 3 batch 1 grade 100 #5 bars (M3-B1-100-#5). These bars performed substantially worse than grade 60 benchmark bars, exhibiting fatigue lives as low as 20% that of the grade 60 bars. Both of these batches had atypical geometric deformations. M1-B2 bars had additional longitudinal ribs that severely reduced the fatigue life of the bars. The bars were effected by inconsistent buckling and likely from stress concentrations occurring at the sections between the additional longitudinal ribs. M3-B1-100-#5 bars had flattened transverse ribs and a longitudinal rib that was a negligible portion of the area and as a result, had the lowest fatigue performance of all #5 bars studied. The atypical bar geometries of the deficient batches are currently allowed by ASTM A706 and A1035 standards. Results from this study therefore highlight the necessity for stricter limits on bar deformations to ensure adequate and consistent fatigue performance in reinforcing bars.

6.2.6 Fatigue Performance Measures

An additional measurement of fatigue performance was tracked for all tests. Fatigue failure was defined in this study as either fracture or the cycle at which the tensile strength at

peak strain dropped to 80% of the first cycle tensile capacity. The latter measure was useful for the quenched and tempered high-strength bars from manufacturer 2 that were able to experience a high number of cycles before fracture, but a significant and gradual loss of strength caused by fatigue cracking. In such cases where a large portion of bar strength is lost prior to fracture, it is important to consider the 80% strength mark as the criteria for bar failure so as not to overestimate the capacity of member when gradual bar strength loss is not modeled explicitly as is common practice.

6.3 RECOMMENDATIONS FOR FUTURE WORK

Additional testing needs to be conducted to fill out the test matrix in totality. In addition to the strain protocols presented, protocols at a lower strain range should be conducted to validate the fatigue model proposed. To clarify the effects of strain range, the effects of mean strain should be considered and its effect on buckling. #11 bars should be considered in future analysis to see if the trends shown prove true for larger size bars. Further investigation into the effects of bar deformation geometry and its effects on buckling and fatigue life are necessary to establish standard specifications to ensure adequate and consistent fatigue life.

REFERENCES

American Concrete Institute (ACI) Committee 117 (2010), "Specification for Tolerances for Concrete Construction and Materials and Commentary (ACI 117-10)", American Concrete Institute, Farmington Hills, MI.

American Concrete Institute (ACI) Committee 318 (2002), "Building Code Requirements for Reinforced Concrete (ACI 318-02)," American Concrete Institute, Farmington Hills, MI.

American Concrete Institute (ACI) Committee 318 (2014), "Building Code Requirements for Reinforced Concrete (ACI 318-14)," American Concrete Institute, Farmington Hills, MI.

American Concrete Institute (ACI), 2010, Design Guide for the Use of ASTM A1035/A1035M Grade 100 Steel Bars for Structural Concrete, ACI ITG-6R-10, American Concrete Institute, Farmington Hills, MI.

ASTM A1035 / A1035M-16a, "Standard Specification for Deformed and Plain, Low-Carbon, Chromium, Steel Bars for Concrete Reinforcement," ASTM International, West Conshohocken, PA, 2016.

ASTM A370-16, "Standard Test Methods and Definitions for Mechanical Testing of Steel Products," ASTM International, West Conshohocken, PA, 2016.

ASTM A615 / A615M-16, "Standard Specification for Deformed and Plain Carbon-Steel Bars for Concrete Reinforcement," ASTM International, West Conshohocken, PA, 2016.

ASTM A706 / A706M-16, "Standard Specification for Deformed and Plain Low-Alloy Steel Bars for Concrete Reinforcement," ASTM International, West Conshohocken, PA, 2016.

ASTM E8 / E8M-16a, "Standard Test Methods for Tension Testing of Metallic Materials," ASTM International, West Conshohocken, PA, 2016.

Brown, Jeff, Kunnath, Sashi K. “Low-Cycle Fatigue Failure of Reinforcing Steel Bars.” ACI Materials Journal 6.110 (2004): 457-65.

Ghannoum, Wassim M. and Chase M. Slavin. “Low-Cycle Fatigue Performance of High-Strength Steel Reinforcing Bars.” ACI Materials Journal 113.06 (2016): 803-814.

Hawileh, R., Rahman, A., Tabatabai, H. “Evaluation of the Low-Cycle Fatigue Life in ASTM A706 and A615 Grade 60 Steel Reinforcing Bars.” Journal of Materials in Civil Engineering 22.1 (2010): 65-76.

Koh, S.K., Stephens, R.I., “Mean Stress Effects on Low Cycle Fatigue for a High Strength Steel,” Fatigue & Fracture of Engineering Materials & Structures, 14.4 (1991): 413-28.

Mander, J. B., Panthaki, F. D., Kasalanati, A. “Low-Cycle Fatigue Behavior of Reinforcing Steel.” Journal of Materials in Civil Engineering 6.4 (1994): 453-68.

MMFX Technologies Corporation, “Material Properties and Design Considerations MMFX2 (ASTM A1035/AASHTO MP18),” MMFX Product Information, December 2012, 36 pp.

NEHRP Consultants Joint Venture, “Use of High-Strength Reinforcement for Earthquake Resistant Concrete Structures,” NIST GCR 14-917-30, Applied Technology Council, Redwood City, CA, 2014.

Slavin, Chase M. and Wassim M. Ghannoum. “Defining Structurally Acceptable Properties of High-Strength Steel Bars through Material and Column Testing, Part I: Material Testing Report.” (05-14), Charles Pankow Foundation, August 2015, pp. 135.

Sokoli, D., and Ghannoum, W.M., “High-strength Reinforcement in Columns under High Shear Stresses,” ACI Structural Journal, 113 (3), 2016.

Sokoli, D., Shekarchi, W., Buenrostro, E., Ghannoum, W.M., “Advancing behavioral understanding and damage evaluation of concrete members using high-resolution digital image correlation data,” Earthquakes and Structures, V. 7, No. 5, pp. 609-26, November 2014.

Sokoli, Drit. “Seismic Performance of Concrete Columns Reinforced with High Strength Steel.” Thesis. University of Texas at Austin, 2014.